# INVESTIGATION OF ROCK-FLUID INTERACTIONS USING GEOMATERIAL MICROFLUIDICS

By

AYUSH JOSHI

Bachelor of Technology in Petroleum Engineering

Rajiv Gandhi Institute of Petroleum Technology

Amethi, India

2021

Submitted to the Faculty of the
Graduate College of the
Oklahoma State University
in partial fulfillment of
the requirements for
the Degree of
MASTER OF SCIENCE
May, 2023

INVESTIGATION OF ROCK-FLUID INTERACTIONS

USING GEOMATERIAL MICROFLUIDICS

Thesis Approved:

Dr. Prem Bikkina

Thesis Adviser & Chair

Dr. Hunjoo Lee

Committee Member

Dr. Javier Vilcaez

Committee Member

# ACKNOWLEDGEMENTS

I appreciate the support and encouragement from those who assisted me during my studies. Without their help, this thesis would not have been of the same quality.

First, I would like to express my appreciation and admiration to my committee chair and advisor Dr. Prem Bikkina for his constant support and guidance throughout my academic pursuit. Dr. Bikkina's expertise and knowledge were integral to the success of this thesis, from conducting experiments to writing it, and his contributions enhanced its significance and effectiveness.

I would also like to extend my sincere thanks to my committee members Professor Dr. Javier Vilcaez and Dr. Hunjoo Lee, for their advice and suggestions in general.

I would be grateful to Brent Johnson from the Microscopy Lab of OSU for their technical support in the microscopic analysis, my colleague Sushobhan Pradhan for helping me on fittings, preparing samples for clay coating characterization, and providing suggestions many times during the experiments, and Rupom Bhattacherjee for creating a foundation for this study.

Finally, I would like to express my appreciation to the Department of Energy (DOE) and Continental Resources (project code 1-578930) for providing funding for this study.

Name: AYUSH JOSHI

Date of Degree: MAY, 2023

Title of Study: INVESTIGATION OF ROCK-FLUID INTERACTIONS USING GEOMATERIAL MICROFLUIDICS

Major Field: Petroleum Engineering

Abstract: Illite and Illite-Smectite clays are reportedly the Caney Shale's most prevalent clay minerals. The swelling and fines migration of clays may occur when water-based fluids contact the clay minerals. This may result in the reduction of pore space and permeability, and wettability alteration. Therefore, we quantified the swelling potentials, fines migration and wettability alteration of Illite and Illite-Smectite clays upon exposure to model brines and a produced water, and a model oil and a crude oil. We measured density, viscosity, pH, TDS, and interfacial tension as they are important in multiphase flow and displacement characteristics.

Geomaterial microfluidics is recently being used to study physicochemical interactions of solid-fluid systems. It facilitates visualizing the surface behavior upon exposure to various fluids. This study includes preparation and characterization of Illite-Smectite clay-coated glass capillary tubes. Illite and Illite-Smectite clay-coated geomaterial microfluidic surfaces were prepared to investigate the effects of first contact fluid, brine salinity, and aging on wettability. In this work, advancing and receding contact angles of model brine-air, model oil-air, produced water-air, crude oil-air, model brine-model oil systems, and produced water-crude oil systems have been measured in the untreated, and clay-coated microfluidic channels of 1000 µm width and 50 µm depth. The aging effect was studied by retaining the non-aqueous and aqueous solutions in the corresponding microfluidic channels for approximately 24 h in the case of channels first contacted by aqueous and non-aqueous solutions, respectively. The advancing and receding contact angles of Caney shale-crude oil-produced water systems were also measured.

The experimental findings indicate the swelling potential, fines migration, and wettability alteration of Illite and Illite-Smectite clays. The results signify the influence of first contact fluid, brine salinity, and aging on wettability of the untreated and clay-coated microfluidic surfaces. The experiments also demonstrate the wetting nature of the Caney shale samples from reservoir and non-reservoir zones.

# TABLE OF CONTENTS

**Chapter** **Page**

Contents

**LIST OF TABLES** ..... viii

**LIST OF FIGURES** ..... ix

**CHAPTER I** ..... 1

**INTRODUCTION** ..... 1

**CHAPTER II** ..... 7

**REVIEW OF LITERATURE** ..... 7

**2.1 A brief introduction of clay minerals** ..... 7

**2.2 Impact of clay on producibility of shale** ..... 8

**2.3 Wettability: A brief introduction** ..... 10

**2.4 Mechanisms that impact the wetting characteristics of surface** ..... 12

**2.4.1 Alteration of interfacial tension between bulk oil and brine** ..... 12

**2.4.2 Multicomponent ion exchange** ..... 13

**2.4.3 pH change** ..... 13

**2.4.4 Mineral dissolution and salting in mechanism** ..... 14

**2.4.5 Expansion of electric double layer** ..... 14

**2.5 Caney shale clay minerology** ..... 15

**2.6 Microfluidics Background** ..... 17

**2.6.1 Geomaterial Micromodels** ..... 17

**CHAPTER III** ..... 20

**MATERIALS AND METHODS** ..... 20

**3.1 Clay Minerals** ..... 20

**3.2 Fluids** ..... 21

**3.3 Solid Substrates** ..... 22

**3.3.1 Capillary tubes** ..... 22

**3.3.2 Thin Bottom flow cells** ..... 22

**3.4 Syringe Pumps** ..... 23

3.5 Tubing and Valve ..... 23
3.6 Microscope, Camera and Light Source ..... 24
3.7 Experimental Procedure ..... 26
3.7.1 Clay solution preparation ..... 26
3.7.2 Clay coating procedure ..... 27
3.7.3 Coating Characterization ..... 29
3.7.4 Experimental procedure for wettability experiments ..... 29
CHAPTER IV ..... 31
RESULTS AND DISCUSSION ..... 31
4.1 Measurements of Swelling Potentials of Illite and Illite-Smectite Clays ..... 31
4.1.1 Swelling potentials of Illite and Illite-Smectite clays to model fluids ..... 31
4.1.2 Swelling potential of Illite and Illite-Smectite to continental fluids ..... 33
4.2 Microscopic characterization of Illite-Smectite coating ..... 35
4.3 Effect of salinity on Illite-Smectite clay coating ..... 36
4.4 Wettability analysis of untreated and clay-coated microfluidic channels ..... 38
4.4.1 DI-Water and n-decane system ..... 39
4.4.1.1 Untreated microfluidic channel ..... 39
4.4.1.2 Illite clay-coated microfluidic channel ..... 42
4.4.1.3 Illite-Smectite coated microfluidic channel ..... 44
4.4.2 5k ppm brine and n-decane system ..... 46
4.4.2.1 Untreated microfluidic channel ..... 46
4.4.2.2 Illite clay-coated microfluidic channel ..... 49
4.4.2.3 Illite-Smectite clay-coated microfluidic channel ..... 51
4.4.3 10k ppm brine and n-decane system ..... 53
4.4.3.1 Untreated microfluidic channel ..... 53
4.4.3.2 Illite clay-coated microfluidic channel ..... 55
4.4.3.3 Illite-Smectite clay-coated microfluidic channel ..... 57
4.4.4 30k ppm brine and n-decane system ..... 59
4.4.4.1 Untreated microfluidic channel ..... 59
4.4.4.2 Illite clay-coated microfluidic channel ..... 61
4.4.4.3 Illite-Smectite clay-coated microfluidic channel ..... 63
4.4.5 Produced water and Crude oil system ..... 65
4.4.5.1 Untreated microfluidic channel ..... 65

**4.4.5.2 Illite clay-coated microfluidic channel** ..... 68
**4.4.5.3 Illite-Smectite clay-coated microfluidic channel** ..... 70
**4.5 Wettability results using Caney shale core sample of reservoir zone** ..... 74
**4.6 Wettability results using Caney shale core sample of non-reservoir zone** ..... 75
**CHAPTER V** ..... 77
**CONCLUSION** ..... 77
**REFERENCES** ..... 79

## LIST OF TABLES

**Table** **Page**

Table 1: Caney shale minerology on the basis of sidewall cores. A calcareous shale deposit known as 'Mayes' formation is found at the base of the Caney shale [52]. ..... 16
Table 2: Chemical composition (mass norm. %) of Illite and Illite-Smectite (70/30 wt.%). ..... 21
Table 3: Density of fluids at 20 ℃, 1 atm, and viscosity, pH, and TDS of fluids at 18 ℃, 1 atm..... 21
Table 4: Interfacial tensions of brine-n-decane systems, and produced water-crude oil system obtained from Continental Resources at 1 atm and 20℃..... 22
Table 5: Specifications of tubing. ..... 24
Table 6: Microscopy components specifications. ..... 24
Table 7: Specifications of microscope used for SEM and SEM-EDS analysis. ..... 26
Table 8: Contribution of different component of Illite-Smectite clay solution prepared in 0 ppm, 5000 ppm, 10,000 ppm, and 30,000 ppm NaCl solution. ..... 38
Table 9: Wettability states of untreated microfluidic channel-brine-oil systems. ..... 73
Table 10: Wettability states of Illite clay-coated microfluidic channel-brine-oil systems. ..... 74
Table 11: Wettability states of Illite-Smectite clay-coated microfluidic channel-brine-oil systems. ..... 74

## LIST OF FIGURES


| Figure | | Page |
|---|---|---|
| Figure 1: | Tetrahedron and Octahedron structure of clay minerals | 8 |
| Figure 2: | Forces acting on particle, Permeability reduction by clogging | 9 |
| Figure 3: | A typical three phase contact angle | 10 |
| Figure 4: | Thin bottom flow cells | 23 |
| Figure 5: | Harvard PHD ULTRA™ Programmable Syringe Pump (Courtesy Harvard Apparatus) | 23 |
| Figure 6: | Components of microscopic system | 25 |
| Figure 7: | Microscopic system | 25 |
| Figure 8: | Schematic of Illite-Smectite clay coating setup for capillary tubes | 28 |
| Figure 9: | Schematic of Illite or Illite-Smectite clay coating setup for thin bottom flow cell | 28 |
| Figure 10: | Schematic of the experimental setup for microfluidics-based wettability experiments | 30 |
| Figure 11: | Swelling Potential of Illite Clay upon exposure to DI water, 5k ppm, 10k ppm, 30k ppm brines, and n-decane | 32 |
| Figure 12: | Swelling Potential of Illite-Smectite clay upon exposure to DI water, 5k ppm, 10k ppm, 30k ppm brines, and n-decane | 32 |
| Figure 13: | (a) Visual appearance of Illite-Smectite clay in DI water, 5k ppm, 10k ppm, and 30k ppm brine solutions just after adding the fluids, (b) after 44 h | 33 |
| Figure 14: | (a) Visual Appearance of Illite and Illite-Smectite in n-decane, and Illite clay in DI water, 5k ppm, 10k ppm, and 30k ppm brine solutions just after adding the fluids, (b) after 27 h | 33 |

**Figure** **Page**


Figure 15: Initial swelling upon exposure to crude oil and produced water ..... 34

Figure 16: Swelling after 24 h upon exposure to crude oil and produced water... 34

Figure 17: (a) Visual appearance of Illite and Illite-Smectite clay in Continental resources crude oil and Produced water just after adding the fluids, (b) after 24 h ..... 35

Figure 18: SEM images of Illite-Smectite coated glass capillary tubes at 20,000x magnification prepared in (a) 0 ppm (DI water), (b) 5000 ppm, (c) 10,000 ppm, (d) 30,000 ppm NaCl brine solutions ..... 35

Figure 19: SEM-EDS images of Illite-Smectite coated glass capillary tube surfaces coated with 10 wt.% clay prepared in (a) 0 ppm (DI water) NaCl, (b) 5000 ppm NaCl, (c) 10,000 ppm NaCl, and (d) 30,000 ppm NaCl solutions ..... 37

Figure 20: Representative image of contact angle measurement ..... 39

Figure 21: The temporal progress of interface shown using image overlay in ImageJ. Arrow indicates the direction of interface movement ..... 39

Figure 22: Untreated microfluidic channel contacted by DI water first: (a) DI water advancing contact angle and (b) DI water receding contact angle in DI water-air system before aging; Untreated microfluidic channel contacted by n-decane first: (c) n-decane advancing contact angle and (d) n-decane receding contact angle in n-decane-air system before aging. Arrow indicates the direction of interface movement ... 40

Figure 23: Untreated microfluidic channel contacted by DI water first: (a) DI water receding contact angle and (b) DI water advancing contact angle in DI water-n-decane system before aging; (c) DI water receding contact angle and (d) DI water advancing contact angle in DI water-n-decane system after aging. Untreated microfluidic channel contacted by n-decane first: (e) DI water advancing contact angle and (f) DI water receding contact angle in DI water-n-decane system before aging; (g) DI water advancing contact angle and (h) DI

water receding contact angle in DI water-n-decane system after aging; Arrow indicates the direction of interface movement ..... 41

Figure 24: Illite clay-coated microfluidic channel contacted by DI water first: (a) DI water advancing contact angle and (b) DI water receding contact angle in DI water-air system before aging; Illite clay-coated microfluidic channel contacted by n-decane first: (c) n-decane advancing contact angle and (d) n-decane receding contact angle in n-decane-air system before aging ..... 42

Figure 25: Illite clay-coated microfluidic channel contacted by DI water first: (a) DI water receding contact angle and (b) DI water advancing contact angle in DI water-n-decane system before aging; (c) DI water receding contact angle and (d) DI water advancing contact angle in DI water-n-decane system after aging. Illite clay-coated microfluidic channel contacted by n-decane first: (e) DI water advancing contact angle and (f) DI water receding contact angle in DI water-n-decane system before aging; (g) DI water advancing contact angle and (h) DI water receding contact angle in DI water-n-decane system after aging; Arrow indicates the direction of interface movement ..... 43

Figure 26: Illite-Smectite clay-coated microfluidic channel contacted by DI water first: (a) DI water advancing contact angle and (b) DI water receding contact angle in DI water-air system before aging; Illite-Smectite clay-coated microfluidic channel contacted by n-decane first: (c) n-decane advancing contact angle and (d) n-decane receding contact angle in n-decane-air system before aging ..... 44

Figure 27: Illite-Smectite clay-coated microfluidic channel contacted by DI water first: (a) DI water receding contact angle and (b) DI water advancing contact angle in DI water-n-decane system before aging; (c) DI water receding contact angle and (d) DI water advancing contact angle in DI water-n-decane system after aging. Illite-Smectite

clay-coated microfluidic channel contacted by n-decane first: (e) DI water advancing contact angle and (f) DI water receding contact angle in DI water-n-decane system before aging; (g) DI water advancing contact angle and (h) DI water receding contact angle in DI water-n-decane system after aging; Arrow indicates the direction of interface movement ..... 45

Figure 28: Untreated microfluidic channel contacted by 5k ppm brine first: (a) 5k ppm brine advancing contact angle and (b) 5k ppm brine receding contact angle in 5k ppm brine-air system before aging ..... 47

Figure 29: Untreated microfluidic channel contacted by 5k ppm brine first: (a) 5k ppm brine receding contact angle and (b) 5k ppm brine advancing contact angle in 5k ppm brine-n-decane system before aging; (c) 5k ppm brine receding contact angle and (d) 5k ppm brine advancing contact angle in 5k ppm brine-n-decane system after aging. Untreated microfluidic channel contacted by n-decane first: (e) 5k ppm brine advancing contact angle and (f) 5k ppm brine receding contact angle in 5k ppm brine-n-decane system before aging; (g) 5k ppm brine advancing contact angle and (h) 5k ppm brine receding contact angle in 5k ppm brine-n-decane system after aging; Arrow indicates the direction of interface movement ..... 48

Figure 30: Illite clay-coated microfluidic channel contacted by 5k ppm brine first: (a) 5k ppm brine advancing contact angle and (b) 5k ppm brine receding contact angle in 5k ppm brine-air system before aging ..... 49

Figure 31: Illite clay-coated microfluidic channel contacted by 5k ppm brine first: (a) 5k ppm brine receding contact angle and (b) 5k ppm brine advancing contact angle in 5k ppm brine-n-decane system before aging; (c) 5k ppm brine receding contact angle and (d) 5k ppm brine advancing contact angle in 5k ppm brine-n-decane system after aging. Illite clay-coated microfluidic channel contacted by n-decane

**Figure** **Page**

first: (e) 5k ppm brine advancing contact angle and (f) 5k ppm brine receding contact angle in 5k ppm brine-n-decane system before aging; (g) 5k ppm brine advancing contact angle and (h) 5k ppm brine receding contact angle in 5k ppm brine-n-decane system after aging; Arrow indicates the direction of interface movement ..... 50

Figure 32: Illite-Smectite clay-coated microfluidic channel contacted by 5k ppm brine first: (a) 5k ppm brine advancing contact angle and (b) 5k ppm brine receding contact angle in 5k ppm brine-air system before aging ..... 51

Figure 33: Illite-Smectite clay-coated microfluidic channel contacted by 5k ppm brine first: (a) 5k ppm brine receding contact angle and (b) 5k ppm brine advancing contact angle in 5k ppm brine-n-decane system before aging; (c) 5k ppm brine receding contact angle and (d) 5k ppm brine advancing contact angle in 5k ppm brine-n-decane system after aging. Illite-Smectite clay-coated microfluidic channel contacted by n-decane first: (e) 5k ppm brine advancing contact angle and (f) 5k ppm brine receding contact angle in 5k ppm brine-n-decane system before aging; (g) 5k ppm brine advancing contact angle and (h) 5k ppm brine receding contact angle in 5k ppm brine-n-decane system after aging; Arrow indicates the direction of interface movement ..... 52

Figure 34: Untreated microfluidic channel contacted by 10k ppm brine first: (a) 10k ppm brine advancing contact angle and (b) 10k ppm brine receding contact angle in 10k ppm brine-air system before aging ..... 53

Figure 35: Untreated microfluidic channel contacted by 10k ppm brine first: (a) 10k ppm brine receding contact angle and (b) 10k ppm brine advancing contact angle in 10k ppm brine-n-decane system before aging; (c) 10k ppm brine receding contact angle and (d) 10k ppm brine advancing contact angle in 10k ppm brine-n-decane system after aging. Untreated microfluidic channel contacted by n-decane

first: (e) 10k ppm brine advancing contact angle and (f) 10k ppm brine receding contact angle in 10k ppm brine-n- decane system before aging; (g) 10k ppm brine advancing contact angle and (h) 10k ppm brine receding contact angle in 10k ppm brine-n-decane system after aging; Arrow indicates the direction of interface movement ..... 54

Figure 36: Illite clay-coated microfluidic channel contacted by 10k ppm brine first: (a) 10k ppm brine advancing contact angle and (b) 10k ppm brine receding contact angle in 10k ppm brine-air system before aging ..... 55

Figure 37: Illite clay-coated microfluidic channel contacted by 10k ppm brine first: (a) 10k ppm brine receding contact angle and (b) advancing contact angle in 10k ppm brine-n-decane system before aging; (c) 10k ppm brine receding contact angle and (d) advancing contact angle in 10k ppm brine-n-decane system after aging. Illite clay-coated microfluidic channel contacted by n-decane first: (e) 10k ppm brine advancing contact angle and (f) receding contact angle in 10k ppm brine-n-decane system before aging; (g) 10k ppm brine advancing contact angle and (h) receding contact angle in 10k ppm brine-n-decane system after aging; Arrow indicates the direction of interface movement ..... 56

Figure 38: Illite-Smectite clay-coated microfluidic channel contacted by 10k ppm brine first: (a) 10k ppm brine advancing contact angle and (b) 10k ppm brine receding contact angle in 10k ppm brine-air system before aging ..... 57

Figure 39: Illite-Smectite clay-coated microfluidic channel contacted by 10k ppm brine first: (a) 10k ppm brine receding contact angle and (b) 10k ppm brine advancing contact angle in 10k ppm brine-n-decane system before aging; (c) 10k ppm brine receding contact angle and (d)10k ppm brine advancing contact angle in 10k ppm brine-n-decane

system after aging. Illite-Smectite clay-coated microfluidic channel contacted by n-decane first: (e) 10k ppm brine advancing contact angle and (f) 10k ppm brine receding contact angle in 10k ppm brine-n-decane system before aging; (g) 10k ppm brine advancing contact angle and (h) 10k ppm brine receding contact angle in 10k ppm brine-n-decane system after aging; Arrow indicates the direction of interface movement ..... 58

Figure 40: Untreated microfluidic channel contacted by 30k ppm brine first: (a) 30k ppm brine advancing contact angle and (b) 30k ppm brine receding contact angle in 30k ppm brine-air system before aging ..... 59

Figure 41: Untreated microfluidic channel contacted by 30k ppm brine first: (a) 30k ppm brine receding contact angle and (b) 30k ppm brine advancing contact angle in 30k ppm brine-n-decane system before aging; (c) 30k ppm brine receding contact angle and (d) 30k ppm brine advancing contact angle in 30k ppm brine-n-decane system after aging. Untreated microfluidic channel contacted by n-decane first: (e) 30k ppm brine advancing contact angle and (f) 30k ppm brine receding contact angle in 30k ppm brine-n-decane system before aging; (g) 30k ppm brine advancing contact angle and (h) 30k ppm brine receding contact angle in 30k ppm brine-n-decane system after aging; Arrow indicates the direction of interface movement ..... 60

Figure 42: Illite clay-coated microfluidic channel contacted by 30k ppm brine first: (a) 30k ppm brine advancing contact angle and (b) 30k ppm brine receding contact angle in 30k ppm brine-air system before aging ..... 61

Figure 43: Illite clay-coated microfluidic channel contacted by 30k ppm brine first: (a) 30k ppm brine receding contact angle and (b) 30k ppm brine advancing contact angle in 30k ppm brine-n-decane system before aging; (c) 30k ppm brine receding contact angle and (d) 30k ppm

brine advancing contact angle in 30k ppm brine-n-decane system after aging. Illite clay-coated microfluidic channel contacted by n-decane first: (e) 30k ppm brine advancing contact angle and (f) receding contact angle in 30k ppm brine-n-decane system before aging; (g) 30k ppm brine advancing contact angle and (h) receding contact angle in 30k ppm brine-n-decane system after aging; Arrow indicates the direction of interface movement ..... 62

Figure 44: Illite-Smectite clay-coated microfluidic channel contacted by 30k ppm brine first: (a) 30k ppm brine advancing contact angle and (b) 30k ppm brine receding contact angle in 30k ppm brine-air system before aging ..... 63

Figure 45: Illite-Smectite clay-coated microfluidic channel contacted by 30k ppm brine first: (a) 30k ppm brine receding contact angle and (b) 30k ppm brine advancing contact angle in 30k ppm brine-n-decane system before aging; (c) 30k ppm brine receding contact angle and (d) 30k ppm brine advancing contact angle in 30k ppm brine-n-decane system after aging. Illite-Smectite clay-coated microfluidic channel contacted by n-decane first: (e) 30k ppm brine advancing contact angle and (f) 30k ppm brine receding contact angle in 30k ppm brine-n-decane system before aging; (g) 30k ppm brine advancing contact angle and (h) 30k ppm brine receding contact angle in 30k ppm brine-n-decane system after aging; Arrow indicates the direction of interface movement ..... 64

Figure 46: Untreated microfluidic channel contacted by produced water first: (a) produced water advancing contact angle and (b) produced water receding contact angle in produced water-air system before aging; Untreated microfluidic channel contacted by crude oil first: (c) crude oil advancing contact angle and (d) crude oil receding contact angle in crude oil-air system before aging ..... 66

**Figure** **Page**

Figure 47: Untreated microfluidic channel contacted by produced water first: (a) produced water receding contact angle and (b) produced water advancing contact angle in produced water-crude oil system before aging; (c) produced water receding contact angle and (d) produced water advancing contact angle in produced water-crude oil system after aging. Untreated microfluidic channel contacted by crude oil first: (e) produced water advancing contact angle and (f) produced water receding contact angle in produced water-crude oil system before aging; (g) produced water advancing contact angle and (h) produced water receding contact angle in produced water-crude oil system after aging; Arrow indicates the direction of interface movement ..... 67

Figure 48: Illite clay-coated microfluidic channel contacted by produced water first: (a) produced water advancing contact angle and (b) produced water receding contact angle in produced water-air system before aging; Illite clay-coated microfluidic channel contacted by crude oil first: (c) crude oil advancing contact angle and (d) crude oil receding contact angle in crude oil-air system before aging ..... 68

Figure 49: Illite clay-coated microfluidic channel contacted by produced water first: (a) produced water receding contact angle and (b) produced water advancing contact angle in produced water-crude oil system before aging; (c) produced water receding contact angle and (d) produced water advancing contact angle in produced water-crude oil system after aging. Illite clay-coated microfluidic channel contacted by crude oil first: (e) produced water advancing contact angle and (f) produced water receding contact angle in produced water-crude oil system before aging; (g) produced water advancing contact angle and (h) produced water receding contact angle in produced water-crude oil system after aging; Arrow indicates the direction of interface

**Figure** **Page**

movement ..... 69

Figure 50: Illite-Smectite clay-coated microfluidic channel contacted by produced water first: (a) produced water advancing contact angle and (b) produced water receding contact angle in produced water-air system before aging; Illite-Smectite clay-coated microfluidic channel contacted by crude oil first: (c) crude oil advancing contact angle and (d) crude oil receding contact angle in crude oil-air system before aging ..... 70

Figure 51: Illite-Smectite clay-coated microfluidic channel contacted by produced water first: (a) produced water receding contact angle and (b) produced water advancing contact angle in produced water-crude oil system before aging; (c) produced water receding contact angle and (d) produced water advancing contact angle in produced water-crude oil system after aging. Illite-Smectite clay-coated microfluidic channel contacted by crude oil first: (e) produced water advancing contact angle and (f) produced water receding contact angle in produced water-crude oil system before aging; (g) produced water advancing contact angle and (h) produced water receding contact angle in produced water-crude oil system after aging; Arrow indicates the direction of interface ..... 71

Figure 52: Snap off phenomenon in Illite-Smectite clay-coated surface contacted by crude oil first ..... 73

Figure 53: (a) Produced water advancing contact angle and (b) produced water receding contact angle in produced water-crude oil-Caney shale rock (reservoir zone) system before aging; (c) produced water advancing contact angle and (d) produced water receding contact angle in produced water-crude oil-Caney shale rock (reservoir zone) system after aging. Arrow indicates the direction of movement of crude oil droplet ..... 75

**Figure** **Page**

Figure 54: (a) Produced water advancing contact angle and (b) produced water receding contact angle in produced water-crude oil-Caney shale rock (non-reservoir zone) system before aging; (c) produced water advancing contact angle and (d) produced water receding contact angle in produced water-crude oil-Caney shale rock (non-reservoir zone) system after aging. Arrow indicates the direction of movement of crude oil droplet..... 76

# CHAPTER I

## INTRODUCTION

The Caney shale is a geological formation rich in organic material and is located in Oklahoma and Arkansas in the United States. The minerals present in the Caney shale include clay minerals such as kaolinite, illite, and smectite, besides quartz and carbonate minerals like calcite and dolomite. The presence of these minerals, along with the organic material, makes the Caney shale a potential source for hydrocarbons. Therefore, it has been the focus of significant exploration and production activity in recent years [1].

Illite and Illite-Smectite clays are reportedly the Caney shale's most prevalent clay minerals. The swelling and fines migration of clays may occur when water-based fluids contact the clay minerals. This may result in the reduction of pore space and permeability, and wettability alteration [2,3].

Although swelling is correlated with clay hydration, all clays do not swell when hydrated. The swelling characteristics of clays differ due to changes in their chemical composition and structure [4]. The silica tetrahedron (T), alumina octahedron (O), and silica tetrahedron (T) layers of the Illite structure are sandwiched together in the ratio of 2:1. The space between these layers is occupied by poorly hydrated potassium cations, which account for the lack of swelling [5]. This contrasts with other types of clay, such as smectite, which have large, plate-like particles that can absorb water and cause swelling. Additionally, Illite clay particles have a higher cation exchange capacity, which means they can hold onto positively charged ions such as potassium and magnesium, making

them less likely to absorb water. The organization of smectites is in quasicrystals, therefore, Smectites swell when water or polar organic solvents are imbibed in between smectite quasicrystals or between the individual layers that make up a quasicrystal. The replacement of small interlayer cations by large organic cations or larger polymeric hydroxyl-metal cations also results in swelling [6].

In unconventional reservoirs like shale, when clay particles are exposed to low salinity injection fluids, fines migration may occur that can plug the narrow pore throats resulting in the formation damage [7]. Fines migration from clays such as Illite and Smectite could also result in formation damage by clogging the narrow pores. Fines migration in shale can cause the formation to become less stable. This is because the fine-grained particles can fill the pores and fractures in the shale, making it more susceptible to deformation and failure [8]. This can lead to issues such as borehole collapse which can cause damage to the well and make it more difficult to extract hydrocarbons. The wettability of the formation is also affected by fines migration as they can change the surface energy and chemical properties of the rock. This could significantly affect the recovery of hydrocarbons.

Microfluidics is a technology that allows real-time visualization of pore-scale phenomena. Microfluidics technology has potential applications in reservoir engineering, a branch of petroleum engineering that deals with the study of subsurface reservoirs to understand their characteristics and behavior in order to optimize hydrocarbon recovery. Microfluidic devices made up of quartz or silicon are used to analyze the fluid behavior in subsurface [9].Microfluidic technology could help in flowing fluids through microchannels where capillary forces are dominant. On a microfluidic chip, a reservoir network pattern can be etched to simulate multiphase flow through porous media. It allows to visualize and quantify wettability of the system [10]. The application of microfluidics also includes the development of miniature, highly sensitive sensors that can detect the presence of oil and gas in subsurface formations. These sensors can be used to measure reservoir parameters

such as pressure, temperature, and fluid saturations, which can help to improve our understanding of the reservoir and optimize hydrocarbon recovery [11].

Another application of microfluidics is in the development of novel fluid systems for enhanced oil recovery (EOR) operations. Microfluidic devices can be used to mimic the rock surface. This can be achieved by coating the microfluidic substrates with the minerals present in the rock. Mimicking the rock surface on microfluidic channel and analyzing its behavior in presence of oil and water can improve oil recovery rates and increase the efficiency of EOR operations. Microfluidics can also be used in developing new methods for injecting fluids into the reservoir to replicate micro-scale injection wells as it provides precise control for fluid injection by adjusting the flowrates to even nanoliters/min. This can significantly improve the efficiency of EOR operations. The application of microfluidics can greatly reduce the cost and risks associated with field testing [12–14].

The wettability of a surface is characterized by the contact angle, a macroscopic quantity that can be experimentally measured. Wettability is an important parameter as it controls the flow, location, and distribution of fluids in a reservoir. The wettability of a reservoir has an impact on its capillary pressure, relative permeability, electrical properties, dispersion, and waterflood behavior [15]. In microfluidics, wettability plays a crucial role in controlling the flow and mixing of fluids in the small channels and structures [16].

A thin film of oil on a rock surface can make the surface hydrophobic, and substantially decrease the amount of oil that can be recovered. In contrast, a thin film of water on a rock surface can make the surface hydrophilic, which makes the rock water-wet and may promote hydrocarbon recovery. In both cases, the thickness and the composition of the thin film are important factors that are affected by the wettability of the rock surface [17]. The oil and water composition, salinity,

temperature, pressure, and the presence of surfactants and other contaminants can affect the properties of the thin film, and ultimately the wettability of the rock surface [18].

Wettability alteration is considered a viable technique by researchers for more efficient oil recovery. For this, the wetting state of a particular rock is altered preferably towards water-wet to increase the ultimate oil recovery. Jadhunandan and Morrow (1995) conducted a study to test the effect of wettability on oil recovery [19]. It was concluded that the ultimate oil recovery reaches its maximum near the intermediate wet state, and not the strongly water-wet state. Salathiel (1973) performed a series of experiments and found that during waterflooding, high oil recovery was obtained from the reservoir of mixed wettability [20]. Therefore, a reservoir's response to waterflooding varies based on its wettability. In the past few decades researchers have reported that maximum oil recovery is achieved when the rock is strongly water-wet [21–24]. Recently, Danial et al. (2022) investigated the wettability in water floods of viscous oil and found that the oil displacement in water-wet systems is mainly governed by capillary phenomenon [25]. C.J. van der waals proposed the concept of "disjoining pressure" to describe the interactions between liquids and solid surfaces, which laid the foundation for the study of wettability. A comparative analysis of conventional techniques was done by Hamid et al. (2022) for evaluating the wettability in shales [26]. This study compares three conventional methods used for evaluating wettability in shale formations: the Amott-Harvey, the U.S. Bureau of Mines (USBM), and the Contact Angle methods. The study revealed that The Amott-Harvey method is relatively easy to perform and provides a measure of the irreducible water saturation, but it can be affected by the presence of clay minerals. The USBM method is less affected by clay minerals and can provide a measure of the residual oil saturation, but it is more time-consuming and requires specialized equipment. The Contact Angle method provides a direct measure of wettability, but it can be affected by the roughness and heterogeneity of the shale surface.

The effect of the first contact fluid on wettability depends on the properties of the fluid and the surface it is in contact with. If the first contact fluid has a lower surface tension and/or a higher chemical affinity for the surface than subsequent fluids, it may be more difficult for subsequent fluids to displace it and change the wettability of the surface.

Fluid characteristics such as salinity, interfacial tension, and pH could also significantly affect the wettability of a surface. Salinity can affect the contact angle by altering the chemical composition of the fluid that is in contact with the solid surface. In general, low salinity fluids tend to make the surface more water-wet, while high salinity fluids tend to make the surface more oil-wet. At low salinities, the double layer at the solid-liquid interface is thick, and water molecules are attracted to the surface, leading to a smaller contact angle and a more water-wet surface. It's important to note that salinity effect on wettability can be complex and depend on the type of surface, type of fluid and the salinity level. The interfacial tension between oil and water can affect the contact angle of the rock surface, which in turn affects the wettability. In general, low interfacial tension tends to make the surface more water-wet, while high interfacial tension tends to make the surface more oil-wet. In Enhanced Oil Recovery (EOR) methods, pH modification of fluids is employed to alter the wettability of the reservoir rock. Alkaline-Surfactant-Polymer (ASP) and Alkaline-Surfactant (AS) are two common EOR methods that employ pH modification to achieve better oil recovery. pH can affect the wettability of a solid surface by altering the surface charge and the chemistry of the fluids that are in contact with the surface.

This thesis focuses on the influence of brine salinity and first contact fluid on wettability of glass, and Illite and Illite-Smectite coated microfluidic surfaces. Advancing and receding contact angle data for DI water-air, brine-air, n-decane-air, produced water-air, crude oil-air, brine-n-decane systems, and crude oil-produced water systems have been measured in the untreated, Illite, and Illite-Smectite coated microfluidic channels. In addition, produced water advancing and receding contact angles were measured for Caney shale reservoir and non-reservoir zone core sample. This

work can be helpful for petroleum industry as swelling potential, fines migration, and wettability alteration of clay minerals are critical aspects for drilling and production operations in shale formations. The applications of this work also include enhanced oil recovery in formations rich in clay and designing injection fluids to increase production from these formations while maintaining the permeability of the formation.

A brief outline of this study is as follows: literature review on clay chemistry, its effect on shale rocks' productivity, literature review on wettability and mechanisms that impact the wetting characteristics of surface, and microfluidics background is provided in chapter 2. Chapter 3 describes the materials and methods utilized to prepare the clay-coated surface and to investigate the effect of salinity and first contact fluid on wettability of untreated and clay-coated microfluidic channels. Chapter 4 discusses the results obtained from the study. Finally, chapter5 discusses the conclusion and recommendations for future work.

# CHAPTER II

# REVIEW OF LITERATURE

## 2.1 A brief introduction of clay minerals

Clay is a naturally occurring material composed of fine-grained minerals, mainly hydrous aluminum phyllosilicates. These minerals are formed from the weathering and alteration of other minerals, such as feldspar and mica, and are made up of aluminum silicate sheets and tetrahedral structures of silica and aluminum oxide. In addition to aluminum phyllosilicates, clay may also contain other minerals, such as quartz, iron oxides, and organic matter [27]. The exact composition of a clay sample depends on the geological conditions under which it was formed, such as the type of parent rock, the climate, and the presence of minerals in the soil.

Clays are classified based on their proportion of sheet structures, such as 1:1 (kaolinite, serpentine) and 2:1 (illite, smectite, vermiculite, smectite). Clay minerals are composed of layered silicate sheets that are held together by the arrangement of tetrahedron and octahedron structures of silica and aluminum oxide. Figure 1 shows the tetrahedron and octahedron structures of clay minerals.

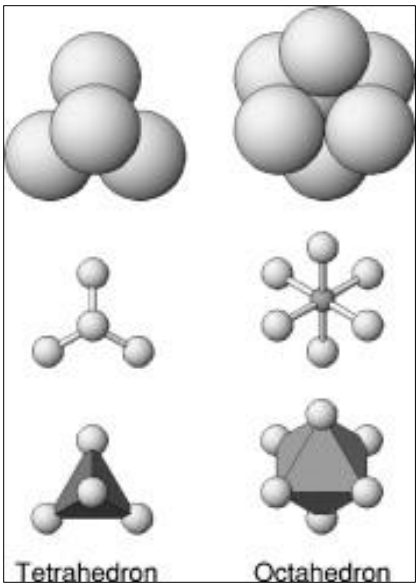


Figure 1: Tetrahedron and Octahedron structure of clay minerals [28].

Illite is a 2:1 clay mineral i.e., one octahedral layer is in between two tetrahedral layers (T-O-T). In the octahedral layer, the aluminum silicate layers contain interlayer cations such as potassium and magnesium. These cations restrict the encroachment of water between the layers. This reduces the swelling potential of the mineral. Whereas, in smectite, the silicate layers are held together by weak van der waals force, and when water is absorbed into the layers they expand and be pushed apart. This causes smectite to swell.

### 2.2 Impact of clay on producibility of shale

Clay minerals can impact the porosity and permeability of shale, which are the key factors that control the flow of the hydrocarbons. Clay minerals have a large surface area owing to their platy structure. Kozeny equation states that permeability is inversely proportional to surface area [29]. Therefore, presence of clay minerals may reduce the permeability of the formation. Variations in the chemical composition, morphology, and physical structure of clay minerals can result in differences in their wetting behavior [30].

Fines migration is another characteristic of clay particles that has a considerable impact on shale producibility. The net sum of attractive van der waals force and the repulsive electrostatic forces and drag forces acting on the particles controls the mobility of the fines. A repulsive electrostatic force acts on the particles because generally both the shale rock grain and the clay particle are negatively charged. At high salt concentration, the formation water ions could shield the negative charge on the clay particles generally resulting in relatively less fines migration than at lower salt concentrations. In addition, the van der waals forces could also be sufficiently high enough to hold the particles to the grain surface. With decrease in the salinity, the repulsive electrostatic and drag force exceeds the attractive van der waals force, hence, resulting in the release of fines in the pore space [31]. This phenomenon is known as fines migration, and it can have a significant impact on productivity of the formation by clogging the narrow pore throats and reducing the permeability of the formation. Figure 2 shows the release of fine particles, and permeability reduction by clogging pore space where $F_{EDL}$, $F_{VLA}$ represents electrostatic force and van der waals force, respectively.

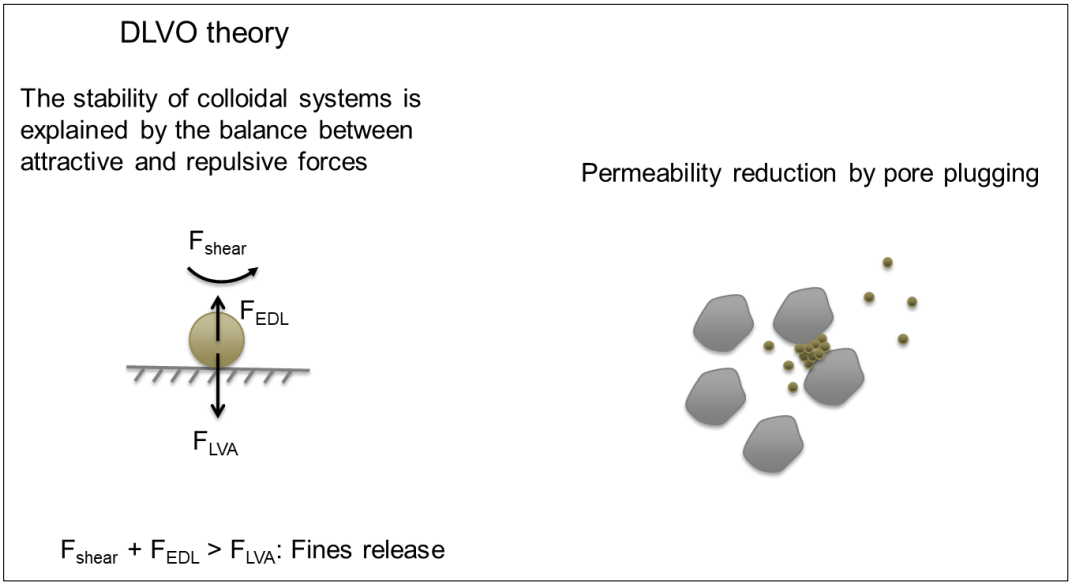


Figure 2: Forces acting on particle (left), Permeability reduction by clogging (right) [32].

### 2.3 Wettability: A brief introduction

Wettability is the preference of a fluid to maintain contact with the solid in the presence of another fluid. Contact angle is a measure of wettability. It is the angle formed by a droplet of liquid on a solid surface at the three-phase contact line as shown in Figure 3.

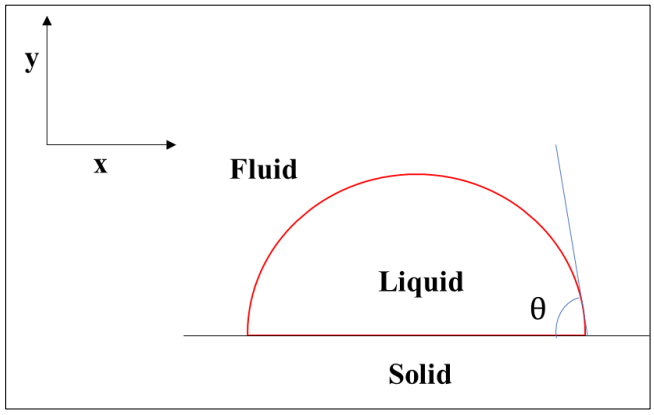


Figure 3: A typical three phase contact angle.

A static contact angle is not sufficient to determine the wettability of rock/brine/oil system. This is because the wettability is determined by multiple contact angles at different three-phase contact regions within the pore spaces of the rock. The contact angle described by Young's equation is a theoretical value that represents the lowest free energy state of a liquid drop on a surface, based on the assumption that the surface is smooth, rigid, chemically homogeneous, insoluble, and non-reactive. However, the real surfaces do not always meet these assumptions. Surface heterogeneities such as roughness or chemical variations can create multiple metastable states for liquid drops, leading to a range of contact angles. Therefore, the advancing and receding contact angles are measured to quantify this range. Consider a system consisting of a solid surface, a liquid droplet, and surrounding fluid, referred to as the solid, liquid, and fluid phase, respectively. The total energy of the interfaces in the system can be calculated using the interfacial tension between the solid-liquid ($\sigma_{sl}$), solid-fluid ($\sigma_{sf}$), and liquid-fluid ($\sigma_{lf}$), and the profiles of the solid wall and the liquid droplet, and is given by the expression:

$$\int_0^X [\sigma_{lf} \sqrt{(1+y')^2} + (\sigma_{sl} - \sigma_{sf}) r(x)] x^k dx \quad (1)$$

In this equation, the variables *x* and *y* represent the distance from the center of the droplet and the droplet profile, respectively. The parameter *x=X* refers to the position of the contact line where the liquid droplet meets the solid surface. The parameter *k* is a value of either 0 or 1, which indicates whether the droplet is two-dimensional or axisymmetric, *r(x)* represents the local ratio between the actual solid surface area and its projection onto a horizontal plane. The system is subjected to a constant liquid volume constraint,

$$V = 2\pi^k \int_0^X x^k (y - y_s) dx \quad (2)$$

In equation 2, V is the volume of the droplet, and $y_s$ is the profile of solid wall. For the system to be in a state of equilibrium, it is necessary to minimize the expression given in equation 1, while also satisfying the condition set by equation 2 [33]. The equation for the apparent contact angle by solving the above-mentioned constraints is given by:

$$cos\theta = \frac{r(X)(\sigma_{sf} - \sigma_{sl})}{\sigma_{lf}(1 - y_s' tan\theta)} \quad (3)$$

If the solid surface is smooth, uniform, rigid, and insoluble, and the interfacial tension between solid-liquid, solid-fluid, and liquid-fluid is constant, then the equation (3) becomes the well-known Young-Dupre equation.

$$cos\theta = \frac{(\sigma_{sf} - \sigma_{sl})}{\sigma_{lf}} \quad (4)$$

In oil-brine-rock (OBR) systems, a thin layer of water or oil (depending on the system is water-wet or oil-wet, respectively) can exist between the liquid droplet and the solid surface, which is due to the equilibrium of different forces i.e., van der waals, electrostatic, and structural forces. Therefore, the traditional Young-Dupre equation cannot be applied to these systems. To overcome this

limitation, Hirasaki (1991) proposed a modified equation for the contact angle of water in OBR systems by using thermodynamic analysis [34]. The equation is given by the expression:

$$cos\theta - 1 = \frac{1}{\sigma_{ob}}\left[\int_{D_o}^{\infty}\Pi(D)\,dD + D_o\Pi(D_o)\right] \quad (5)$$

The equation for the contact angle of water in OBR systems involves two components, namely Π(D), also referred to as the disjoining pressure denotes the overall pressure between the oil-brine interface and the brine-rock interface at a distance D, and $D_0$, which signifies the thickness of the equilibrium water film.

Equation (5) shows that the wetting behavior of a typical OBR system is influenced by three key factors: the interfacial tension between the oil and brine, the disjoining pressure across the water film, and equilibrium water/oil film thickness. These factors are determined by various interfacial interactions i.e., electrical double layer interaction, van der waals force, structural force, hydrogen bond, and chemical interaction [35].

### 2.4 Mechanisms that impact the wetting characteristics of surface

As described in previous section, the wettability of an oil-bearing rock system depends on the interactions between the oil, water, and rock interfaces, particularly the interaction across the thin films. Therefore, any process that affects these interfacial interactions also affects the wettability. This section reviews the currently proposed mechanisms that affect wettability.

#### 2.4.1 Alteration of interfacial tension between bulk oil and brine

When mechanisms affect the overlapping electrical double layers (EDLs) across the thin water film in an oil-brine system, it also impacts the EDL at the bulk oil-brine interface away from the thin water film. This change in the EDL alters the free energy, which in turn changes the interfacial tension. According to equation 5, a smaller oil-brine interfacial tension leads to a more water-wet condition. This is because a decrease in tension causes the bulk oil-brine interface to expand,

resulting in an increased oil contact angle. Although experiments confirm a decrease in bulk oil-brine interfacial tension, the resulting variation is often not significant enough to cause a notable wettability change [41-43]. As a result, the decrease in bulk oil-brine interfacial tension is usually considered a supplementary mechanism.

### 2.4.2 Multicomponent ion exchange

The multicomponent ion exchange (MIE) mechanism suggests that high valence ions act as bridges to form ion and ligand bindings between oil and rock. Lowering the concentration of these ions during low salinity water (LSW) flooding breaks the bindings, weakening the attraction between oil and rock and making the system more water-wet [38]. This mechanism also explains the significant impact of certain ions, such as sulfate in carbonate reservoirs, which are referred to as potential determining ions. Sulfate tends to precipitate with calcium in carbonates, suppressing the formation of calcium bonds and altering wettability.

The researchers performed LSW flooding on a core sample and observed improved oil recovery. Next, they washed the core with NaCl solution until there were no high valence ions present. After aging the core, they repeated LSW with NaCl solution but found no additional oil recovery [45,46]. This suggests that the expansion of the electrical double layer (EDL) without MIE does not contribute significantly to enhanced oil recovery. However, this conclusion contradicts some other studies that considered EDL expansion a more dominant mechanism than MIE [40].

### 2.4.3 pH change

The pH level has a significant impact on surface interactions, such as the adsorption of organic components to rock surfaces as shown in equation 6 and 7.

$$Clay - NHR_3^+ + OH^- \rightleftharpoons Clay + R_3N + H_20 \quad (6)$$

$$Clay - RCOOH + OH^- \rightleftharpoons Clay + RCOO^- + H_20 \quad (7)$$

During low salinity water (LSW) flooding, the increase in pH level is typically due to the replacement of hydrogen ions with adsorbed high valence ions on the rock surface as shown in equation 8 [41].

$$Clay - Ca_2^+ + H_2O \rightleftharpoons Clay - H^+ + Ca_2^+ + OH^- \quad (8)$$

This phenomenon is like multicomponent ion exchange (MIE), and some have suggested that this type of pH increase is only a phenomenon of MIE [42].

The equilibrium of these interactions can be altered by changing the pH level. For instance, increasing the pH level will desorb both acidic and basic components, which can break the bonds between oil and rock and modify the surface charging property, resulting in more water-wet conditions. The impact of pH change on surface charging properties can be calculated using the corresponding surface complexation model [41].

### 2.4.4 Mineral dissolution and salting in mechanism

The salting-in effect refers to the increased solubility of organic components on rock surfaces as ion concentrations decrease during LSW flooding, resulting in a more water-wet surface due to changes in surface charges and thus EDL interactions [43]. However, the validity of the salting-in mechanism is a subject of debate, as there is limited evidence supporting it [44]. Another related mechanism is mineral dissolution during LSW, which emphasizes the role of ions released by dissolution, but this mechanism is also widely challenged [45,46]. Additionally, neither of these two mechanisms is expected to have a significant impact at a field scale due to brine equilibration during the process [47-48, 50].

### 2.4.5 Expansion of electric double layer

Ligthelm et al. proposed that the EDL expansion mechanism is a key factor in wettability alteration [39]. The surfaces of rocks and oil are usually negatively charged in brine, creating a repulsive force across the thin water film due to overlapping EDLs. The length of the EDL is inversely

proportional to the Debye parameter, and during LSW flooding, the EDL thickness increases due to the lower ionic concentration. This leads to an enhanced repulsive force across the water film, making the system more water-wet as shown in equation 9:

$$\Pi_{EDL}(D) = nk_bT\left(\frac{2\phi_1\phi_2\cosh(\kappa D)-\phi_1^2-\phi_2^2}{(sinh(\kappa D))^2}\right) \quad (9)$$

where, $\Pi_{EDL}(D)$ is the pressure across water film owing to the EDL interaction, n is the bulk ion concentration, $k_b$ the Boltzmann constant, T the temperature, $\phi_1, \phi_2$ are the electric potential at the oil-brine and brine-rock interface, respectively, and κ is the Debye parameter given by equation 10:

$$\kappa = \sqrt{\frac{2e^2N_AI}{\varepsilon_0\varepsilon_r k_bT}} \quad (10)$$

where, $N_A$ is the Avogadro constant, I the ionic strength, $\epsilon_0$ the vacuum permittivity, and $\epsilon_r$ the relative permittivity of solution.

Several experiments have found a correlation between the change in zeta potential and contact angle when brines of different salinity are used, which confirms the contribution of EDL interaction to wettability alteration [35,48]. EDL expansion is just one mechanism that affects EDL interaction. The EDL interaction is determined by the Poisson-Boltzmann equation, the electrostatic equilibrium condition, and the surface complexation model. Therefore, any change related to the chemical equilibrium in the surface complexation model, such as changes in pH, will have an impact on EDL interaction. If oil and rock surfaces are oppositely charged, the interaction will be attractive. The mechanism of EDL expansion is just a special case of the change of EDL interaction energy resulting from the change of salt ion concentration.

### 2.5 Caney shale clay minerology

Caney shale is a newly discovered unconventional formation situated in the southern mid-continent Anadarko, Ardmore, Marietta, and Arkoma basins. The formation ranges from 60 to 300 meters

Table 1: Caney shale minerology on the basis of sidewall cores. A calcareous shale deposit known as ‘Mayes’ formation is found at the base of the Caney shale [52].

Caney Shale
"Mayes" Formation

**Richardson 2-33**

| Sample | CLAYS | | | | CARBONATES | | | OTHER MINERALS | | | | | SUM | | |
|---|---|---|---|---|---|---|---|---|---|---|---|---|---|---|---|
| Depth (ft) | Chlorite | Kaolinite | Illite | Mx I/S* | Calcite† | Dol/Ank** | Siderite | Quartz | K-spar | Plag. | Pyrite | Apatite | Clays | Carbonates | Other Minerals |
| 5908.0 | 4 | 3 | 13 | 1 | 1 | trc | 2 | 61 | 1 | 3 | 1 | 10 | 21 | 3 | 76 |
| 5927.0 | 2 | 7 | 29 | 2 | 1 | 1 | 3 | 33 | 2 | 5 | 2 | 13 | 40 | 5 | 55 |
| 5996.0 | 3 | 4 | 20 | 9 | 28 | 4 | 0 | 27 | 1 | 2 | 2 | 0 | 36 | 32 | 32 |
| 6142.0 | 1 | 0 | 3 | trc | 14 | 66 | Tr | 11 | 2 | 3 | trc | Tr | 4 | 80 | 16 |
| 6208.0 | 1 | 1 | 14 | 3 | 14 | 7 | Tr | 50 | 3 | 6 | trc | 1 | 19 | 21 | 60 |

**Rogers Trust 1-24**

| Sample | CLAYS | | | | CARBONATES | | | OTHER MINERALS | | | | | SUM | | |
|---|---|---|---|---|---|---|---|---|---|---|---|---|---|---|---|
| Depth (ft) | Chlorite | Kaolinite | Illite | Mx I/S* | Calcite† | Dol/Ank** | Siderite | Quartz | K-spar | Plag. | Pyrite | Apatite | Clays | Carbonates | Other Minerals |
| 6778.00 | trc | 10 | 16 | 18 | 4 | 5 | 0 | 31 | 1 | 4 | 2 | 9 | 44 | 9 | 47 |
| 6826.00 | trc | 6 | 19 | 16 | 10 | 2 | 0 | 36 | 0 | 5 | 4 | 2 | 41 | 12 | 47 |
| 6846.00 | 4 | trc | 22 | 25 | 13 | 3 | 0 | 25 | trc | 4 | 4 | trc | 51 | 16 | 33 |
| 7059.00 | 0 | 0 | 17 | 4 | 12 | 21 | 0 | 40 | trc | 3 | 3 | trc | 21 | 33 | 46 |

*Ordered interstratified mixed-layer illite/smectite, with 35% expandable interlayers for samples with abundant mixed-layers
**Includes dolomite and iron-bearing dolomites (i.e., Fe-dolomite and ankerite
***No mixed illite, all smectite
†Includes the Fe-rich varieties

thick and has a high total organic carbon content of 0.5 to 11%. It is part of the South Central Oklahoma Oil Province (SCOOP) and is of Mississippian age. Caney shale is located above the Woodford shale. Woodford shale is the primary oil-bearing formation in the area, and has significant oil and gas resources [51]. X-ray Diffraction (XRD) data on various Caney core samples from different depths show that Illite is the dominant clay mineralogy present in Caney [52–54]. Although there are some mixed Illite-Smectite clays, the contribution of Illite predominates over Smectite. Table 1 represents the Caney shale minerology on the basis of sidewall cores.

### 2.6 Microfluidics Background

Microfluidics is the study of fluid behavior in small channels with dimensions of tens to hundreds of micrometers, where surface forces rather than bulk forces control the flow [54]. Microfluidic chips, also known as micromodels, are typically made of transparent materials like glass, polydimethylsiloxane (PDMS), polystyrene, or polycarbonate, which allow direct visualization of the flow networks created by etching based on a predesigned geometric shape. Microfluidics first emerged in the early 1980s and has influenced various fields such as physics, chemistry, biochemistry, and biotechnology [55]. Recently, microfluidics has started to be used in petroleum industry to study multiphase flow through porous media. The customizable flow network in micromodels enables researchers to visually study the fluid flow and the impact of surface and interfacial forces, while also allowing for the representation of complex rock networks [56,57]. Detailed information on micromodel fabrication can be found in Amirian T.'s (2019) work [58].

#### 2.6.1 Geomaterial Micromodels

While traditional micromodels made of glass or PDMS can accurately depict the subsurface flow network through microfabrication, they are limited in their ability to account for the unique surface chemistry associated with different rock types. Although these micromodels can partially represent fluid flow in sandstone rocks due to the shared silica composition, they are inadequate for simulating the flow of fluids in other types of hydrocarbon-bearing rocks such as carbonates (e.g.

limestone and dolomite) and shales, which have completely different mineralogies. Carbonates are predominantly composed of two crystal forms of $CaCO_3$, Calcite and Aragonite, while shales are mainly comprised of clay-rich formations.

To overcome the limitation of traditional glass micromodels in representing the unique surface chemistry of different types of rocks, researchers have developed geomaterial micromodels. These micromodels can be created by laser-etching real-rock samples or functionalizing traditional micromodels with geomaterials such as coal, calcite, and clay. For instance, Gerami et al. (2017) developed a coal micromodel by etching fractures on an actual coal surface and observed fluid transport in the micromodel [59]. Shaik et al. (2020) created calcite-coated glass capillary tubes and micromodels for studying the effects of cleaning, silane agent, and supersaturation on $CaCO_3$ deposition on glass surfaces [60]. On the other hand, Song and Kovescek (2015) developed a method for preparing clay-coated micromodels by injecting a Kaolinite suspension into silicon micromodels [61]. They created a reversible coating by drying the micromodel with flowing air and an irreversible coating baked in an oven at 120 °C for 25 minutes. The reversible coating was utilized to study clay particle migration during low salinity water flooding, while the irreversible coating was used to examine wettability alteration in sandstone reservoirs resulting from clay presence. Rupom et al. (2022) coated the glass capillary tubes and straight channel borosilicate glass micromodels with Illite clay to represent the pore-scale clay chemistry of Caney shale, a Mississippian unconventional play in Southern Oklahoma, USA. The coated microfluidic surfaces are heat-treated at low (25 °C) and high temperature (125 °C), and the heat treatment results are compared. Also, they aimed to investigate the effect of salinity on clay adsorption on the glass surface and overall coating quality [62]. Amirian et al. (2017) developed Illite and Kaolinite coated geomaterial surfaces, which were used to investigate low salinity water flooding in sandstone reservoirs. The coated micromodel was air-dried at 80 °C for 2 hours to produce a reversible layer of clay particles on the glass surface [58]. In contrast to this method, Zhang et al. (2018) developed

a layer-by-layer coating technique to functionalize glass and PDMS micromodels with Kaolinite and Montmorillonite clay minerals. The process involved injecting Poly(diallyldimethylammonium chloride) solution to adhere clay minerals on the substrate surface. Static and dynamic flooding of brines were used to evaluate the stability of the coated surface, and the coating was found to be more stable than the one achieved by simply injecting clay solution through the micromodels [63]. Despite this, the physical adsorption method was used in this study for coating to achieve the following: to restrict the use of synthetic materials except clay; to mimic the subsurface conditions as much as possible.

The next chapter will discuss the materials and methods used in this study.

# CHAPTER III

# MATERIALS AND METHODS

## 3.1 Clay Minerals

The study utilized Illite (IMt-1) and Illite-Smectite mixed layer (70/30 wt.%) clay minerals sourced from the Cambrian shales of Silver Hill in Jefferson Canyon, Montana, USA. The clays were obtained from the Clay Minerals Society's repository of source clays and were used to coat thin bottom flow cells. Since this study is continuation of work by Rupom et al. (2022) [62], therefore, Illite-Smectite mixed layer (70/30) was used to coat the capillary tubes for coating characterization. Before coating, the clay chips were ground into powder using a ball mill for a period of less than five minutes. To prevent any contamination of iron (Fe) or aluminum (Al), tungsten canister and balls were used during the grinding process. The chemical composition (mass norm. %) of Illite (IMt-1) and Illite-Smectite mixed layer (70/30 wt.%) are as shown in table 2.

Table 2: Chemical composition (mass norm. %) of Illite and Illite-Smectite (70/30 wt.%).

| Compound | Illite (IMt-1) | Illite-Semctite (70/30) |
|---|---|---|
| $SiO_2$ | 49.3 | 51.6 |
| $Al_2O_3$ | 24.25 | 25.6 |
| $TiO_2$ | 0.55 | 0.039 |
| $Fe_2O_3$ | 7.32 | 1.11 |
| FeO | 0.55 | <0.01 |
| MnO | 0.03 | 0.04 |
| MgO | 2.56 | 2.46 |
| CaO | 0.43 | 0.67 |
| $Na_2O$ | 0 | 0.32 |
| $K_2O$ | 7.83 | 5.36 |
| $P_2O_5$ | 0.03 | 0.04 |

### 3.2 Fluids

The NaCl (99%) and n-decane (99%) were purchased from Sigma Aldrich. For this study we have used NaCl brine solutions of four different salinities i.e., DI water (0 ppm), 5k ppm brine, 10k ppm brine, 30k ppm brine, and a produced water, and a crude oil obtained from Continental Resources. The viscosity measurements were conducted by using RheoSense microVISC. It calculates the viscosity based on the pressure drop when fluid passes through the rectangular channel. Interfacial tension was measured by using the pendant drop method and the image analysis was carried out using drop analysis plugin of ImageJ software. This method requires the density contrast between the two fluids i.e., oil and water. Therefore, the densities of fluids were measured by using Mettler Toledo DA-100M density meter. It measures the density of fluids by oscillating body method. The pH and TDS of produced water were measured using Oakton PC multimeter.

Table 3: Density of fluids at 20 °C, 1 atm, and viscosity, pH, and TDS of fluids at 18 °C, 1 atm.

| Fluid | Viscosity (cP) | Density ($g/cm^3$) | pH | TDS (ppt) |
|---|---|---|---|---|
| DI water | 1.04 | 0.994 | | |
| 5,000 ppm brine | 1.12 | 1.001 | | |
| 10,000 ppm brine | 1.23 | 1.004 | - | - |
| 30,000 ppm brine | 1.26 | 1.018 | | |
| n-decane | 0.92 | 0.732 | | |
| Crude oil | 2.25 | 0.790 | | |
| Produced water | 1.15 | 1.020 | 7.25 | 36.7 |

Table 4: Interfacial tensions of brine-n-decane systems, and produced water-crude oil system obtained from Continental Resources at 1 atm and 20°C.

| Non-Aqueous Phase | Aqueous Phase | IFT (mN/m) |
|---|---|---|
| n-decane | DI water | 51.18 |
| | 5,000 ppm brine | 47.51 |
| | 10,000 ppm brine | 46.27 |
| | 30,000 ppm brine | 43.81 |
| Crude oil | Produced water | 4.9 |

Table 3 represents the fluids properties. Table 4 represents the interfacial tension between model/crude oil(s) and model/produced brine(s).

### 3.3 Solid Substrates

#### 3.3.1 Capillary tubes

To investigate the impact of the salinity of the base fluid on the adsorption of clay particles onto a glass surface, borosilicate glass capillary tubes (90 mm in length, outer diameter ranging from 1.2 to 1.5 mm, and wall thickness of 0.2 mm) purchased from DWK Life Sciences Kimble (catalog no. 34505-99) were utilized to develop the coating technique.

3.3.2 Thin Bottom flow cells

Thin bottom flow cells purchased from Micronit Microtechnologies (Enschede, Netherlands), were used to conduct the wettability experiments (Figure 4). The flow cells are made up of borosilicate glass. The flow cells have three different channels. The length of top and bottom channels is 42 mm, and the middle channel is 40 mm. The width of top, middle and bottom channel is 0.5 mm, 1.5, and 1 mm, respectively. The thickness of the flow cell is 1.8 mm. The depth of each channel is 50 µm. The distance of channels from the top and bottom surfaces are 1050 µm and 145 µm, respectively.

Figure 4: Thin bottom flow cells.

### 3.4 Syringe Pumps

A single Standard Infuse/Withdraw PHD ULTRA™ Programmable Syringe Pump (Figure 5), procured from Harvard Apparatus, was utilized for the transportation of fluids to and from the glass micromodels and capillary tubes. The pump can deliver fluids continuously at a nanoscale flow rate (45 nl/min) by using the glass syringes obtained from Harvard Apparatus, and its programmable feature facilitates the automation of the process steps.


Figure 5: Harvard PHD ULTRA™ Programmable Syringe Pump (Courtesy Harvard Apparatus).

### 3.5 Tubing and Valve

FEP (Fluorinated ethylene propylene) tubing, having an inner diameter of 0.25 mm and an outer diameter of 1.6 mm (1/16"), was used to connect the capillary tube and the pump. PEEK tubing, with an outer diameter of 3.175 mm and an inner diameter of 1.6 mm, was employed to connect the syringe pump with the microfluidic chip. These components are chemically compatible with both aqueous and organic phase liquids used in the study. Swagelok three-way valves were also used in this study. Table 5 represents the specifications of tubing.

Table 5: Specifications of tubing.

| | |
|---|---|
| FEP Transparent Tubing | • Dimension: 1.16" OD x 0.25 mm ID<br>• Max. operating pressure: 200 bar<br>• Operating temperature range: -51 °C to 50 °C |
| PEEK Tubing | • 1/8" OD x 1.6 mm ID<br>• Max. operating pressure: 276 bar |

### 3.6 Microscope, Camera and Light Source

In the microfluidic setup, a 50MP 1080P 60FPS 4K camera, fitted with a 0.7X-4.5X magnification C-mount lens, was employed to capture high-quality images and videos of the glass surfaces during wettability experiments. To provide illumination, an LED-ring light source, coupled with an adjustable 1.5-36 mm optical iris diaphragm, was used. The camera and lens were procured from Eakins Repair Tools, the light source from Insein Li Fung Store, and the iris from Walley Optics Store of AliExpress.

Table 6: Microscopy components specifications.

| | |
|---|---|
| Camera | Type: Digital HDMI/USB powered<br>Picture pixel: 50MP<br>Video frame rate: 4K@30FPS; 1920x1080@60FPS<br>CMOS censer:1/2.33 inch<br>CMOS pixel:1.55 μm x 1.55 μm |
| Lens | Type: C-mount lens<br>Working distance: 95 mm<br>Adapter: 0.5X Barlow Lens (Increase working distance)<br>Zoom ratio: 6.5:1<br>Objective magnification power: 0.7 - 4.5X<br>Size: 168 mm (L) * 50 mm (D) |
| Light source | Type: Adjustable brightness LED bottom light source<br>Outside Diameter: 90 mm<br>Inside Diameter: 63 mm |
| Iris | Outside diameter: 56 mm<br>Minimum aperture diameter: 1.5 mm<br>Maximum aperture diameter: 36 mm<br>Thickness: 6 mm<br>Material: Metal<br>Blades: 14 pieces |

Figure 6 illustrates the components of the microscopic system utilized in the microfluidic setup, and Figure 7 depicts the system. The specifications of the components can be found in Table 6.


Figure 6: Components of microscopic system.

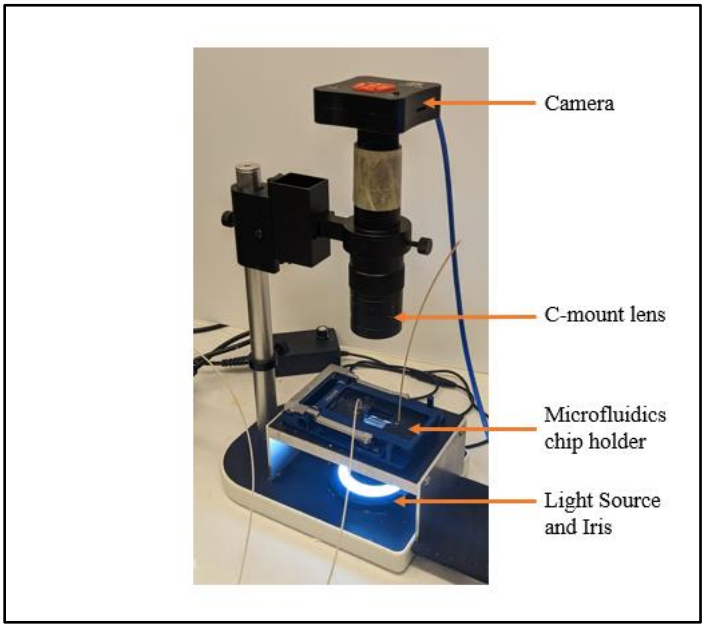


Figure 7: Microfluidic system.

Coating characterization and stability evaluations were conducted using FEI Quanta 600 field-emission gun Environmental Scanning Electron Microscope (SEM), Bruker Energy-Dispersive X-ray Spectroscope (SEM-EDS) in the Microscopic Laboratory of Oklahoma State University, USA. SEM and SEM-EDS were used for coating characterization as described in section 3.7.3. The technical specifications of the microscope can be found in Table 7. The data sources used for this study include the vendor's website [64] and the microscopy lab of Oklahoma State University [65].

Table 7: Specifications of microscope used for SEM and SEM-EDS analysis.

| Microscope | Specifications |
|---|---|
| FEI Quanta 600 Field-Emission Gun Environmental SEM with Bruker Energy-Dispersive X-Ray Spectroscope | • Resolution of 1.2 nm at 30 kV, 1.5 nm at low vacuum mode, and 1.5 nm at ESEM mode<br>• Accelerating voltages up to 30 kV<br>• Digital camera system<br>• XFlash®6 detector series with active areas from 10 to 100 $mm^2$ |

## 3.7 Experimental Procedure

### 3.7.1 Clay solution preparation

To coat glass capillary tubes a slurry of Illite-Smectite (70:30 wt.%) clay with a concentration of 10 wt.% was prepared in NaCl brine. Also, a slurry of Illite clay or Illite-Smectite clay with a concentration of 2 wt.% was prepared to coat the thin bottom flow cells for wettability experiments. The concentration of clay was determined through several trial experiments, considering the requirement for an adequate amount of clay particles to be adsorbed on the surface, and to avoid clogging the microchannels. NaCl brine was chosen as the base fluid to replicate subsurface reservoir conditions and minimize in situ migration of fines and swelling of clay induced by freshwater interaction with clay.

The impact of salinity on clay adsorption to the glass surface was assessed by utilizing slurries prepared with brines of four distinct salinities. The properties of these brines are presented in Table

2. As the salinity of the solvent was increased, the clay particles tended to aggregate and settle due to a reduction in double layer repulsive forces. Therefore, to keep the clay particles dispersed in the solution, the slurries were subjected to ultrasonication using a Branson 2800 Ultrasonic Cleaner for 30 minutes before being injected into the capillary tubes and the thin bottom flow cells.

### 3.7.2 Clay coating procedure

The objective of coating glass capillary tubes with Illite-Smectite clay was to establish the coating procedure and investigate the impact of salinity on clay adsorption to the glass surface. In this study, the approach of physical adsorption was utilized to develop the coated surface to achieve several objectives, such as avoiding the use of any artificial compounds, replicating the subsurface porous environment as closely as possible, and investigating the effect of salinity on physical adsorption to the glass surface. The method was adapted from the work of Rupom et al. (2022) [62].

As physical adsorption between the glass surface and clay particles is influenced by Van der waals attractive forces, a series of 100 clay solution infusion and withdrawal cycles were executed to enhance the interaction of clay particles with the glass surface. Each cycle comprised three steps: infusion, delay, and withdrawal. Prior to injection, the solid substrates undergo cleaning with Nitrogen Plasma utilizing the PE-50 Plasma Cleaner, acquired from Plasma Etch, USA, to remove organic contaminants.

To maintain the dispersion of clay particles in the solution, the clay solutions were ultrasonicated every ten cycles. The syringe pump was utilized to infuse fluids into the capillary tubes at a velocity of 26.5 meters/hour, and the fluids were withdrawn at 2.65 meters/hour once the channel was fully saturated with clay slurry. A delay of 2 minutes between infusion and withdrawal was maintained to allow for adequate time for the clay particles to be adsorbed. The flow rates were determined via numerous trial tests to ensure that the clay slurry was evenly delivered into the flow volume and

that the fluid carrying unadsorbed and loosely attached particles was displaced without affecting the coating. Figure 8 presents a simplified schematic of the clay coating process for glass capillary

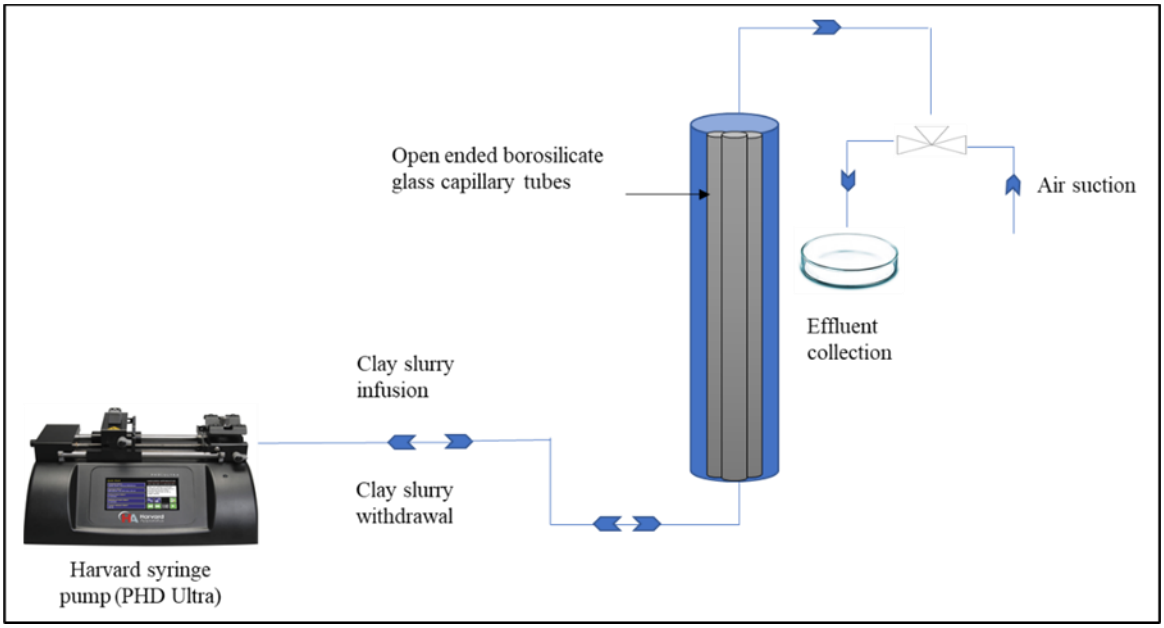


Figure 8: Schematic of Illite-Smectite clay coating setup for capillary tubes.

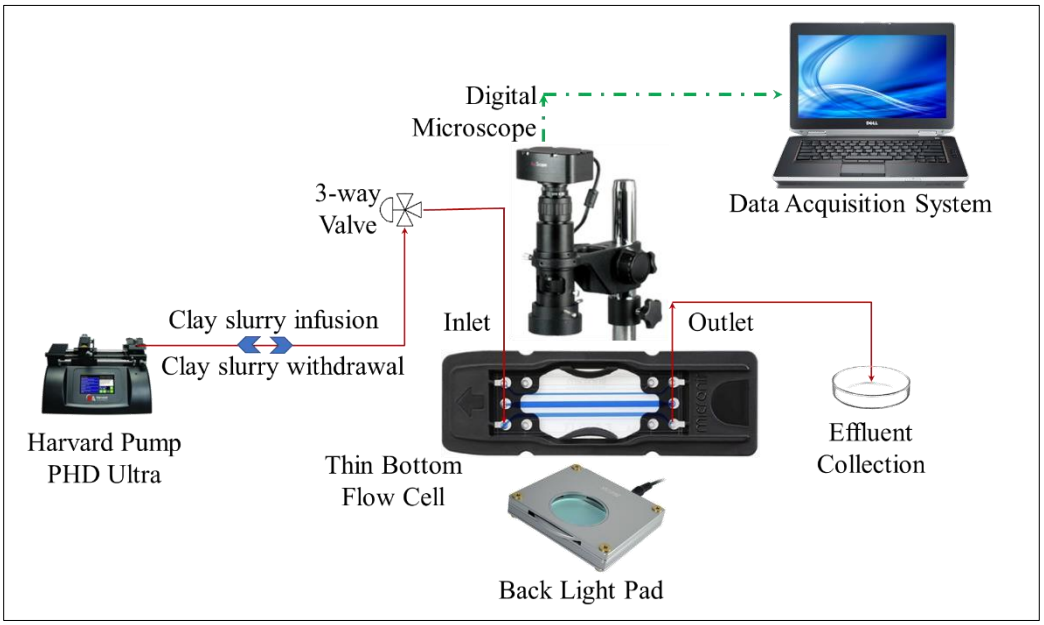


Figure 9: Schematic of Illite or Illite-Smectite clay coating setup for thin bottom flow cell.

tubes. Following the coating, the capillary tubes were air-dried at 125 °C for 1 hour. The procedure for coating thin bottom flow cells (Figure 9) was quite similar. However, unlike the capillary tubes, the thin bottom flow cells allowed for visualization of the surface after each coating cycle, and only three cycles were observed to be sufficient to uniformly coat the glass surface.

### 3.7.3 Coating Characterization

The coated capillary tubes were fragmented into small pieces using tweezers to expose the coated surfaces for microscopic characterization. Coating morphology and elemental atomic percentages were evaluated using a FEI Quanta 600 Field-Emission Gun Environmental Scanning Electron Microscope (SEM) and a Bruker Energy-Dispersive X-ray Spectroscope (SEM-EDS), respectively.

### 3.7.4 Experimental procedure for wettability experiments

The flow rate used to perform the experiment was 50 nl/min to maintain the capillary numbers in the range of $10^{-7}$ to $10^{-5}$. Each experiment consists of two different cases i.e., the microfluidic chip was contacted by water at first, and oil at first. In both cases, fluids were injected and withdrawn at 50 nl/min for obtaining the advancing and receding contact angle data. In the case of a microfluidic chip contacted by water first, the water advancing and receding contact angles were measured in water-air system, by infusing and withdrawing water at 50 nl/min, respectively. The water injection is followed by the oil injection at 50 nl/min to obtain the oil advancing contact angle data for the water-oil system. Similarly, oil receding contact angles were measured by withdrawing the oil at 50 nl/min.

In the case of a microfluidic chip contacted by oil first, the oil advancing and receding contact angles were measured in oil-air system, by infusing and withdrawing oil at 50 nl/min, respectively. The oil injection is followed by the water injection at 50 nl/min to obtain the water advancing contact angle data for the water-oil system. Similarly, water receding contact angles were measured

by withdrawing the water at 50 nl/min. The aging effect was studied by retaining the oil and water in the corresponding microfluidic channels for approximately 24 h in the case of channels first contacted by water and oil, respectively. Figure 10 shows the schematic of the experimental setup.

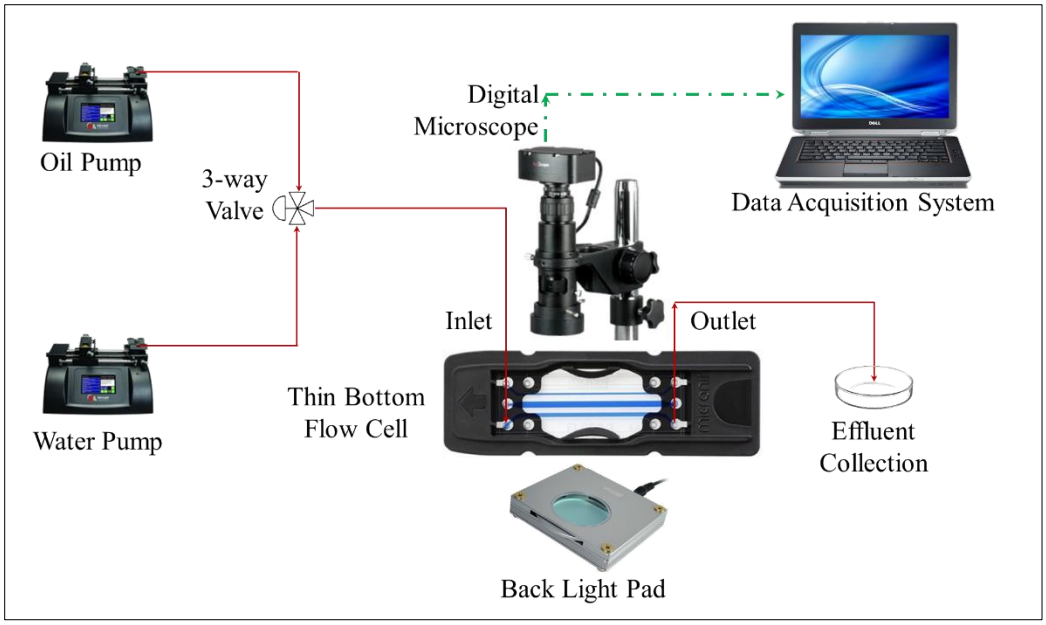


Figure 10: Schematic of the experimental setup for microfluidics-based wettability experiments.

The next chapter will discuss the results obtained from clay coating, swelling potential, fines migration and wettability experiments.

# CHAPTER IV

# RESULTS AND DISCUSSION

## 4.1 Measurements of Swelling Potentials of Illite and Illite-Smectite Clays

### 4.1.1 Swelling potentials of Illite and Illite-Smectite clays to model fluids

Swelling potentials of Illite and Illite-Smectite (70:30 by wt.%) clays upon exposure to DI water, 5k ppm brine, 10k ppm brine, and 30k ppm brines, and n-decane are evaluated. The aqueous brine solutions were prepared by using NaCl and DI water. For this experiment, we used borosilicate glass vials of 15 mm diameter and 45 mm height. The Illite swelling potential experiment was conducted for about a day as it was showing a minor increase in height. In contrast, the Illite-Smectite clay swelled immediately after it encountered DI water and the brine solutions. However, there was minor swelling in case of exposure to n-decane. The experiment for swelling potential of Illite-Smectite clay was run for 44 h i.e., approximately two days for brine solutions while for n-decane the experiment was conducted for 27 h. Figures 11 and 12 represents the Clay height (in mm) vs time plot(s) for Illite and Illite-Smectite clay, respectively. Figures 13 and 14 represent the visual appearance of Illite-Smectite clay in model oil and brines, and visual appearance of Illite and Illite-Smectite in model oil and Illite clay in model brines, respectively.

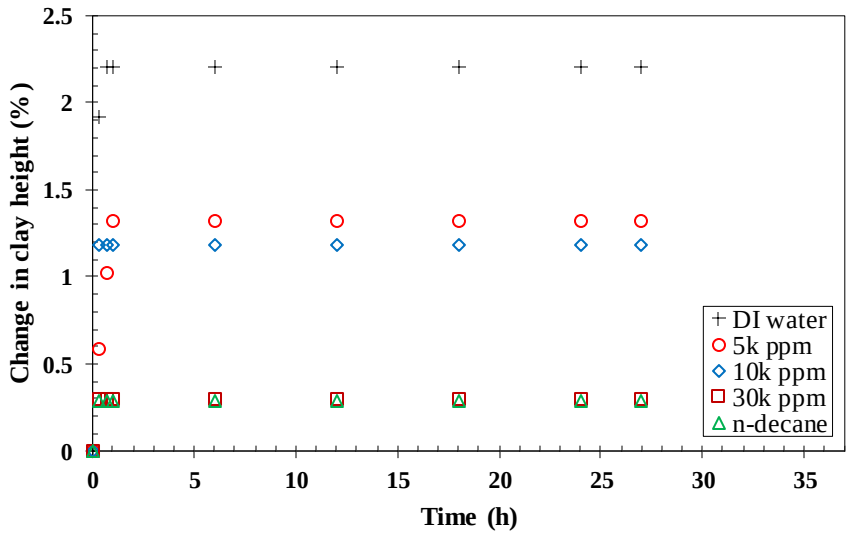


Figure 11: Swelling Potential of Illite Clay upon exposure to DI water, 5k ppm, 10k ppm, 30k ppm brines, and n-decane.

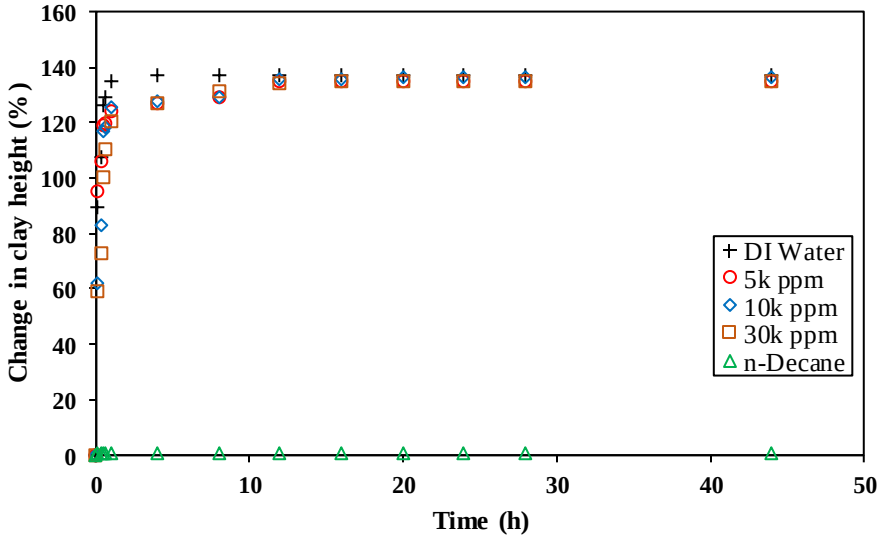


Figure 12: Swelling Potential of Illite-Smectite clay upon exposure to DI water, 5k ppm, 10k ppm, 30k ppm brines, and n-decane.

.

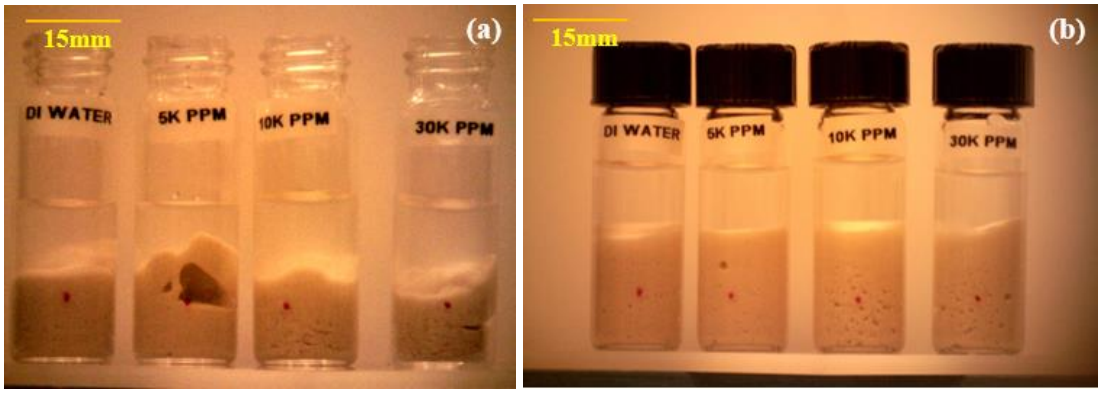


Figure 13: (a) Visual appearance of Illite-Smectite clay in DI water, 5k ppm, 10k ppm, and 30k ppm brine solutions just after adding the fluids, (b) after 44 h.

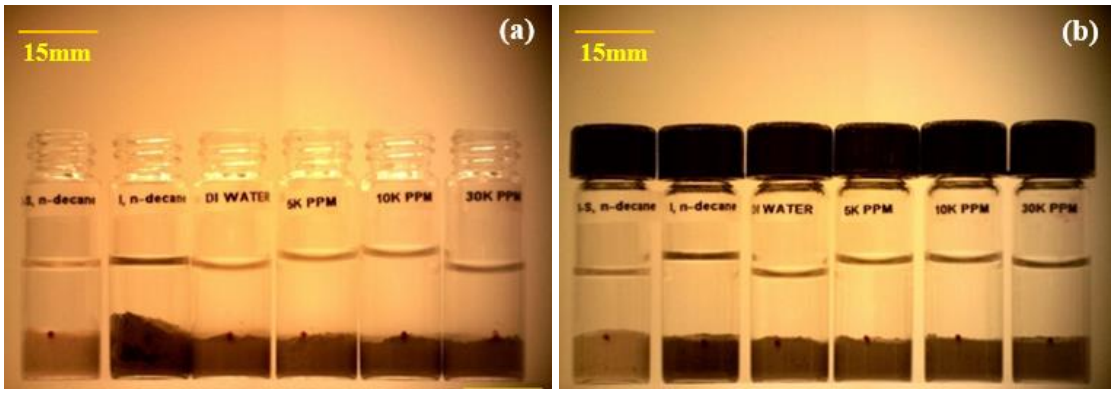


Figure 14: (a) Visual Appearance of Illite and Illite-Smectite in n-decane, and Illite clay in DI water, 5k ppm, 10k ppm, and 30k ppm brine solutions just after adding the fluids, (b) after 27 h.

### 4.1.2 Swelling potential of Illite and Illite-Smectite to continental fluids

A similar procedure as described in section 4.1.1 was used to conduct the swelling potential of Illite and Illite Smectite clay with the crude oil and produced water obtained from Continental Resources. The experiment was conducted for a day. Figures 15 and 16 represent the clay height (in mm) vs time plots for initial swelling, and after 24 h, respectively. Figure 17 represents the visual appearance of Illite and Illite-Smectite clay in crude oil and produced water.

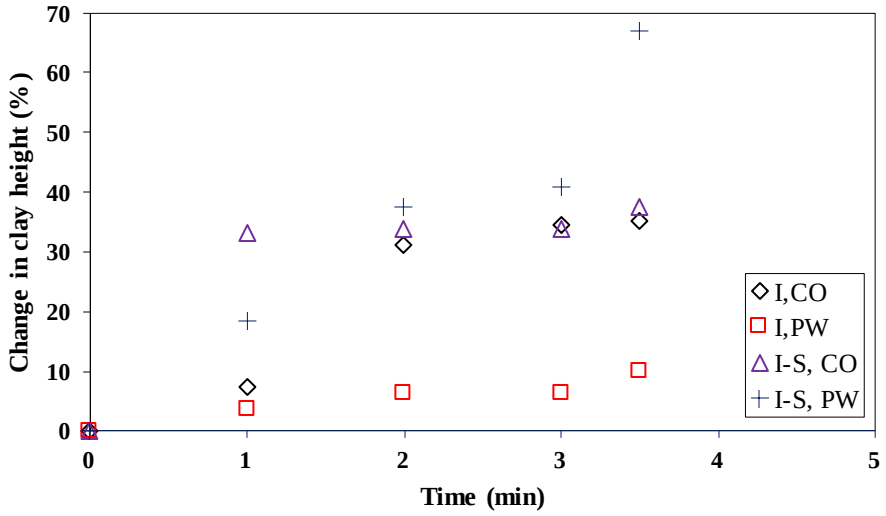


Figure 15: Initial swelling upon exposure to crude oil and produced water.

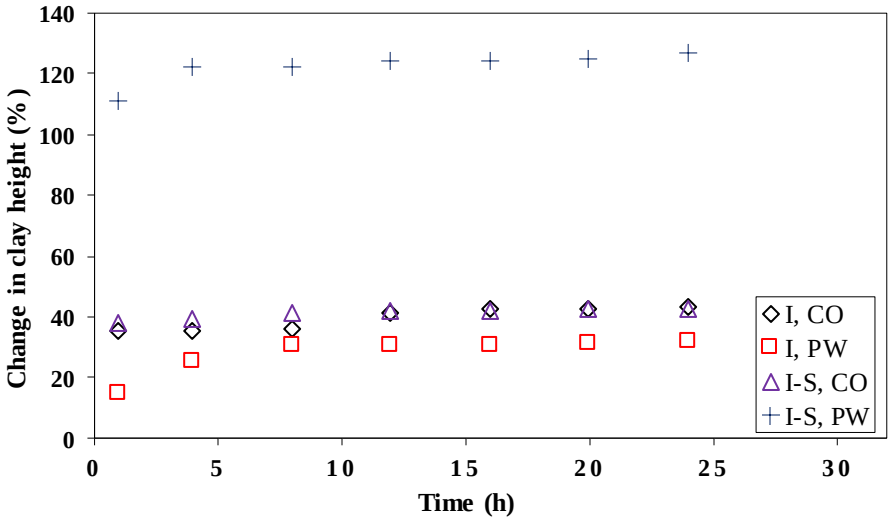


Figure 16: Swelling after 24 h upon exposure to crude oil and produced water.

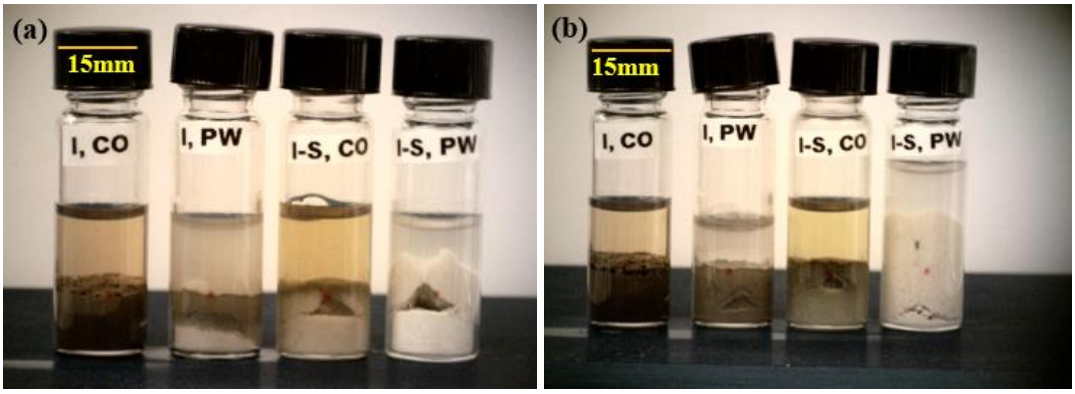


Figure 17: (a) Visual appearance of Illite and Illite-Smectite clay in Continental resources crude oil and produced water just after adding the fluids, (b) after 24 h.

### 4.2 Microscopic characterization of Illite-Smectite coating

The coating procedure was adapted from the work of Rupom et al. (2022) [62] as described in section 3.7.2.

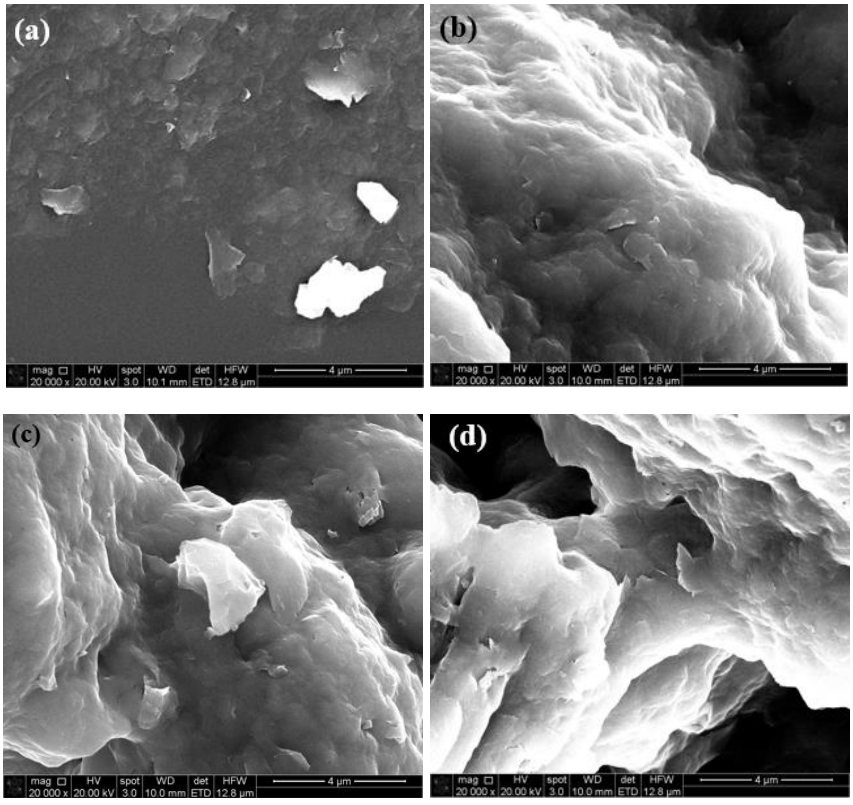


Figure 18: SEM images of Illite-Smectite coated glass capillary tubes at 20,000x magnification prepared in (a) 0 ppm (DI water), (b) 5000 ppm, (c) 10,000 ppm, (d) 30,000 ppm NaCl brine solutions.

Figure 18 shows the 20,000x Scanning Electron Microscopic (SEM) images of the Illite-Smectite clay-coated surface with clay solutions prepared in 0 ppm (DI water), 5000 ppm, 10,000 ppm, and 30,000 ppm.

### 4.3 Effect of salinity on Illite-Smectite clay coating

Glass capillary tubes were coated with 10 wt.% Illite-Smectite clay in NaCl solutions of 4 different concentrations (0 ppm, 5000 ppm, 10000 ppm, and 30000 ppm). The surfaces of the coated tubes were examined using SEM-EDS, and the results showed that increasing the concentration of the NaCl solution led to an improvement in the coverage of the coating. In contrast, when the clay slurry was prepared using deionized (DI) water, no adsorption of clay particles onto the glass surface was observed. The number of adsorbed particles increased with higher concentrations of brine, and with 30000 ppm brine, a quasi-homogeneous coating was achieved. An EDS elemental maps of the coated surfaces revealed a higher degree of clay particle adsorption on the glass surface when the slurry was prepared using higher salinity brine. These maps show the presence of different chemical elements on the coated surface with different color indexes. Figure 19 depicts the results of this analysis, with Figure 19(a) showing that the surface coated with clay slurry prepared in 5000 ppm of brine had an elemental map dominated by the presence of silicon (Si). While Si is a primary constituent of both the solid substrate and the clay minerals, the significant dominance of silica indicates that the uncoated borosilicate glass surface was the primary source of it otherwise, there would have been a significant contribution of other clay components (e.g., Mg, Al, K, Ca, Fe, etc.) on the elemental map, as observed in Figures 19(b) and 19(c). An increased concentration of brine (10,000 ppm and 30,000 ppm) resulted in an increased adsorption of clay particles, leading to the coated surfaces displaying a more even distribution of other clay constituents besides Si on the EDS elemental map as shown in Figures 19(c) and 19(d).

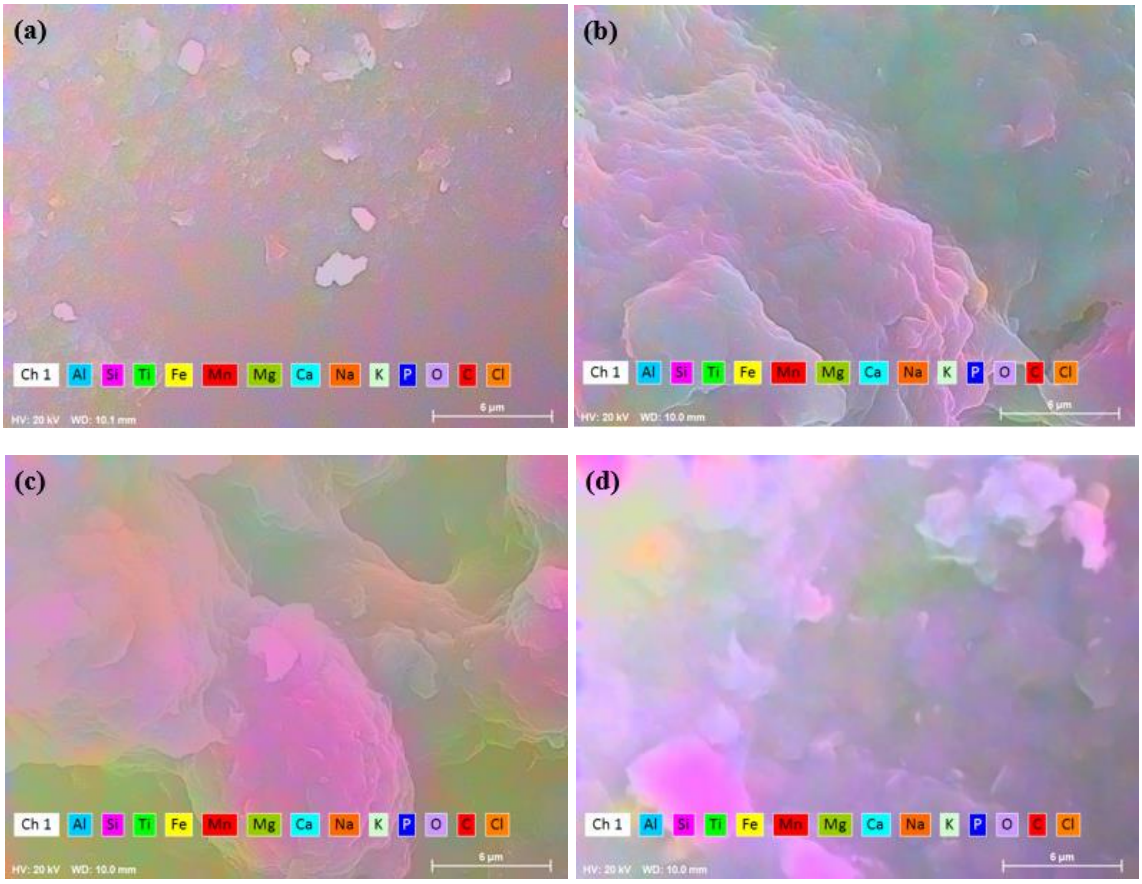


Figure 19: SEM-EDS images of Illite-Smectite coated glass capillary tube surfaces coated with 10 wt.% clay prepared in (a) 0 ppm (DI water) NaCl, (b) 5000 ppm NaCl, (c) 10,000 ppm NaCl, and (d) 30,000 ppm NaCl solutions.

Table 8 represents the contribution of different components of Illite-Smectite clay slurry prepared in 0 ppm, 5000 ppm, 10,000 ppm, and 30,000 ppm NaCl solution. The increase in atom % of Mg, Al, and Fe along with the corresponding decrease in Si is the indication of efficient coating.

Table 8: Contribution of different component of Illite-Smectite clay solution prepared in 0 ppm, 5000 ppm, 10,000 ppm, and 30,000 ppm NaCl solution.

| | Average Atom [%] | | | |
|---|---|---|---|---|
| **Element** | **0 ppm** | **5000 ppm** | **10,000 ppm** | **30,000 ppm** |
| Carbon | 12.19±1.32 | 11.62±1.16 | 11.37±0.19 | 11.55±0.54 |
| Oxygen | 53.41±2.01 | 60.03±2.59 | 58.92±2.20 | 57.14±2.32 |
| Sodium | 3.96±0.41 | 0.00 | 0.19±0.10 | 1.15±0.52 |
| Magnesium | 0.1±0.06 | 0.22±0.04 | 0.21±0.08 | 0.26±0.01 |
| Aluminum | 3.36±0.23 | 7.37±1.53 | 7.49±2.32 | 9.05±0.74 |
| Silicon | 25.32±0.76 | 18.14±2.14 | 18.24±1.76 | 16.21±0.84 |
| Phosphorus | 0.00 | 0.00 | 0.00 | 0.00 |
| Chlorine | 0.00 | 0.00 | 0.33±0.16 | 1.28±0.55 |
| Potassium | 1.4±0.12 | 2.04±0.58 | 2.68±0.66 | 2.65±0.39 |
| Calcium | 0.23±0.03 | 0.00 | 0.00 | 0.00 |
| Titanium | 0.00 | 0.00 | 0.02±0.02 | 0.00 |
| Manganese | 0.00 | 0.01±0.01 | 0.00 | 0.00 |
| Iron | 0.04±0.02 | 0.59±0.18 | 0.54±0.30 | 0.71±0.09 |
| Total | 100 | 100.00 | 100.00 | 100.00 |

### 4.4 Wettability analysis of untreated and clay-coated microfluidic channels

Advancing and receding contact angle data for DI water-air, brine-air, n-decane-air, produced water-air, crude oil-air, brine-n-decane systems, and crude oil-produced water systems have been measured in the untreated, Illite clay-coated, and Illite-Smectite clay-coated microfluidic channels of 1000 µm width and 50 µm depth. Contact angles were measured using an online protractor as shown in Figure 20. The contact angle between n-decane and DI water system as shown in Figure 20 is 57° (=180°-123°) as we always measure the contact angle in the denser phase. The advantage of using microfluidic channel is that we can measure multiple contact angles along the channel. Figure 21 represents the DI water advancing contact angle in DI water-air system by using overlay feature in ImageJ software. The darkest (rightmost) interface in the image indicates its current position.

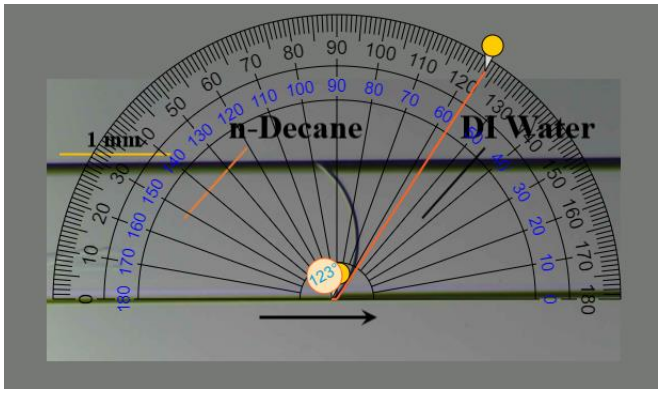


Figure 20: Representative image of contact angle measurement.

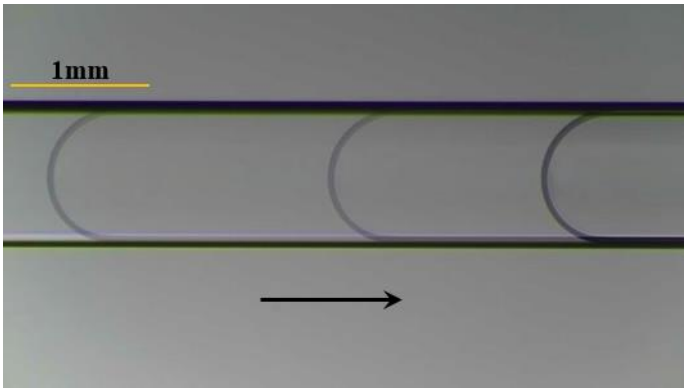


Figure 21: The temporal progress of interface shown using image overlay in ImageJ. Arrow indicates the direction of interface movement.

### 4.4.1 DI-Water and n-decane system

#### 4.4.1.1 Untreated microfluidic channel

Figure 22 represents the advancing and receding contact angles of DI water-air and n-decane-air systems. Figure 23 represents the advancing and receding contact angles of DI water-n-decane before and after aging (DI water contacted the channel surface first), n-decane-DI water before and after aging (n-decane contacted the channel surface first) systems. The before aging base case advancing and receding contact angles of DI water-air, n-decane-air, and the DI water-n-decane systems in the untreated microfluidic channel contacted by DI water first were ~0°. DI water advancing and receding contact angles in the case of surface contacted by n-decane first were ~180° indicating that the surface is behaving as strongly oil-wet before aging. The aging effect was studied

by retaining the n-decane and DI water in the corresponding microfluidic channels for approximately 24 h in the case of channels first contacted by DI water and n-decane, respectively.

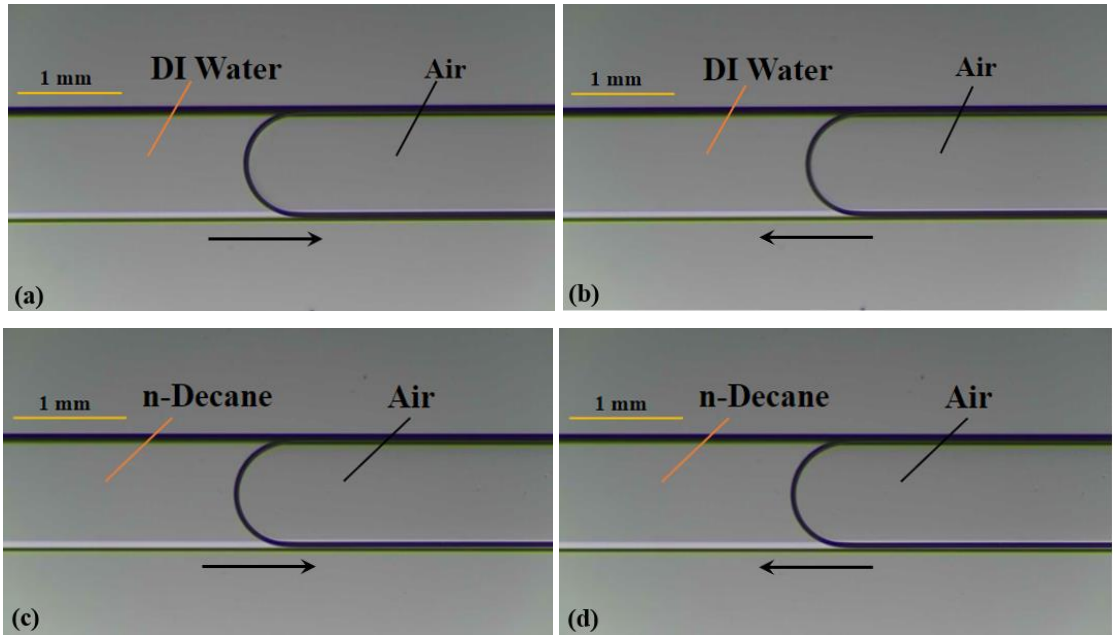


Figure 22: Untreated microfluidic channel contacted by DI water first: (a) DI water advancing contact angle and (b) DI water receding contact angle in DI water-air system before aging; Untreated microfluidic channel contacted by n-decane first: (c) n-decane advancing contact angle and (d) n-decane receding contact angle in n-decane-air system before aging. Arrow indicates the direction of interface movement.

In the case of DI water first contacted the channel, the DI water receding and advancing contact angles in DI water-n-decane system were ~60°–70° and ~80°–90°, respectively. This indicates that during DI water receding the surface is behaving as water-wet while when the DI water advances the surface behaves as intermediate wet after aging. In the case of n-decane first contacted the channel, the DI water advancing and receding contact angles were ~85°–95° and ~50°–65°, respectively. This indicates that during DI water advancing the surface is behaving as intermediate wet while when the DI water recedes the surface behaves as water-wet after aging.

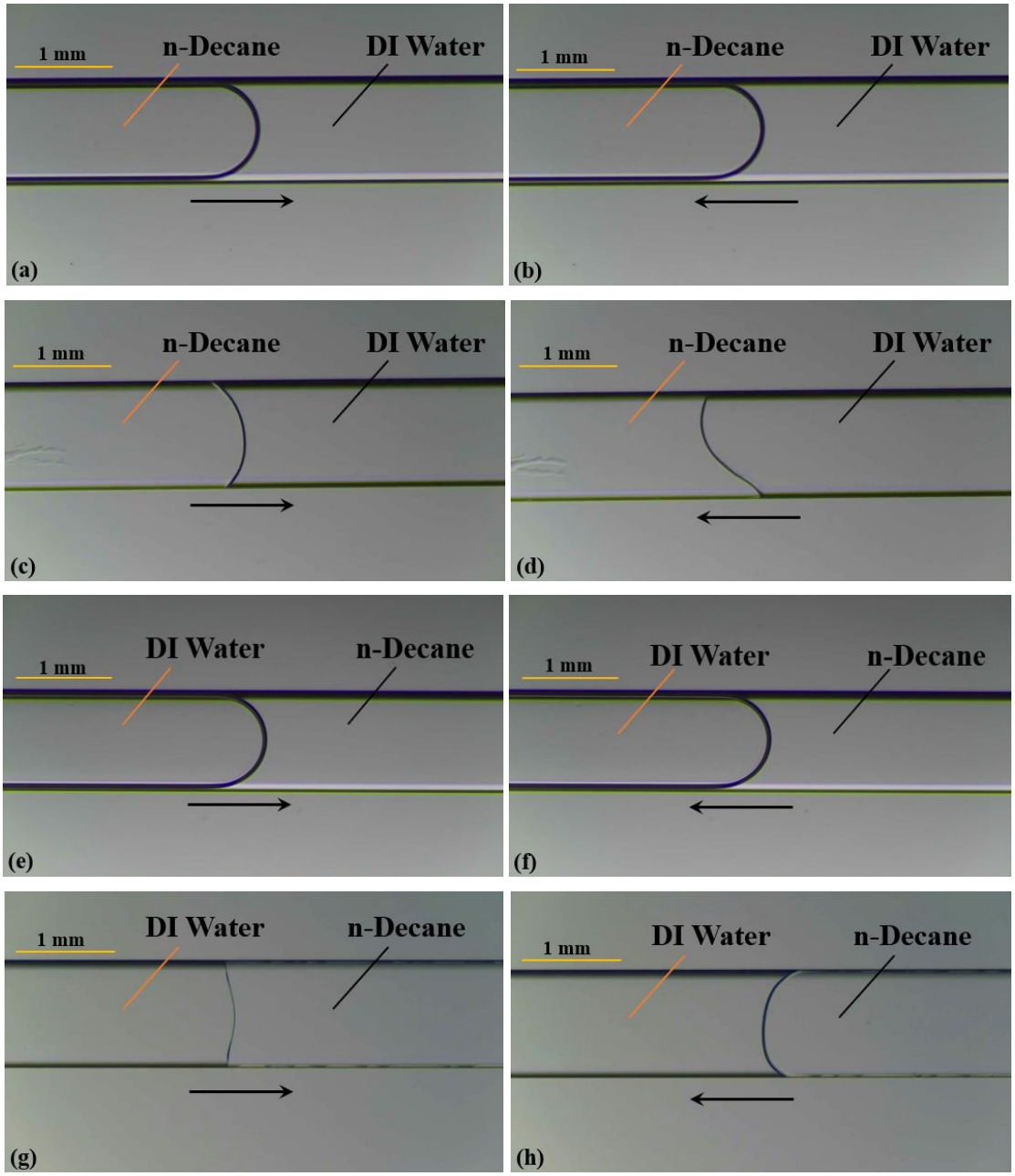


Figure 23: Untreated microfluidic channel contacted by DI water first: (a) DI water receding contact angle and (b) DI water advancing contact angle in DI water-n-decane system before aging; (c) DI water receding contact angle and (d) DI water advancing contact angle in DI water-n-decane system after aging. Untreated microfluidic channel contacted by n-decane first: (e) DI water advancing contact angle and (f) DI water receding contact angle in DI water-n-decane system before aging; (g) DI water advancing contact angle and (h) DI water receding contact angle in DI water-n-decane system after aging; Arrow indicates the direction of interface movement.

#### 4.4.1.2 Illite clay-coated microfluidic channel

Figure 24 represents the advancing and receding contact angles of DI water-air and n-decane-air system. Figure 25 represents the advancing and receding contact angles of DI water-n-decane system before and after aging (DI water contacted the channel surface first), n-decane-DI water before and after aging (n-decane contacted the channel surface first) systems. The before aging advancing and receding contact angles of DI water-air, n-decane-air, and the DI water-n-decane systems in the Illite clay-coated microfluidic channel contacted by DI water first were ~0°. The DI water advancing and receding contact angles in the case of surface contacted by n-decane first were ~180° indicating that the surface is behaving as strongly oil-wet before aging. The aging effect was studied by retaining the n-decane and DI water in the corresponding microfluidic channels for approximately 24 h in the case of channels first contacted by DI water and n-decane, respectively.

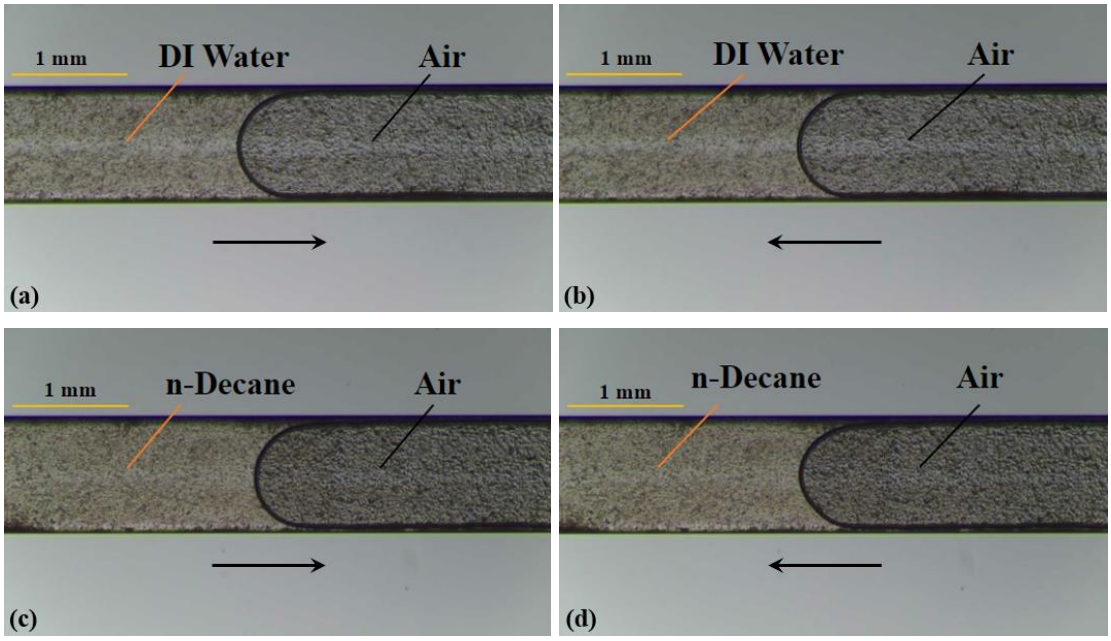


Figure 24: Illite clay-coated microfluidic channel contacted by DI water first: (a) DI water advancing contact angle and (b) DI water receding contact angle in DI water-air system before aging; Illite clay-coated microfluidic channel contacted by n-decane first: (c) n-decane advancing contact angle and (d) n-decane receding contact angle in n-decane-air system before aging.

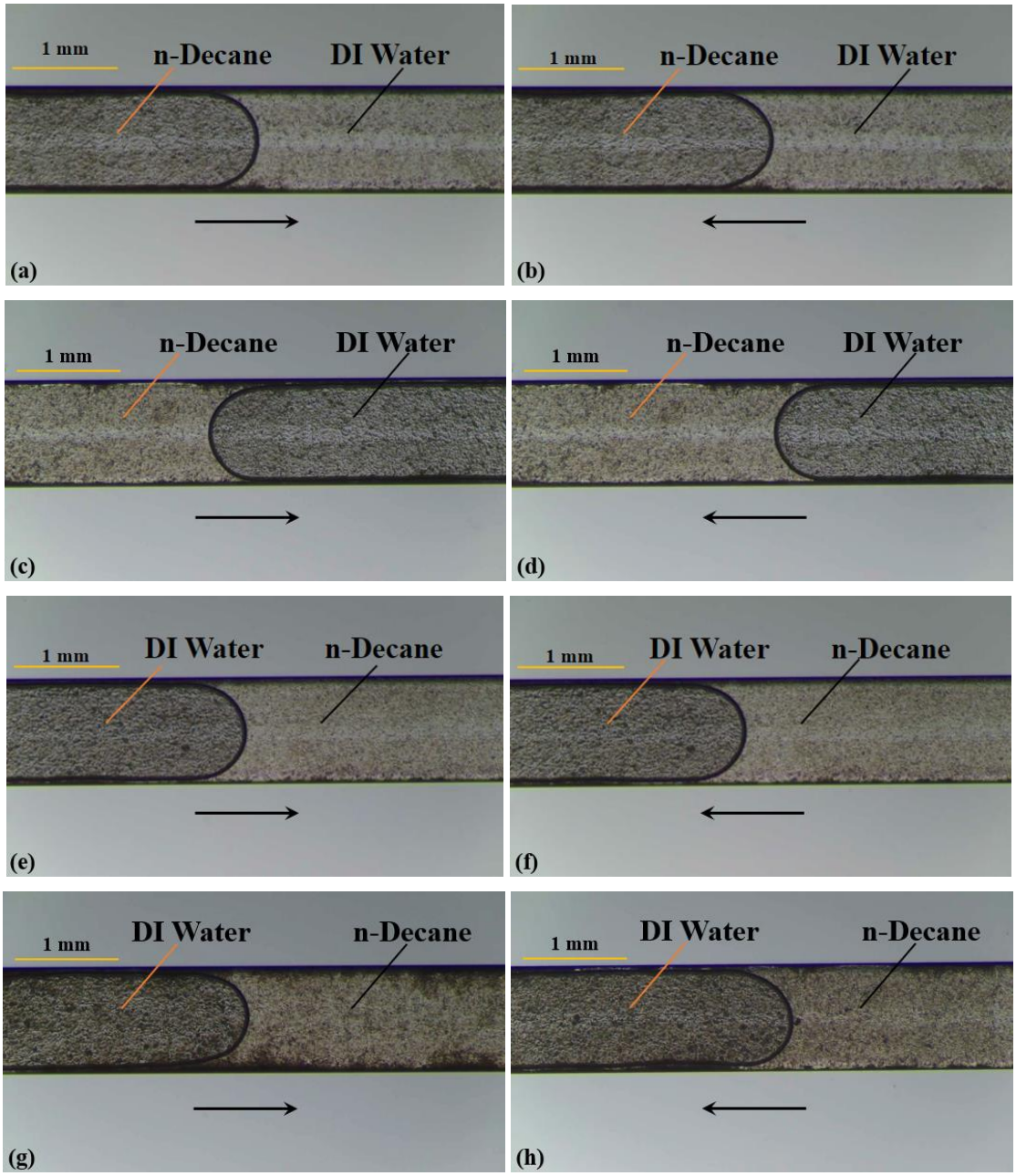


Figure 25: Illite clay-coated microfluidic channel contacted by DI water first: (a) DI water receding contact angle and (b) DI water advancing contact angle in DI water-n-decane system before aging; (c) DI water receding contact angle and (d) DI water advancing contact angle in DI water-n-decane system after aging. Illite clay-coated microfluidic channel contacted by n-decane first: (e) DI water advancing contact angle and (f) DI water receding contact angle in DI water-n-decane system before aging; (g) DI water advancing contact angle and (h) DI water receding contact angle in DI water-n-decane system after aging; Arrow indicates the direction of interface movement.

In the case of DI water first contacted the channel surface, both DI water advancing and receding angles were ~180° indicating the surface became strongly oil-wet after aging. In the case of n-decane first contacted the channel surface, both DI water advancing and receding angles were ~180° indicating the surface is still strongly oil-wet after aging.

#### 4.4.1.3 Illite-Smectite coated microfluidic channel

Figure 26 represents the advancing and receding contact angles of DI water-air and n-decane-air system. Figure 27 represents the advancing and receding contact angles of DI water-n-decane before and after aging (DI water contacted the channel surface first), n-decane-DI water before and after aging (n-decane contacted the channel surface first) systems.

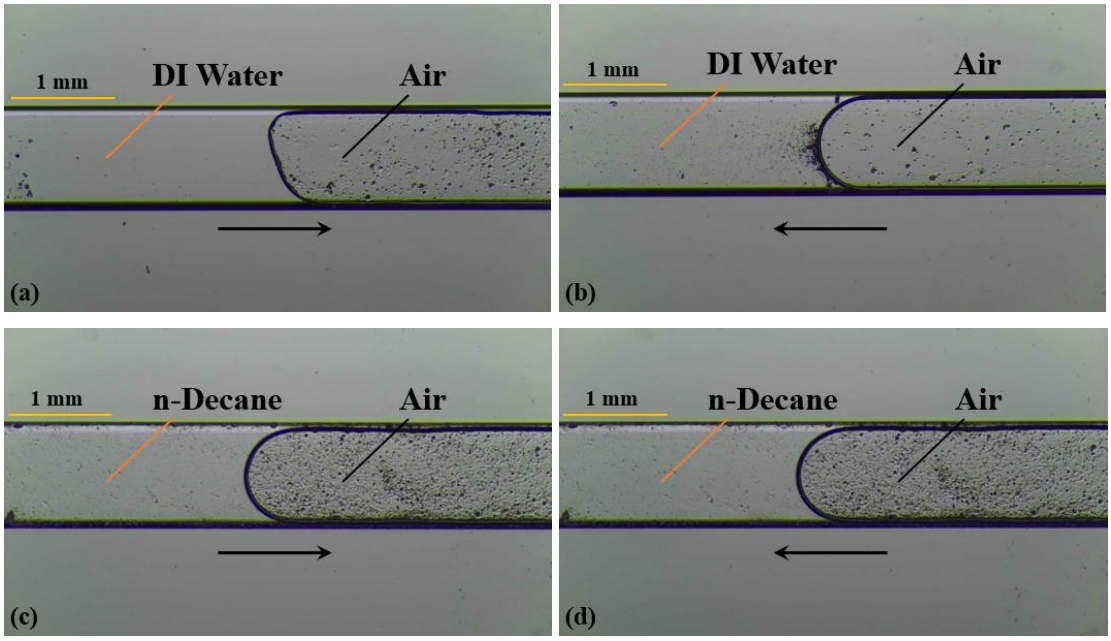


Figure 26: Illite-Smectite clay-coated microfluidic channel contacted by DI water first: (a) DI water advancing contact angle and (b) DI water receding contact angle in DI water-air system before aging; Illite-Smectite clay-coated microfluidic channel contacted by n-decane first: (c) n-decane advancing contact angle and (d) n-decane receding contact angle in n-decane-air system before aging.

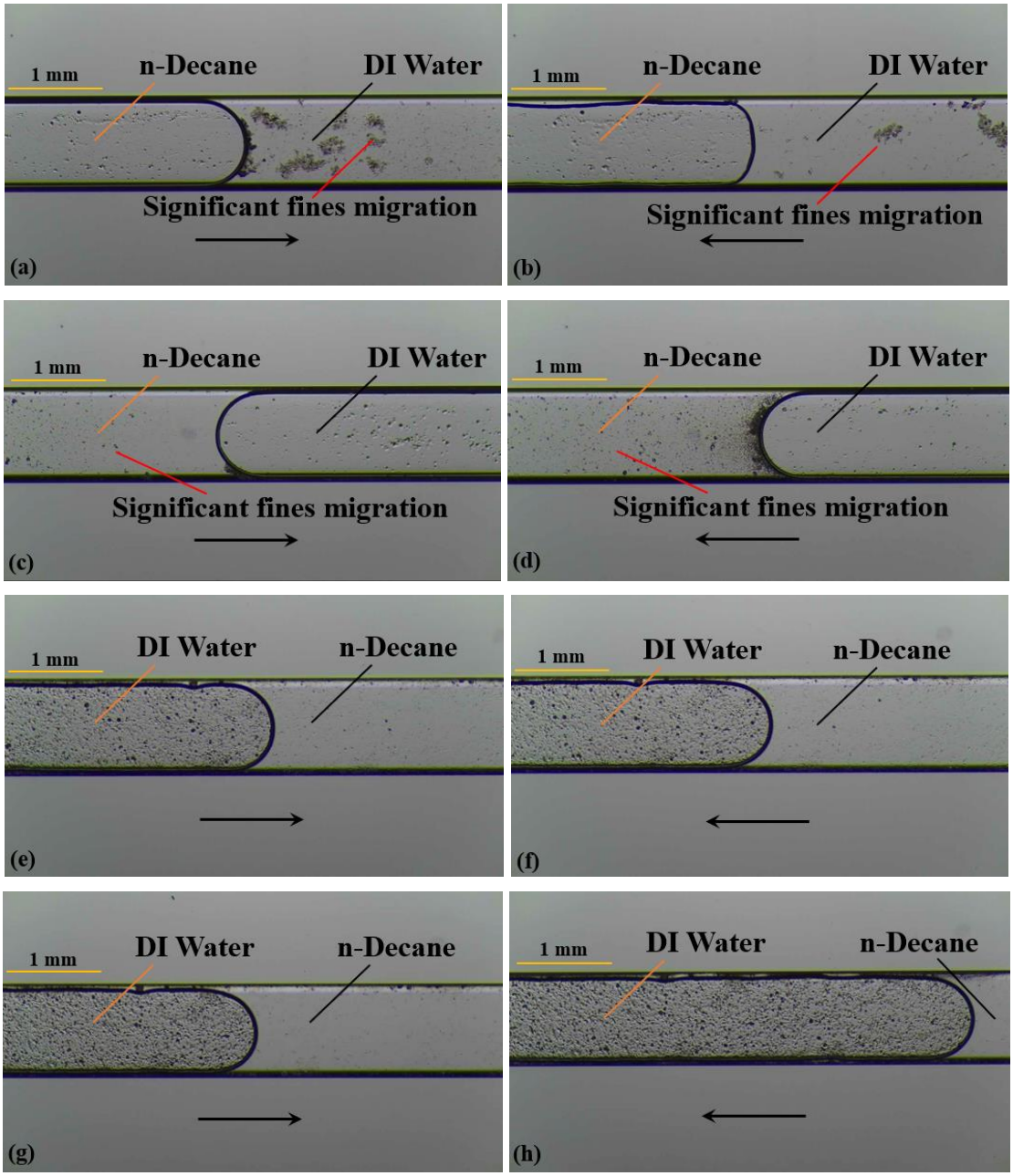


Figure 27: Illite-Smectite clay-coated microfluidic channel contacted by DI water first: (a) DI water receding contact angle and (b) DI water advancing contact angle in DI water-n-decane system before aging; (c) DI water receding contact angle and (d) DI water advancing contact angle in DI water-n-decane system after aging. Illite-Smectite clay-coated microfluidic channel contacted by n-decane first: (e) DI water advancing contact angle and (f) DI water receding contact angle in DI water-n-decane system before aging; (g) DI water advancing contact angle and (h) DI water receding contact angle in DI water-n-decane system after aging; Arrow indicates the direction of interface movement.

The before aging advancing and receding contact angles of DI water-air, n-decane-air, and the DI water-n-decane systems in the Illite-Smectite clay-coated microfluidic channel contacted by DI water first were ~0°. The DI water advancing and receding contact angles in the case of surface contacted by n-decane first were ~180° indicating that the surface is behaving as strongly oil-wet before aging. The aging effect was studied by retaining the n-decane and DI water in the corresponding microfluidic channels for approximately 24 h in the case of channels first contacted by DI water and n-decane, respectively. In the case of DI water first contacted the channel surface, both DI water advancing and receding angles were ~0° indicating the surface is preferentially strongly water-wet even after aging. In the case of n-decane first contacted the channel surface, both DI water advancing and receding angles were ~180° indicating the surface is preferentially strongly oil-wet even after aging.

Significant fines migration was observed in the case of DI water-air system (Figures 26 (a) and (b)), and in the case of DI water-n-decane system when DI water first contacted the microfluidic channel (Figures 27 (a), (b), (c), and (d)). This is because of the electric double layer repulsion between clay and water molecules. Generally, most substrates carry negative charge after being exposed to water because of high dielectric constant of water. When positive ions in the aqueous medium are not sufficient to shield the negative charge on clay surface, clay particles are released.

### 4.4.2 5k ppm brine and n-decane system

#### 4.4.2.1 Untreated microfluidic channel

Figure 28 represents the advancing and receding contact angles of 5k ppm brine-air system. Figure 29 represents the advancing and receding contact angles of 5k ppm brine-n-decane before and after aging (5k ppm brine contacted the channel surface first), n-decane-5k ppm brine before and after aging (n-decane contacted the channel surface first) systems. The before aging base case advancing and receding contact angles of 5k ppm brine-air, n-decane-air, and the 5k ppm brine-n-decane systems in the untreated microfluidic channel contacted by 5k ppm brine first were ~0°. 5k ppm

brine advancing and receding contact angles in the case of surface contacted by n-decane first were ~180° indicating that the surface is behaving as strongly oil-wet before aging. The aging effect was studied by retaining the n-decane and 5k ppm brine in the corresponding microfluidic channels for approximately 24 h in the case of channels first contacted by 5k ppm brine and n-decane, respectively.

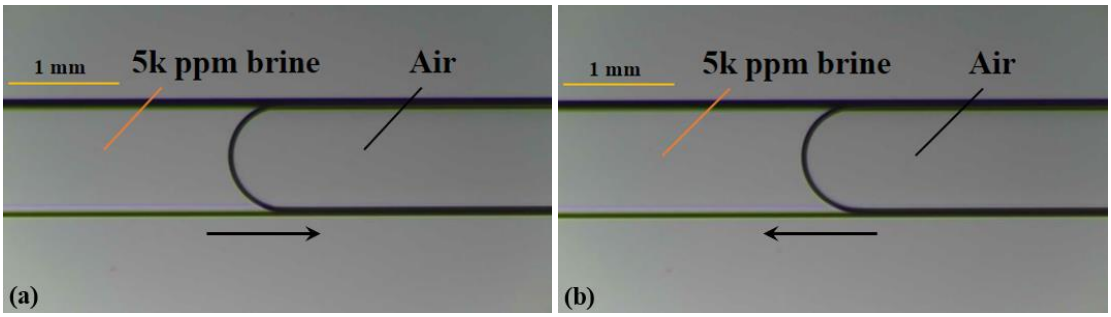


Figure 28: Untreated microfluidic channel contacted by 5k ppm brine first: (a) 5k ppm brine advancing contact angle and (b) 5k ppm brine receding contact angle in 5k ppm brine-air system before aging.

In the case of 5k ppm brine first contacted the channel, the 5k ppm brine receding and advancing contact angles in 5k ppm brine-n-decane system were ~0° indicating the surface is still strongly water-wet after aging. In the case of n-decane first contacted the channel, the 5k ppm brine advancing and receding contact angles were ~0° indicating that the surface changed the wettability from oil-wet to water-wet after aging. This can be attributed to the effect of low salinity water flooding.

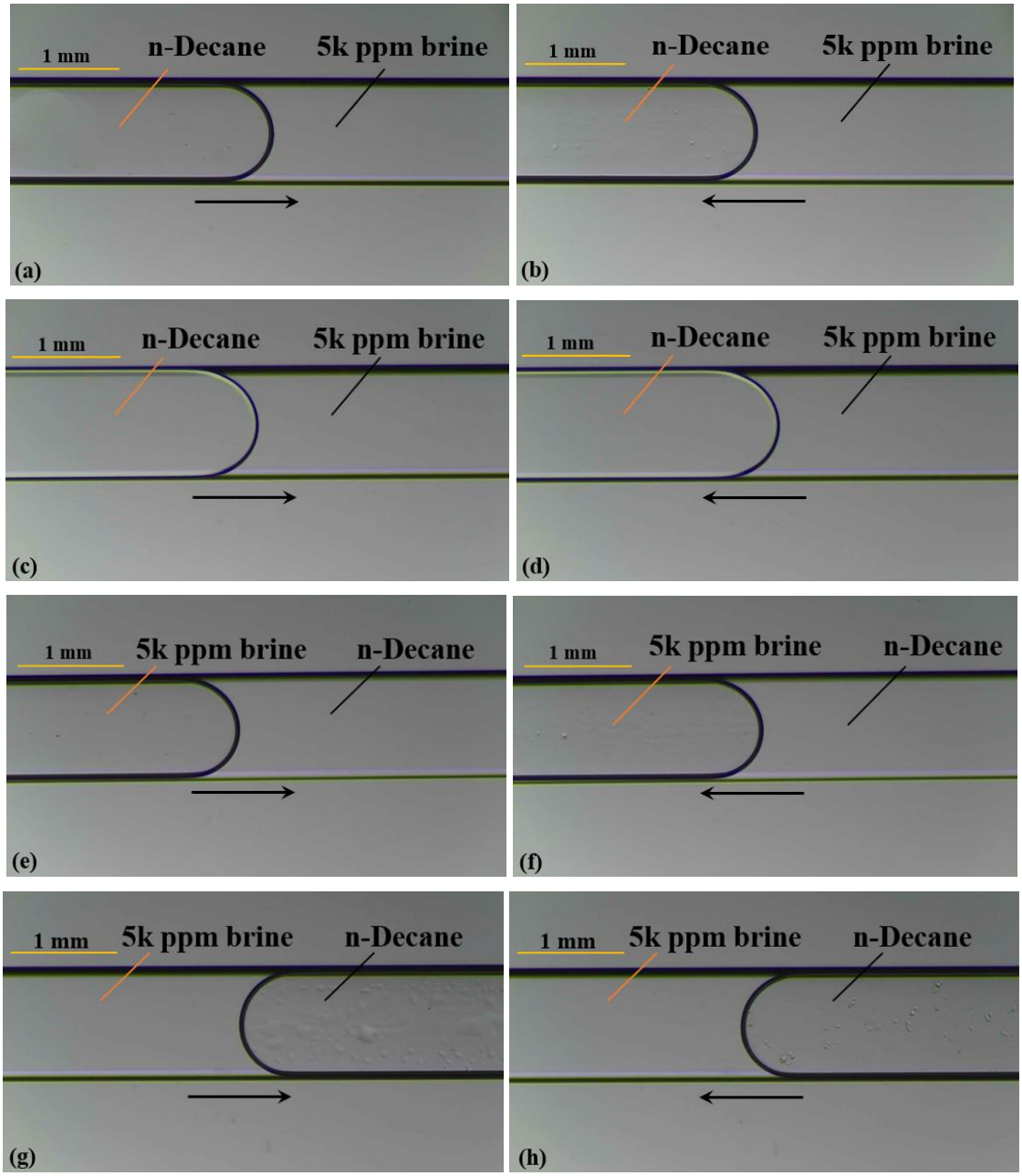


Figure 29: Untreated microfluidic channel contacted by 5k ppm brine first: (a) 5k ppm brine receding contact angle and (b) 5k ppm brine advancing contact angle in 5k ppm brine-n-decane system before aging; (c) 5k ppm brine receding contact angle and (d) 5k ppm brine advancing contact angle in 5k ppm brine-n-decane system after aging. Untreated microfluidic channel contacted by n-decane first: (e) 5k ppm brine advancing contact angle and (f) 5k ppm brine receding contact angle in 5k ppm brine-n-decane system before aging; (g) 5k ppm brine advancing contact angle and (h) 5k ppm brine receding contact angle in 5k ppm brine-n-decane system after aging; Arrow indicates the direction of interface movement.

#### 4.4.2.2 Illite clay-coated microfluidic channel

Figure 30 represents the advancing and receding contact angles of 5k ppm brine-air system. Figure 31 represents the advancing and receding contact angles of 5k ppm brine-n-decane before and after aging (5k ppm brine contacted the channel surface first), n-decane-5k ppm brine before and after aging (n-decane contacted the channel surface first) systems.

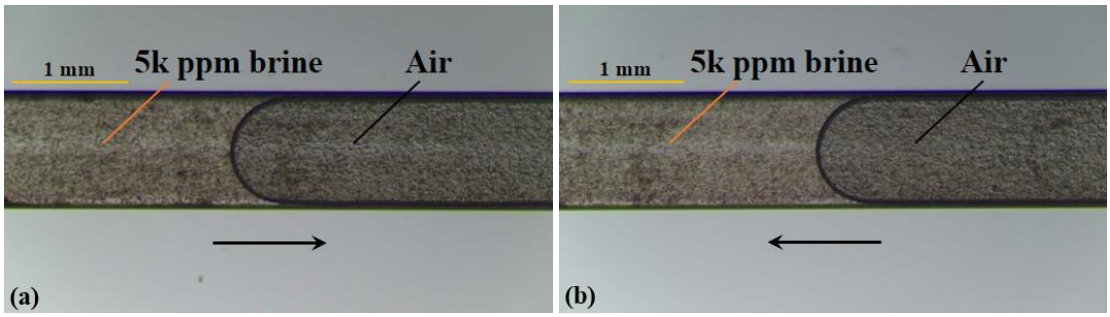


Figure 30: Illite clay-coated microfluidic channel contacted by 5k ppm brine first: (a) 5k ppm brine advancing contact angle and (b) 5k ppm brine receding contact angle in 5k ppm brine-air system before aging.

The before aging advancing and receding contact angles of 5k ppm brine-air, n-decane-air, and the 5k ppm brine-n-decane systems in the Illite clay-coated microfluidic channel contacted by 5k ppm brine first were ~0°. 5k ppm brine advancing and receding contact angles in the case of surface contacted by n-decane first were ~180° indicating that the surface is behaving as strongly oil-wet before aging. The aging effect was studied by retaining the n-decane and 5k ppm brine in the corresponding microfluidic channels for approximately 24 h in the case of channels first contacted by 5k ppm brine and n-decane, respectively. In the case of 5k ppm brine first contacted the channel, the 5k ppm brine receding and advancing contact angles in 5k ppm brine-n-decane system were ~0° indicating the surface is still strongly water-wet after aging. In the case of n-decane first contacted the channel, the 5k ppm brine advancing and receding contact angles were ~0° indicating that the surface changed the wettability from oil-wet to water-wet after aging. This can be attributed to the effect of low salinity water flooding.

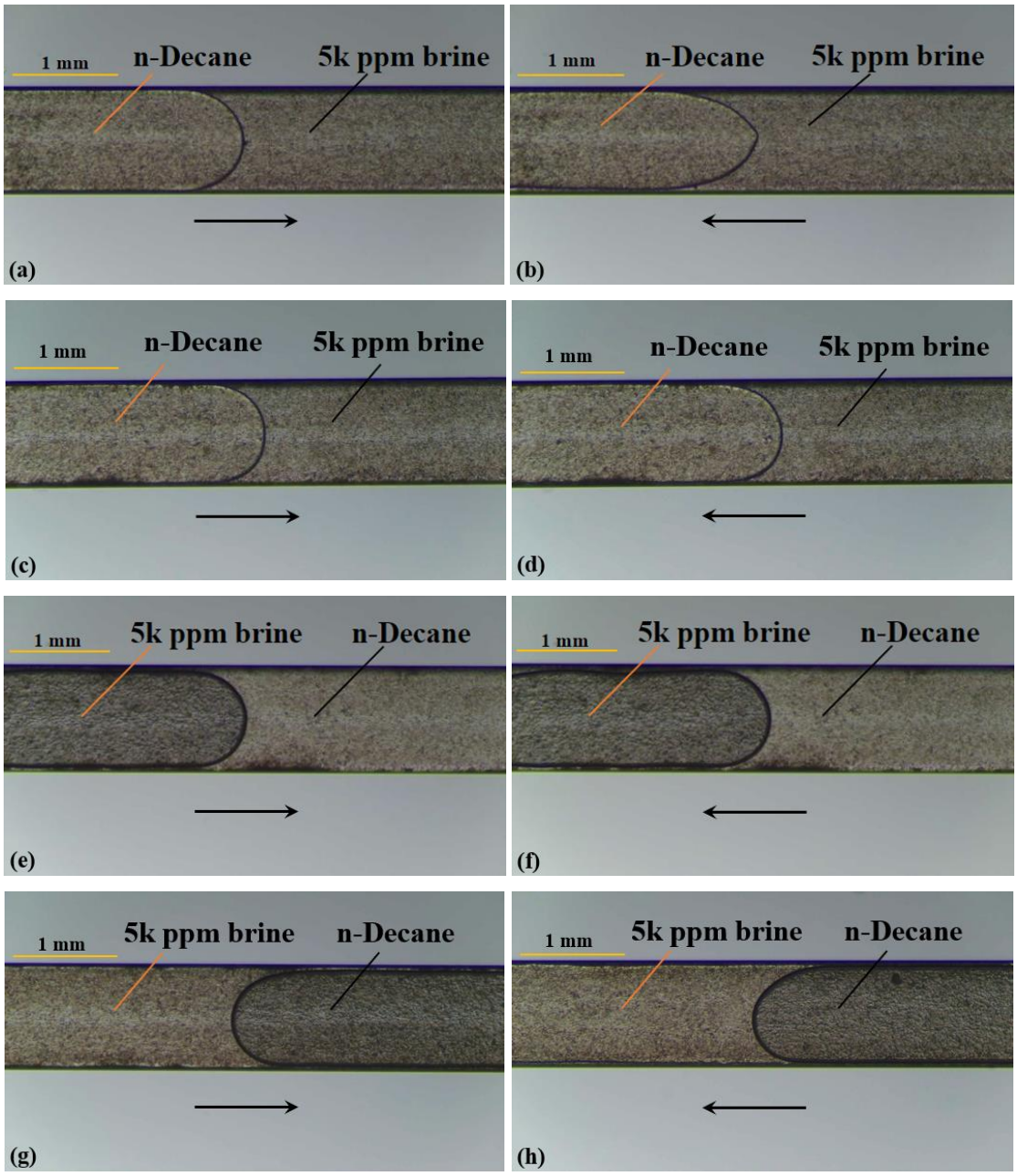


Figure 31: Illite clay-coated microfluidic channel contacted by 5k ppm brine first: (a) 5k ppm brine receding contact angle and (b) 5k ppm brine advancing contact angle in 5k ppm brine-n-decane system before aging; (c) 5k ppm brine receding contact angle and (d) 5k ppm brine advancing contact angle in 5k ppm brine-n-decane system after aging. Illite clay-coated microfluidic channel contacted by n-decane first: (e) 5k ppm brine advancing contact angle and (f) 5k ppm brine receding contact angle in 5k ppm brine-n-decane system before aging; (g) 5k ppm brine advancing contact angle and (h) 5k ppm brine receding contact angle in 5k ppm brine-n-decane system after aging; Arrow indicates the direction of interface movement.

#### 4.4.2.3 Illite-Smectite clay-coated microfluidic channel

Figure 32 represents the advancing and receding contact angles of 5k ppm brine-air system. Figure 33 represents the advancing and receding contact angles of 5k ppm brine-n-decane before and after aging (5k ppm brine contacted the channel surface first), n-decane-5k ppm brine before and after aging (n-decane contacted the channel surface first) systems. The before aging advancing and receding contact angles of 5k ppm brine-air, n-decane-air, and the 5k ppm brine-n-decane systems in the Illite-Smectite clay-coated microfluidic channel contacted by 5k ppm brine first were ~0°. 5k ppm brine advancing and receding contact angles in the case of surface contacted by n-decane first were ~180° indicating that the surface is behaving as strongly oil-wet before aging.

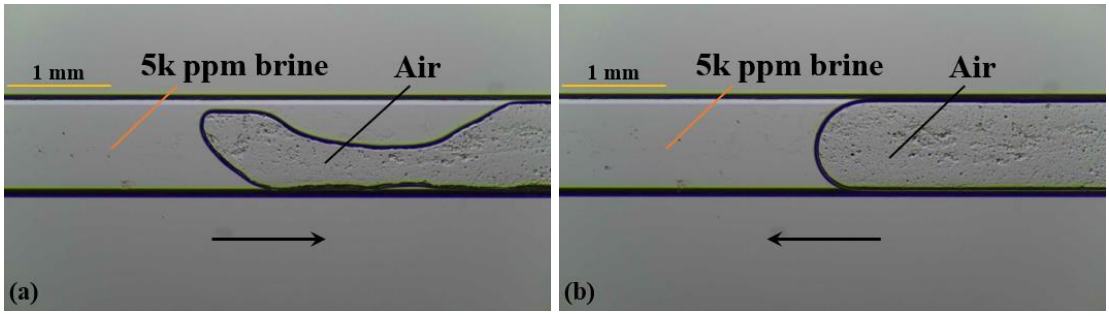


Figure 32: Illite-Smectite clay-coated microfluidic channel contacted by 5k ppm brine first: (a) 5k ppm brine advancing contact angle and (b) 5k ppm brine receding contact angle in 5k ppm brine-air system before aging.

The aging effect was studied by retaining the n-decane and 5k ppm brine in the corresponding microfluidic channels for approximately 24 h in the case of channels first contacted by 5k ppm brine and n-decane, respectively. In the case of 5k ppm brine first contacted the channel, the 5k ppm brine receding and advancing contact angles in 5k ppm brine-n-decane system were ~0° indicating the surface is behaving as strongly water-wet after aging. In the case of n-decane first contacted the channel, the 5k ppm brine advancing and receding contact angles were ~0° indicating that the surface changed the wettability from oil-wet to water-wet after aging. This can be attributed to the effect of low salinity water flooding.

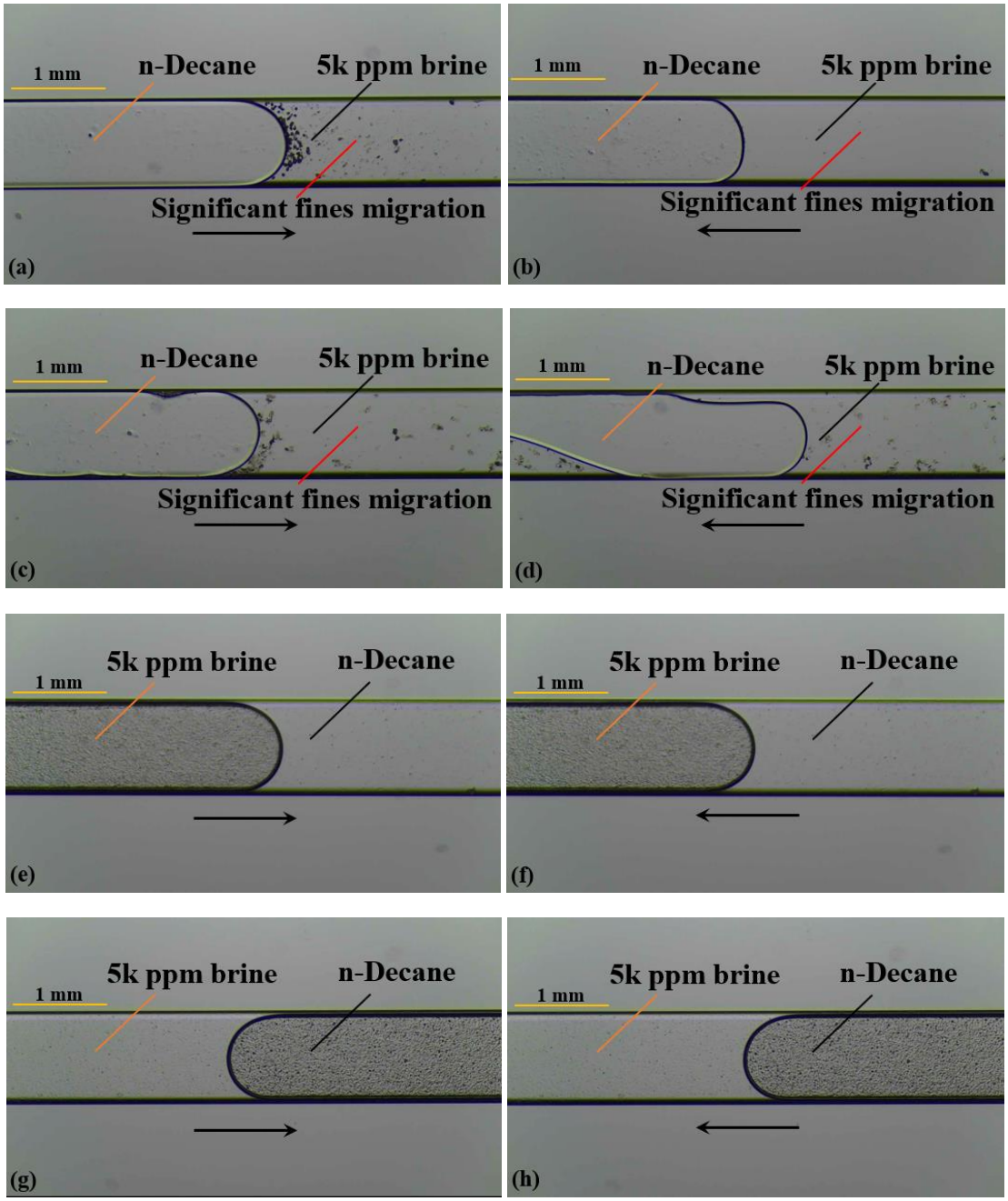


Figure 33: Illite-Smectite clay-coated microfluidic channel contacted by 5k ppm brine first: (a) 5k ppm brine receding contact angle and (b) 5k ppm brine advancing contact angle in 5k ppm brine-n-decane system before aging; (c) 5k ppm brine receding contact angle and (d) 5k ppm brine advancing contact angle in 5k ppm brine-n-decane system after aging. Illite-Smectite clay-coated microfluidic channel contacted by n-decane first: (e) 5k ppm brine advancing contact angle and (f) 5k ppm brine receding contact angle in 5k ppm brine-n-decane system before aging; (g) 5k ppm brine advancing contact angle and (h) 5k ppm brine receding contact angle in 5k ppm brine-n-decane system after aging; Arrow indicates the direction of interface movement.

Significant fines migration was observed in the case of 5k ppm brine-air system (Figures 32 (a) and (b)), and in the case of 5k ppm brine-n-decane system when 5k ppm brine first contacted the microfluidic channel (Figures 33 (a), (b), (c), and (d)).

### 4.4.3 10k ppm brine and n-decane system

#### 4.4.3.1 Untreated microfluidic channel

Figure 34 represents the advancing and receding contact angles of 10k ppm brine-air system. Figure 35 represents the advancing and receding contact angles of 10k ppm brine-n-decane before and after aging (10k ppm brine contacted the channel surface first), n-decane-10k ppm brine before and after aging (n-decane contacted the channel surface first) systems. The before aging base case advancing and receding contact angles of 10k ppm brine-air, n-decane-air, and the 10k ppm brine-n-decane systems in the untreated microfluidic channel contacted by 10k ppm brine first were ~$0^{o}$. 10k ppm brine advancing and receding contact angles in the case of surface contacted by n-decane first were ~$180^{o}$ indicating that the surface is behaving as strongly oil-wet before aging. The aging effect was studied by retaining the n-decane and 10k ppm brine in the corresponding microfluidic channels for approximately 24 h in the case of channels first contacted by 10k ppm brine and n-decane, respectively.

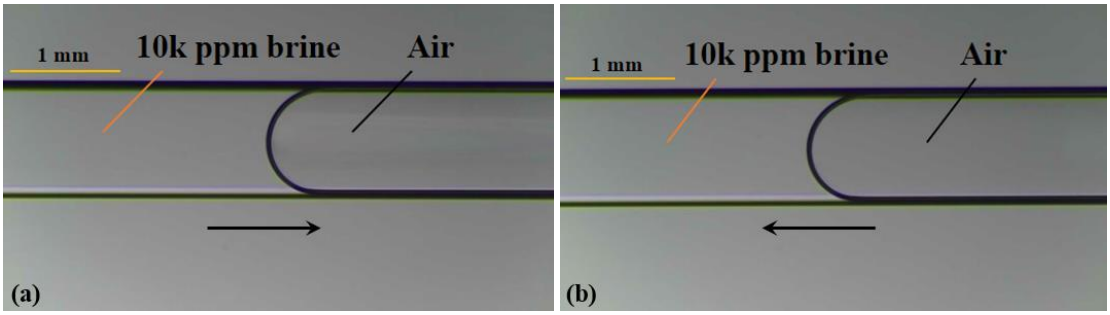


Figure 34: Untreated microfluidic channel contacted by 10k ppm brine first: (a) 10k ppm brine advancing contact angle and (b) 10k ppm brine receding contact angle in 10k ppm brine-air system before aging.

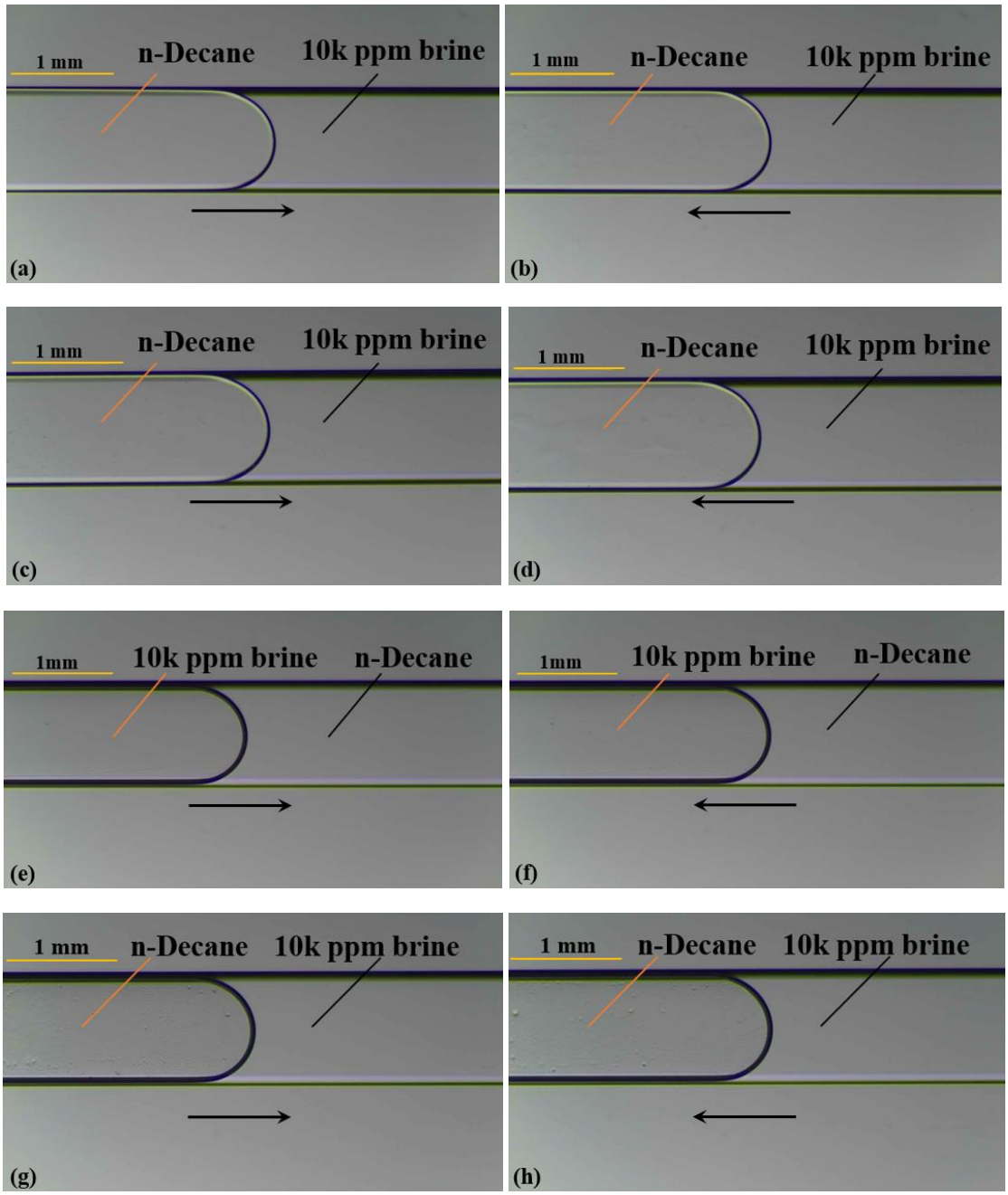


Figure 35: Untreated microfluidic channel contacted by 10k ppm brine first: (a) 10k ppm brine receding contact angle and (b) 10k ppm brine advancing contact angle in 10k ppm brine-n-decane system before aging; (c) 10k ppm brine receding contact angle and (d) 10k ppm brine advancing contact angle in 10k ppm brine-n-decane system after aging. Untreated microfluidic channel contacted by n-decane first: (e) 10k ppm brine advancing contact angle and (f) 10k ppm brine receding contact angle in 10k ppm brine-n-decane system before aging; (g) 10k ppm brine advancing contact angle and (h) 10k ppm brine receding contact angle in 10k ppm brine-n-decane system after aging; Arrow indicates the direction of interface movement.

In the case of 10k ppm brine first contacted the channel surface, both 10k ppm brine advancing and receding angles were ~0° indicating the surface is still strongly water-wet after aging. In the case of n-decane contacted the channel surface, both 10k ppm brine advancing and receding angles were ~180° indicating the surface is still strongly oil-wet even after aging.

#### 4.4.3.2 Illite clay-coated microfluidic channel

Figure 36 represents the advancing and receding contact angles of 10k ppm brine-air system. Figure 37 represents the advancing and receding contact angles of 10k ppm brine-n-decane before and after aging (10k ppm brine contacted the channel surface first), n-decane-10k ppm brine before and after aging (n-decane contacted the channel surface first) systems. The before aging advancing and receding contact angles of 10k ppm brine-air, n-decane-air, and the 10k ppm brine-n-decane systems in the Illite clay-coated microfluidic channel contacted by 10k ppm brine first were ~0°. 10k ppm brine advancing and receding contact angles in the case of surface contacted by n-decane first were ~180° indicating that the surface is behaving as strongly oil-wet before aging. The aging effect was studied by retaining the n-decane and 10k ppm brine in the corresponding microfluidic channels for approximately 24 h in the case of channels first contacted by 10k ppm brine and n-decane, respectively.

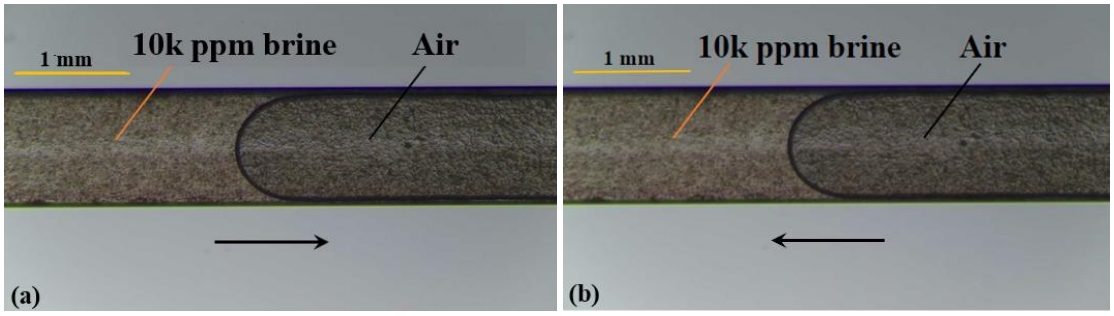


Figure 36: Illite clay-coated microfluidic channel contacted by 10k ppm brine first: (a) 10k ppm brine advancing contact angle and (b) 10k ppm brine receding contact angle in 10k ppm brine-air system before aging.

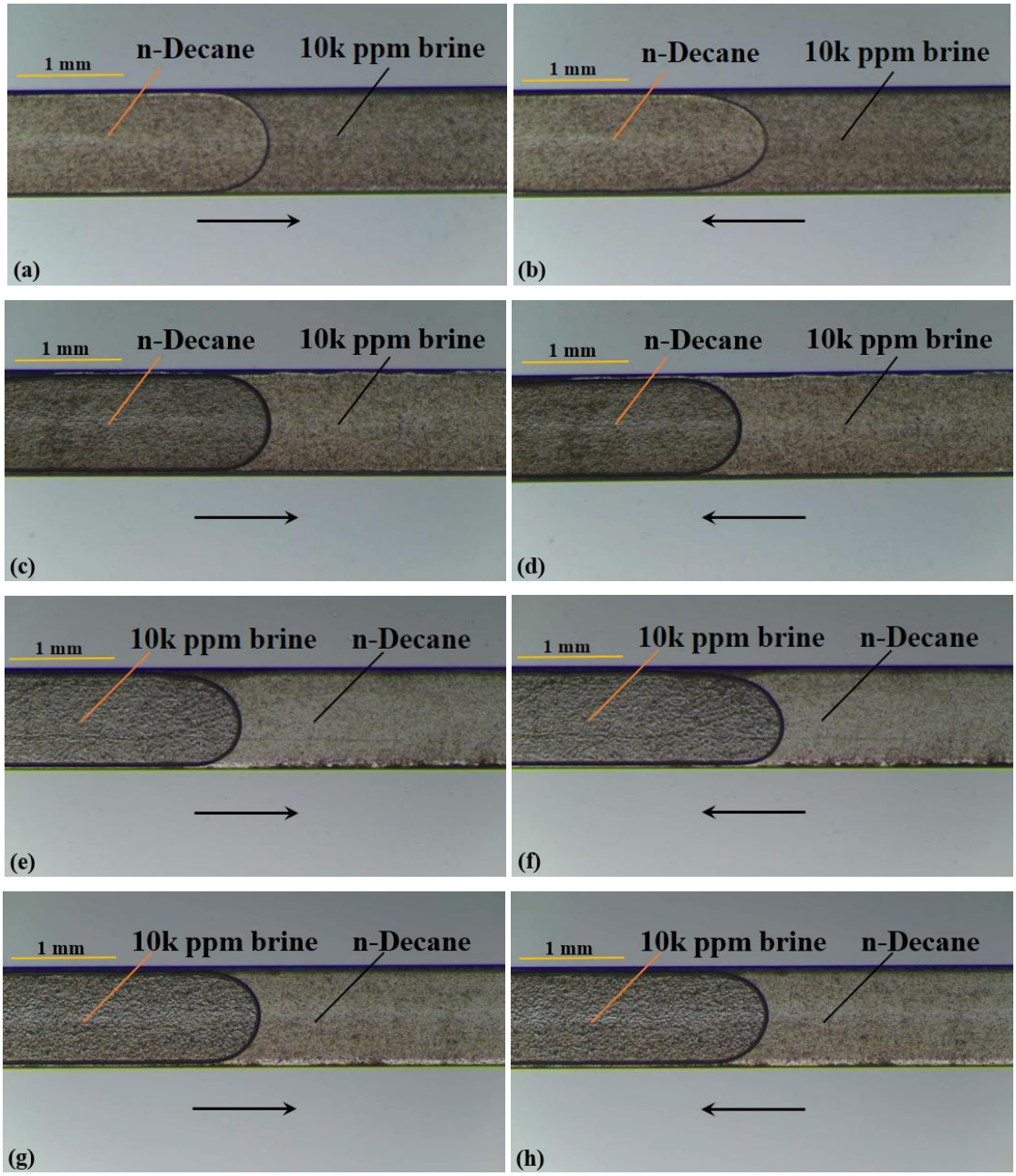


Figure 37: Illite clay-coated microfluidic channel contacted by 10k ppm brine first: (a) 10k ppm brine receding contact angle and (b) 10k ppm brine advancing contact angle in 10k ppm brine-n-decane system before aging; (c) 10k ppm brine receding contact angle and (d) 10k ppm brine advancing contact angle in 10k ppm brine-n-decane system after aging. Illite clay-coated microfluidic channel contacted by n-decane first: (e) 10k ppm brine advancing contact angle and (f) 10k ppm brine receding contact angle in 10k ppm brine-n-decane system before aging; (g) 10k ppm brine advancing contact angle and (h) 10k ppm brine receding contact angle in 10k ppm brine-n-decane system after aging; Arrow indicates the direction of interface movement.

In the case of 10k ppm brine first contacted the channel surface, both 10k ppm brine advancing and receding angles were ~0° indicating the surface is still strongly water-wet even after aging. In the case of n-decane contacted the channel surface, both 10k ppm brine advancing and receding angles were ~180° indicating the surface is still strongly oil-wet even after aging.

#### 4.4.3.3 Illite-Smectite clay-coated microfluidic channel

Figure 38 represents the advancing and receding contact angles of 10k ppm brine-air system. Figure 39 represents the advancing and receding contact angles of 10k ppm brine-n-decane before and after aging (10k ppm brine contacted the channel surface first), n-decane-10k ppm brine before and after aging (n-decane contacted the channel surface first) systems. The before aging advancing and receding contact angles of 10k ppm brine-air, n-decane-air, and the 10k ppm brine-n-decane systems in the Illite-Smectite clay-coated microfluidic channel contacted by 10k ppm brine first were ~0°. 10k ppm brine advancing and receding contact angles in the case of surface contacted by n-decane first were ~180° indicating that the surface is behaving as strongly oil-wet before aging. The aging effect was studied by retaining the n-decane and 10k ppm brine in the corresponding microfluidic channels for approximately 24 h in the case of channels first contacted by 10k ppm brine and n-decane, respectively.

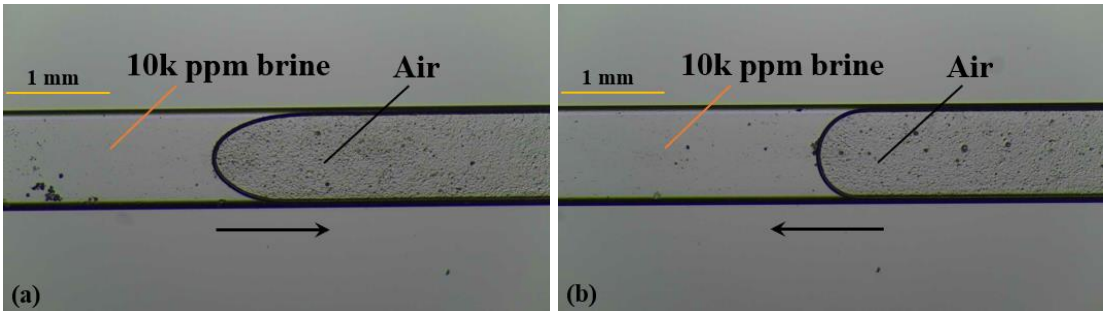


Figure 38: Illite-Smectite clay-coated microfluidic channel contacted by 10k ppm brine first: (a) 10k ppm brine advancing contact angle and (b) 10k ppm brine receding contact angle in 10k ppm brine-air system before aging.

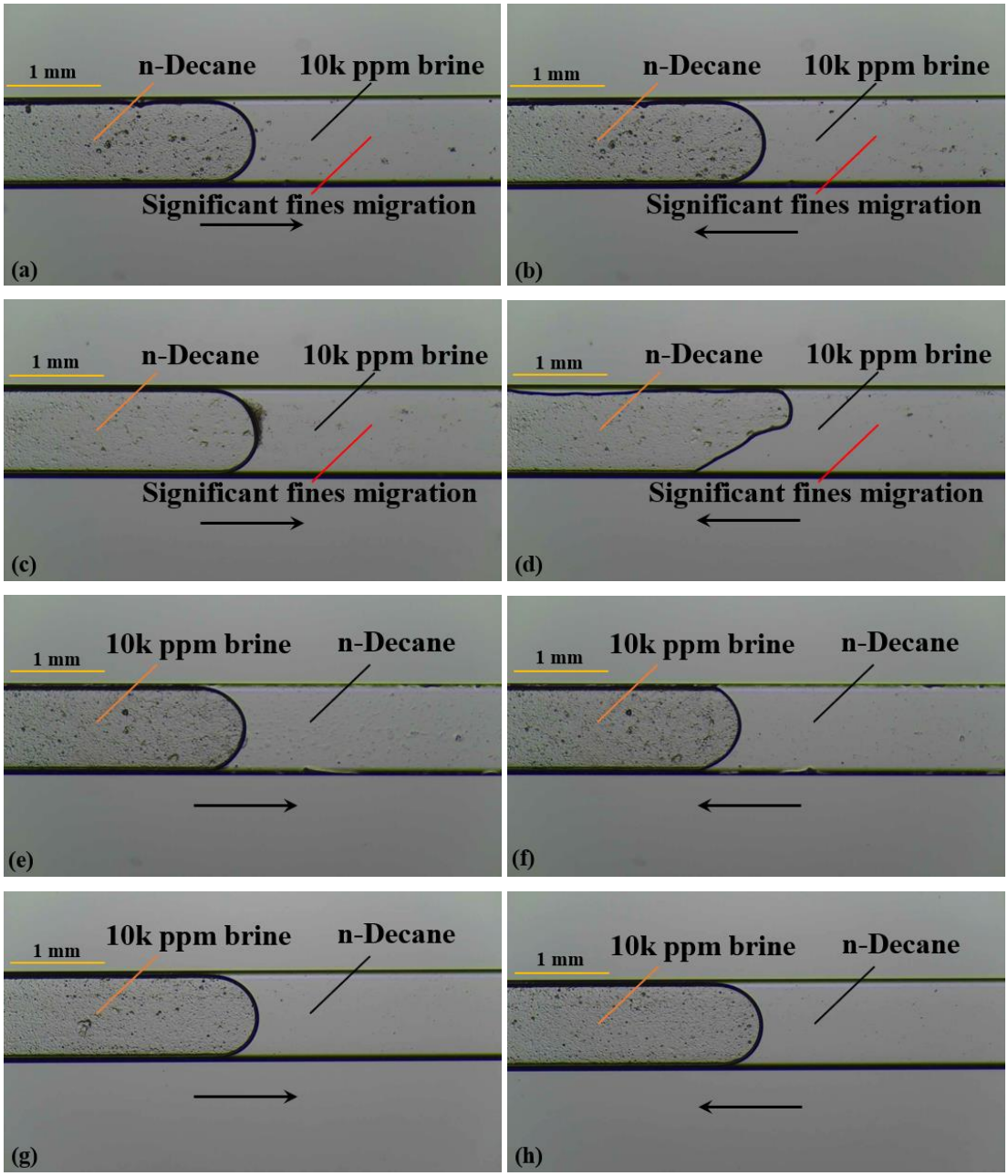


Figure 39: Illite-Smectite clay-coated microfluidic channel contacted by 10k ppm brine first: (a) 10k ppm brine receding contact angle and (b) 10k ppm brine advancing contact angle in 10k ppm brine-n-decane system before aging; (c) 10k ppm brine receding contact angle and (d) 10k ppm brine advancing contact angle in 10k ppm brine-n-decane system after aging. Illite-Smectite clay-coated microfluidic channel contacted by n-decane first: (e) 10k ppm brine advancing contact angle and (f) 10k ppm brine receding contact angle in 10k ppm brine-n-decane system before aging; (g) 10k ppm brine advancing contact angle and (h) 10k ppm brine receding contact angle in 10k ppm brine-n-decane system after aging; Arrow indicates the direction of interface movement.

In the case of 10k ppm brine first contacted the channel surface, both 10k ppm brine advancing and receding angles were ~0° indicating the surface is still strongly water-wet even after aging. In the case of n-decane contacted the channel surface, both 10k ppm brine advancing and receding angles were ~180° indicating the surface is still strongly oil-wet even after aging. Significant fines migration was observed in the case of 10k ppm brine-air system (Figures 38 (a) and (b)), and in the case of 10k ppm brine-n-decane system when 10k ppm brine first contacted the microfluidic channel (Figures 39 (a), (b), (c), and (d)).

### 4.4.4 30k ppm brine and n-decane system

#### 4.4.4.1 Untreated microfluidic channel

Figure 40 represents the advancing and receding contact angles of 30k ppm brine-air system. Figure 41 represents the advancing and receding contact angles of 30k ppm brine-n-decane before and after aging (30k ppm brine contacted the channel surface first), n-decane-30k ppm brine before and after aging (n-decane contacted the channel surface first) systems. The before aging base case advancing and receding contact angles of 30k ppm brine-air, n-decane-air systems in the untreated microfluidic channel were ~25°–30° and ~180°, respectively. In the case of surface contacted by n-decane first, 30k ppm brine advancing and receding contact angles before aging were ~180° indicating that the surface is behaving as strongly oil-wet before aging.

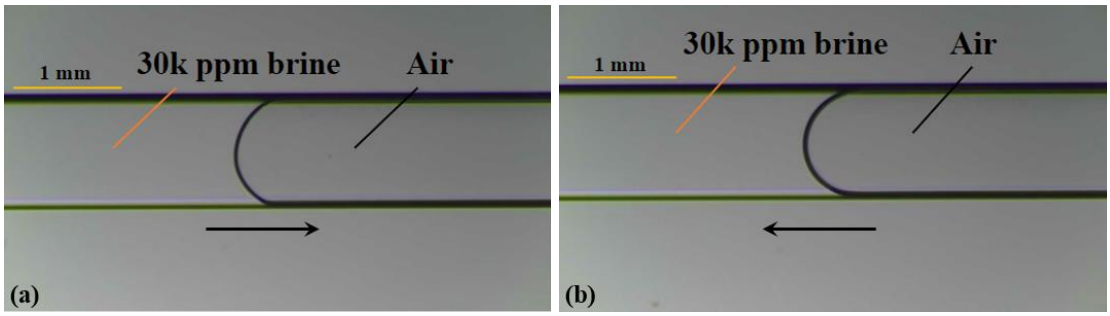


Figure 40: Untreated microfluidic channel contacted by 30k ppm brine first: (a) 30k ppm brine advancing contact angle and (b) 30k ppm brine receding contact angle in 30k ppm brine-air system before aging.

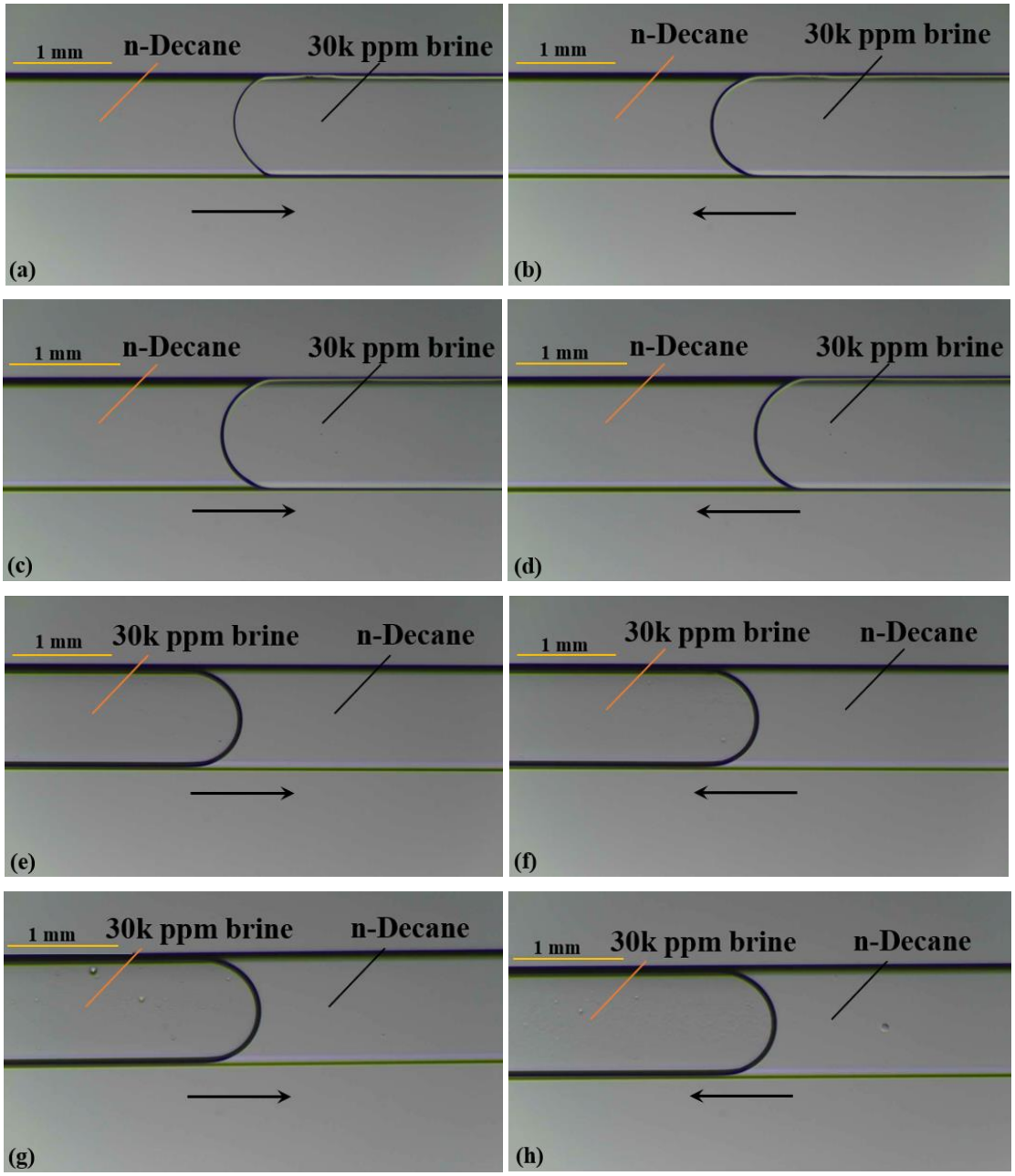


Figure 41: Untreated microfluidic channel contacted by 30k ppm brine first: (a) 30k ppm brine receding contact angle and (b) 30k ppm brine advancing contact angle in 30k ppm brine-n-decane system before aging; (c) 30k ppm brine receding contact angle and (d) 30k ppm brine advancing contact angle in 30k ppm brine-n-decane system after aging. Untreated microfluidic channel contacted by n-decane first: (e) 30k ppm brine advancing contact angle and (f) 30k ppm brine receding contact angle in 30k ppm brine-n-decane system before aging; (g) 30k ppm brine advancing contact angle and (h) 30k ppm brine receding contact angle in 30k ppm brine-n-decane system after aging; Arrow indicates the direction of interface movement.

In the case of surface contacted by 30k ppm brine first, 30k ppm brine advancing and receding contact angles before aging were ~150° and 145° indicating that the surface is behaving as oil-wet soon after it encounters n-decane which is attributed to the effect of salinity. The aging effect was studied by retaining the n-decane and 30k ppm brine in the corresponding microfluidic channels for approximately 24 h in the case of channels first contacted by 30k ppm brine and n-decane, respectively. In the case of 30k ppm brine first contacted the channel surface, both 30k ppm brine advancing and receding angles were ~150° indicating the surface is still oil-wet after aging. In the case of n-decane contacted the channel surface, both 30k ppm brine advancing and receding angles were ~180° indicating the surface is still strongly oil-wet after aging.

#### 4.4.4.2 Illite clay-coated microfluidic channel

Figure 42 represents the advancing and receding contact angles of 30k ppm brine-air system. Figure 43 represents the advancing and receding contact angles of 30k ppm brine-n-decane before and after aging (30k ppm brine contacted the channel surface first), n-decane-30k ppm brine before and after aging (n-decane contacted the channel surface first) systems. The before aging advancing and receding contact angles of 30k ppm brine-air, n-decane-air systems in the Illite clay-coated microfluidic channel were ~0°. In the case of surface contacted by n-decane first, 30k ppm brine advancing and receding contact angles before aging were ~180° indicating that the surface is behaving as strongly oil-wet before aging.

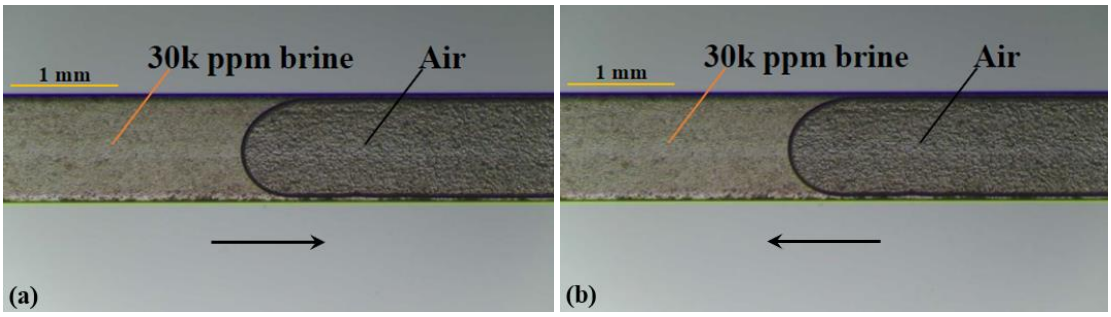


Figure 42: Illite clay-coated microfluidic channel contacted by 30k ppm brine first: (a) 30k ppm brine advancing contact angle and (b) 30k ppm brine receding contact angle in 30k ppm brine-air system before aging.

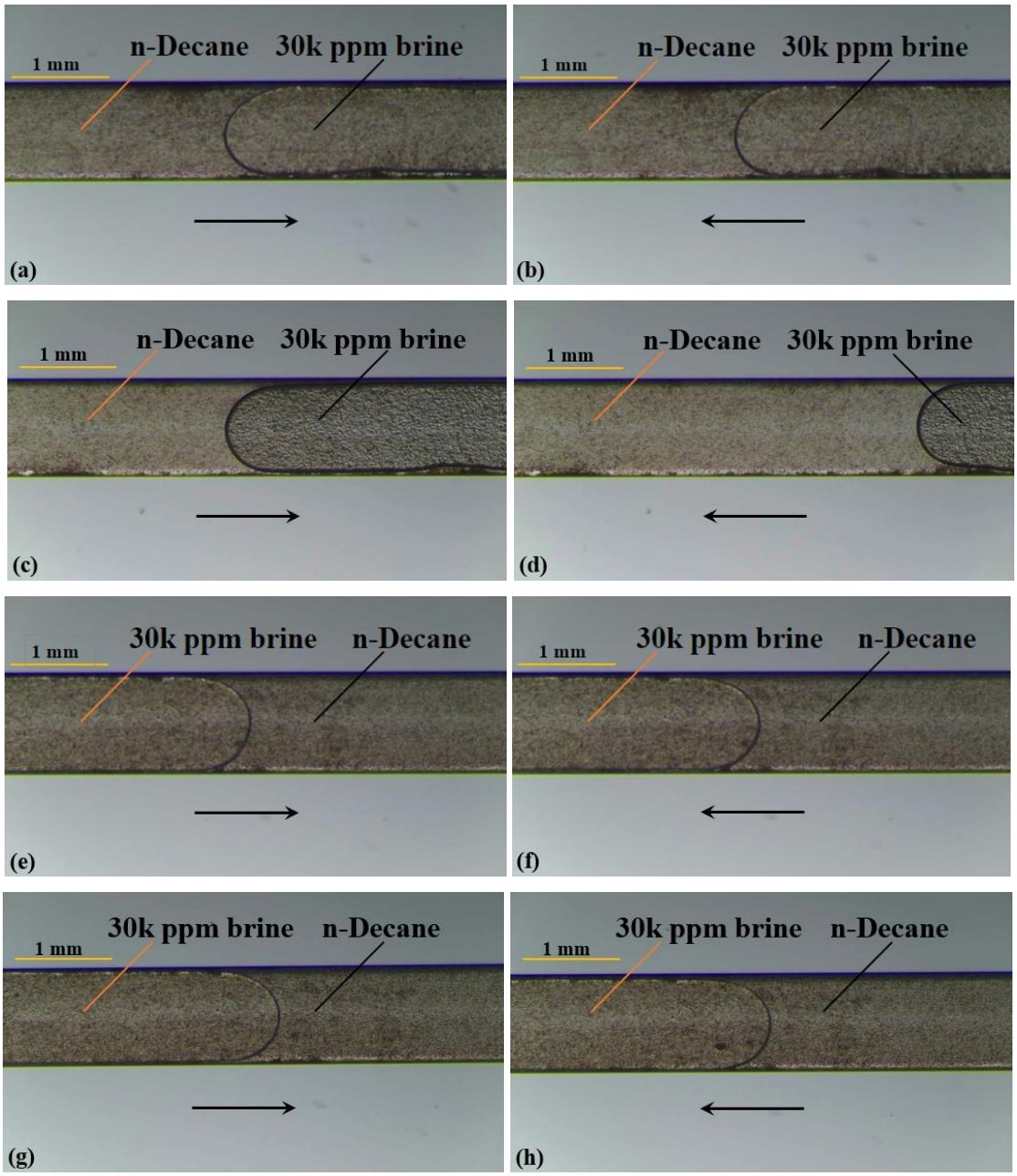


Figure 43: Illite clay-coated microfluidic channel contacted by 30k ppm brine first: (a) 30k ppm brine receding contact angle and (b) 30k ppm brine advancing contact angle in 30k ppm brine-n-decane system before aging; (c) 30k ppm brine receding contact angle and (d) 30k ppm brine advancing contact angle in 30k ppm brine-n-decane system after aging. Illite clay-coated microfluidic channel contacted by n-decane first: (e) 30k ppm brine advancing contact angle and (f) 30k ppm brine receding contact angle in 30k ppm brine-n-decane system before aging; (g) 30k ppm brine advancing contact angle and (h) 30k ppm brine receding contact angle in 30k ppm brine-n-decane system after aging; Arrow indicates the direction of interface movement.

In the case of surface contacted by 30k ppm brine first, 30k ppm brine advancing and receding contact angles before aging were ~180° indicating that the surface is behaving as strongly oil-wet soon after it encounters n-decane which is attributed to the effect of salinity. The aging effect was studied by retaining the n-decane and 30k ppm brine in the corresponding microfluidic channels for approximately 24 h in the case of channels first contacted by 30k ppm brine and n-decane, respectively. In the case of 30k ppm brine first contacted the channel surface, both 30k ppm brine advancing and receding angles were ~180° indicating the surface is preferentially strongly oil-wet even after aging. In the case of n-decane contacted the channel surface, both 30k ppm brine advancing and receding angles were ~180° indicating the surface is preferentially strongly oil-wet even after aging.

#### 4.4.4.3 Illite-Smectite clay-coated microfluidic channel

Figure 44 represents the advancing and receding contact angles of 30k ppm brine-air system. Figure 45 represents the advancing and receding contact angles of 30k ppm brine-n-decane before and after aging (30k ppm brine contacted the channel surface first), n-decane-30k ppm brine before and after aging (n-decane contacted the channel surface first) systems. The before aging advancing and receding contact angles of 30k ppm brine-air, n-decane-air, and the 30k ppm brine-n-decane systems in the Illite-Smectite clay-coated microfluidic channel contacted by 30k ppm brine first were ~0°.

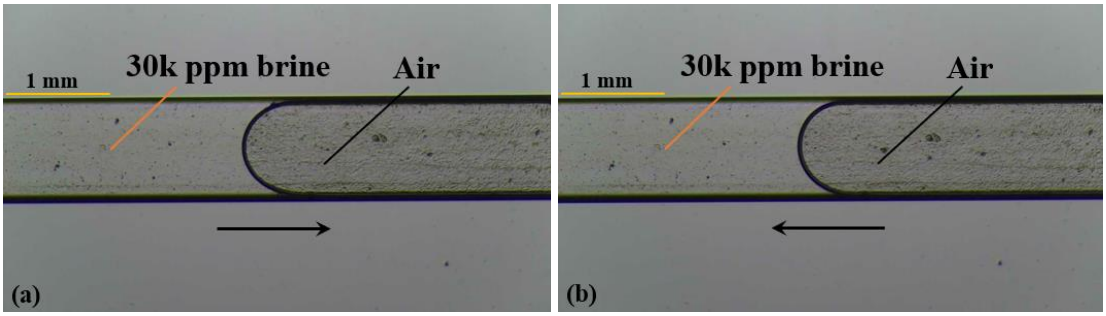


Figure 44: Illite-Smectite clay-coated microfluidic channel contacted by 30k ppm brine first: (a) 30k ppm brine advancing contact angle and (b) 30k ppm brine receding contact angle in 30k ppm brine-air system before aging.

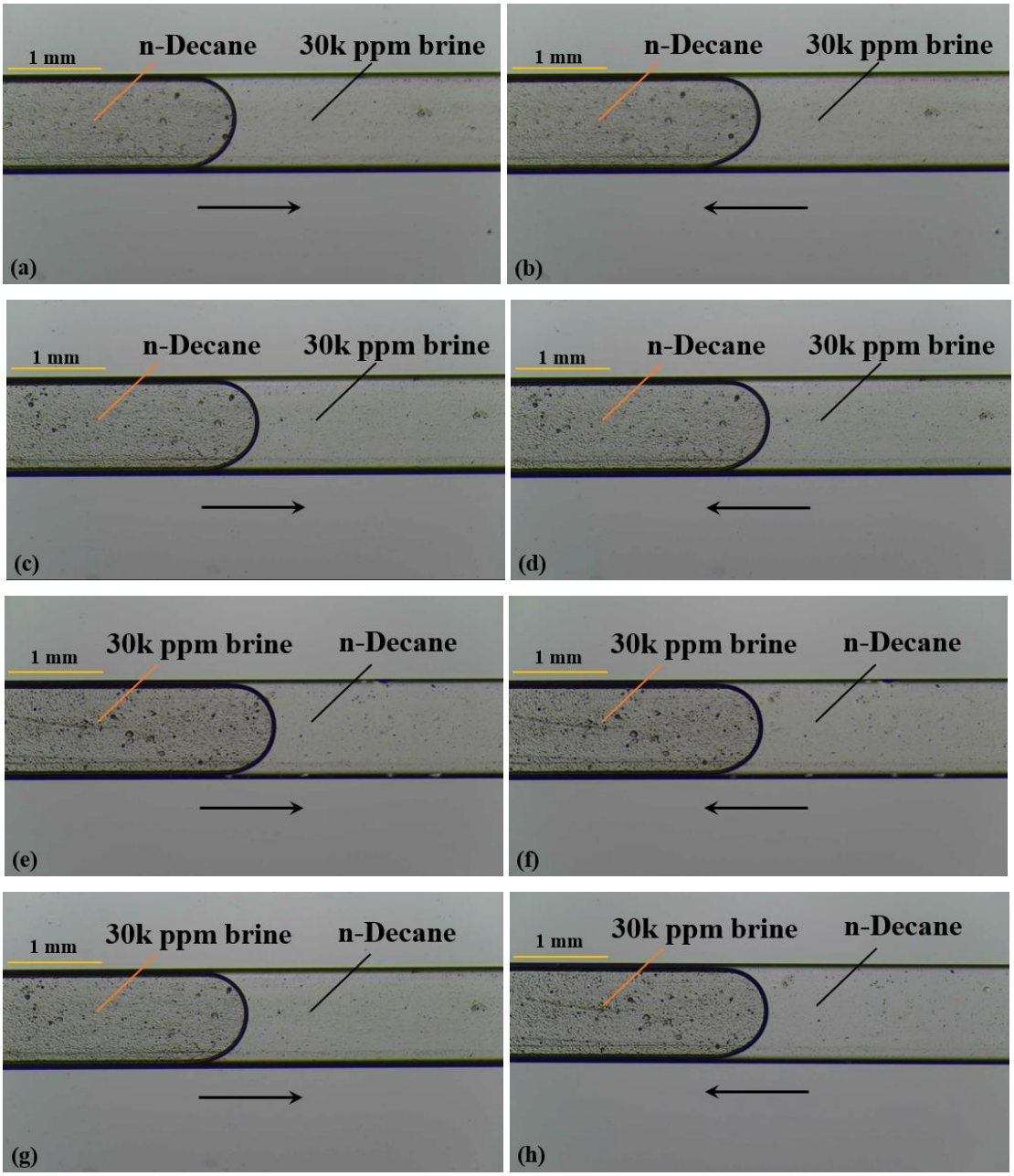


Figure 45: Illite-Smectite clay-coated microfluidic channel contacted by 30k ppm brine first: (a) 30k ppm brine receding contact angle and (b) 30k ppm brine advancing contact angle in 30k ppm brine-n-decane system before aging; (c) 30k ppm brine receding contact angle and (d) 30k ppm brine advancing contact angle in 30k ppm brine-n-decane system after aging. Illite-Smectite clay-coated microfluidic channel contacted by n-decane first: (e) 30k ppm brine advancing contact angle and (f) 30k ppm brine receding contact angle in 30k ppm brine-n-decane system before aging; (g) 30k ppm brine advancing contact angle and (h) 30k ppm brine receding contact angle in 30k ppm brine-n-decane system after aging; Arrow indicates the direction of interface movement.

30k ppm brine advancing and receding contact angles in the case of surface contacted by n-decane first were ~180° indicating that the surface is behaving as strongly oil-wet before aging. The aging effect was studied by retaining the n-decane and 30k ppm brine in the corresponding microfluidic channels for approximately 24 h in the case of channels first contacted by 30k ppm brine and n-decane, respectively. In the case of 30k ppm brine first contacted the channel surface, both 30k ppm brine advancing and receding angles were ~0° indicating the surface is still strongly water-wet even after aging. In the case of n-decane contacted the channel surface, both 30k ppm brine advancing and receding angles were ~180° indicating the surface is still strongly oil-wet even after aging. In addition, fines migration was not observed in this case.

### 4.4.5 Produced water and Crude oil system

#### 4.4.5.1 Untreated microfluidic channel

Figure 46 represents the advancing and receding contact angles of produced water-air and crude oil-air system. Figure 47 represents the advancing and receding contact angles of produced water-crude oil before and after aging (produced water contacted the channel surface first), crude oil-produced water before and after aging (crude oil contacted the channel surface first) systems. In untreated microfluidic channels, the before aging base case advancing and receding contact angles of produced water-air system were ~45° and ~30°, respectively, and crude oil-air system were ~0°. In the case of produced water contacted the channel first, the produced water advancing and receding contact angles before aging were ~90° and ~25°–30°, respectively, indicating that during produced water advancing, the surface is behaving as intermediate wet and during produced water receding, the surface is behaving as water-wet. In the case of crude oil contacted the channel first, the produced water advancing and receding contact angles before aging were ~180° indicating that the surface is behaving as strongly oil-wet. The aging effect was studied by retaining the crude oil and produced water in the corresponding microfluidic channels for approximately 24 h in the case of channels first contacted by produced water and crude oil, respectively.

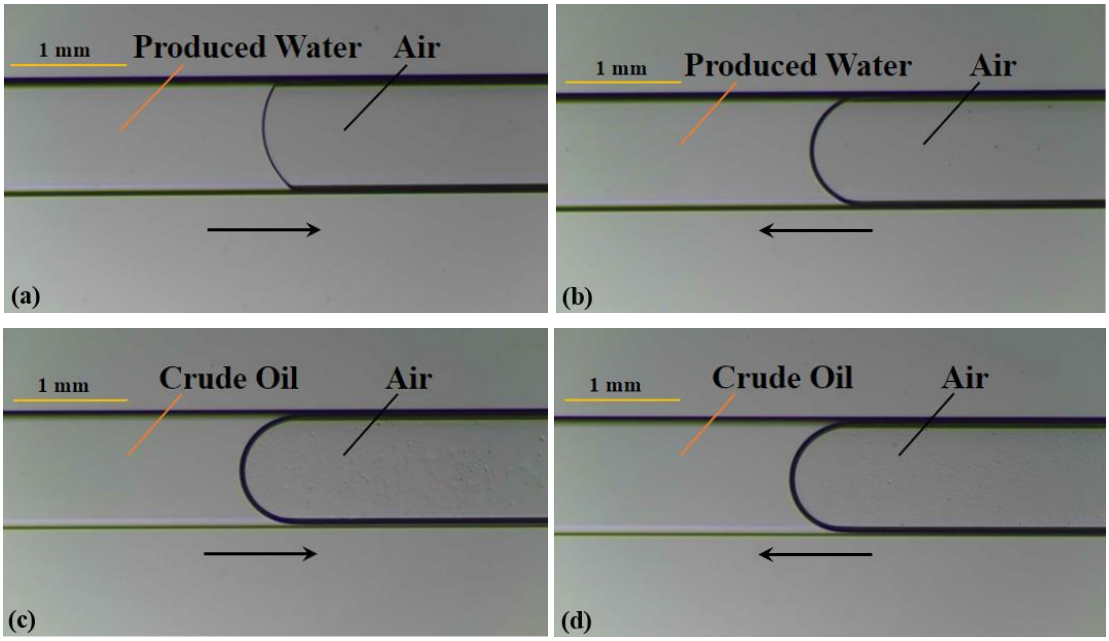


Figure 46: Untreated microfluidic channel contacted by produced water first: (a) produced water advancing contact angle and (b) produced water receding contact angle in produced water-air system before aging; Untreated microfluidic channel contacted by crude oil first: (c) crude oil advancing contact angle and (d) crude oil receding contact angle in crude oil-air system before aging.

In the case of produced water first contacted the channel surface, the produced water advancing and receding angles after aging were ~130°–140° and ~30° indicating that during produced water advancing surface is behaving as oil-wet and during produced water receding surface is behaving as water-wet after aging. In the case of crude oil first contact the channel surface, both the produced water advancing and receding angles were ~180° indicating that the surface is still strongly oil-wet after aging.

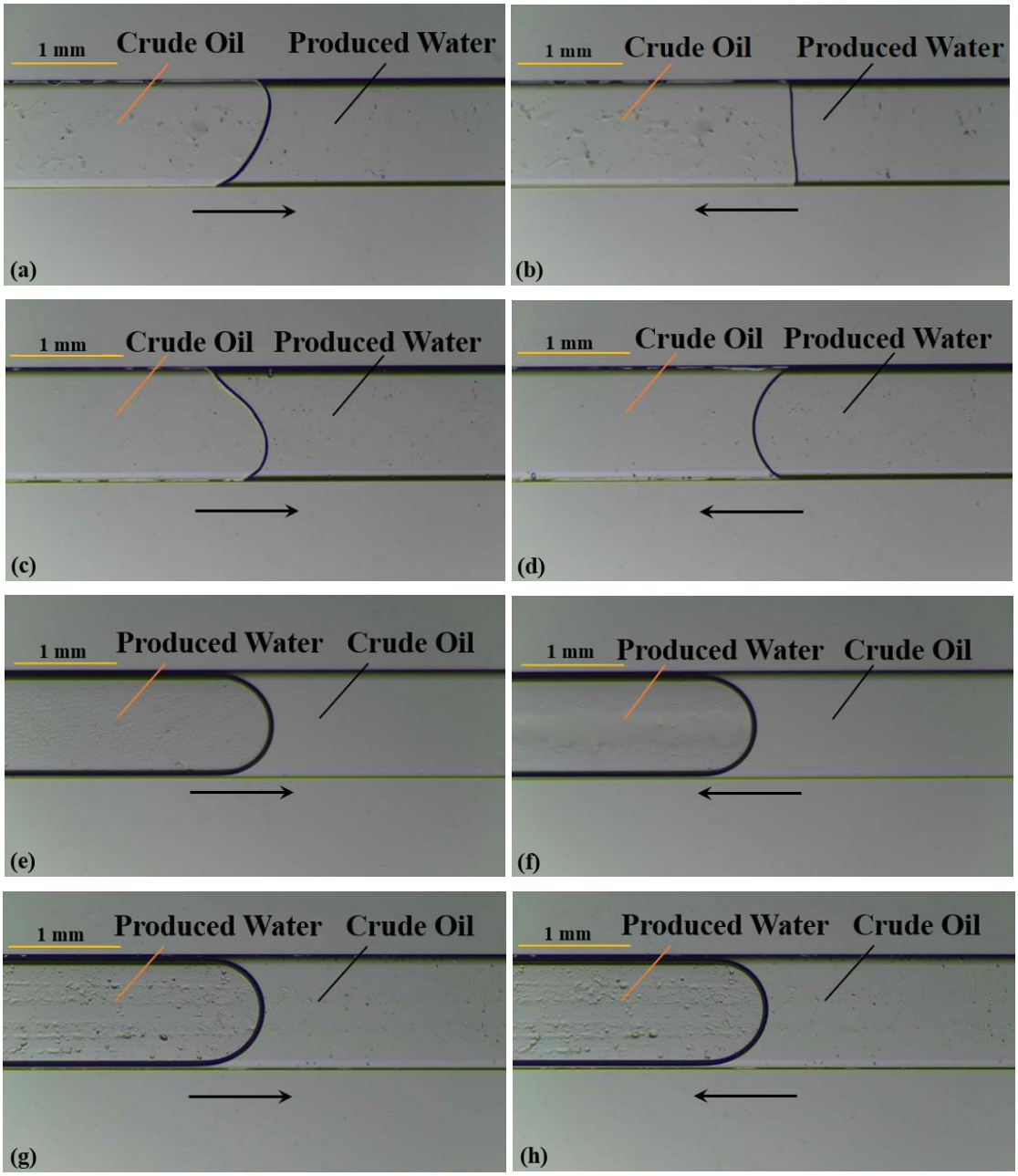


Figure 47: Untreated microfluidic channel contacted by produced water first: (a) produced water receding contact angle and (b) produced water advancing contact angle in produced water-crude oil system before aging; (c) produced water receding contact angle and (d) produced water advancing contact angle in produced water-crude oil system after aging. Untreated microfluidic channel contacted by crude oil first: (e) produced water advancing contact angle and (f) produced water receding contact angle in produced water-crude oil system before aging; (g) produced water advancing contact angle and (h) produced water receding contact angle in produced water-crude oil system after aging; Arrow indicates the direction of interface movement.

#### 4.4.5.2 Illite clay-coated microfluidic channel

Figure 48 represents the advancing and receding contact angles of produced water-air and crude oil-air system. Figure 49 represents the advancing and receding contact angles of produced water-crude oil before and after aging (produced water contacted the channel surface first), crude oil-produced water before and after aging (crude oil contacted the channel surface first) systems. The before aging advancing and receding contact angles of produced water-air, and crude oil-air systems in Illite clay-coated microfluidic channels were ~0°.

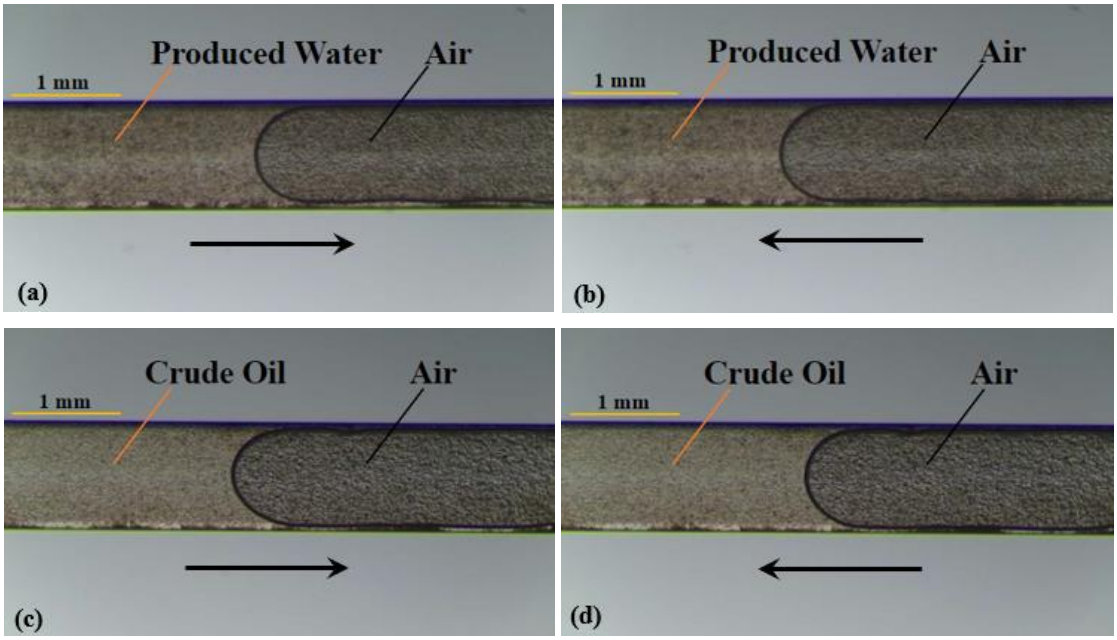


Figure 48: Illite clay-coated microfluidic channel contacted by produced water first: (a) produced water advancing contact angle and (b) produced water receding contact angle in produced water-air system before aging; Illite clay-coated microfluidic channel contacted by crude oil first: (c) crude oil advancing contact angle and (d) crude oil receding contact angle in crude oil-air system before aging.

In the case of crude oil contacted the channel first, both produced water advancing and receding contact angles before aging were ~180°, indicating the surface is strongly oil-wet. In the case of produced water contacted the channel first, produced water advancing contact angle before aging were ~0°, indicating the surface is strongly water-wet. The aging effect was studied by retaining the crude oil and produced water in the corresponding microfluidic channels for approximately 24 h in the case of channels first contacted by produced water and crude oil, respectively.

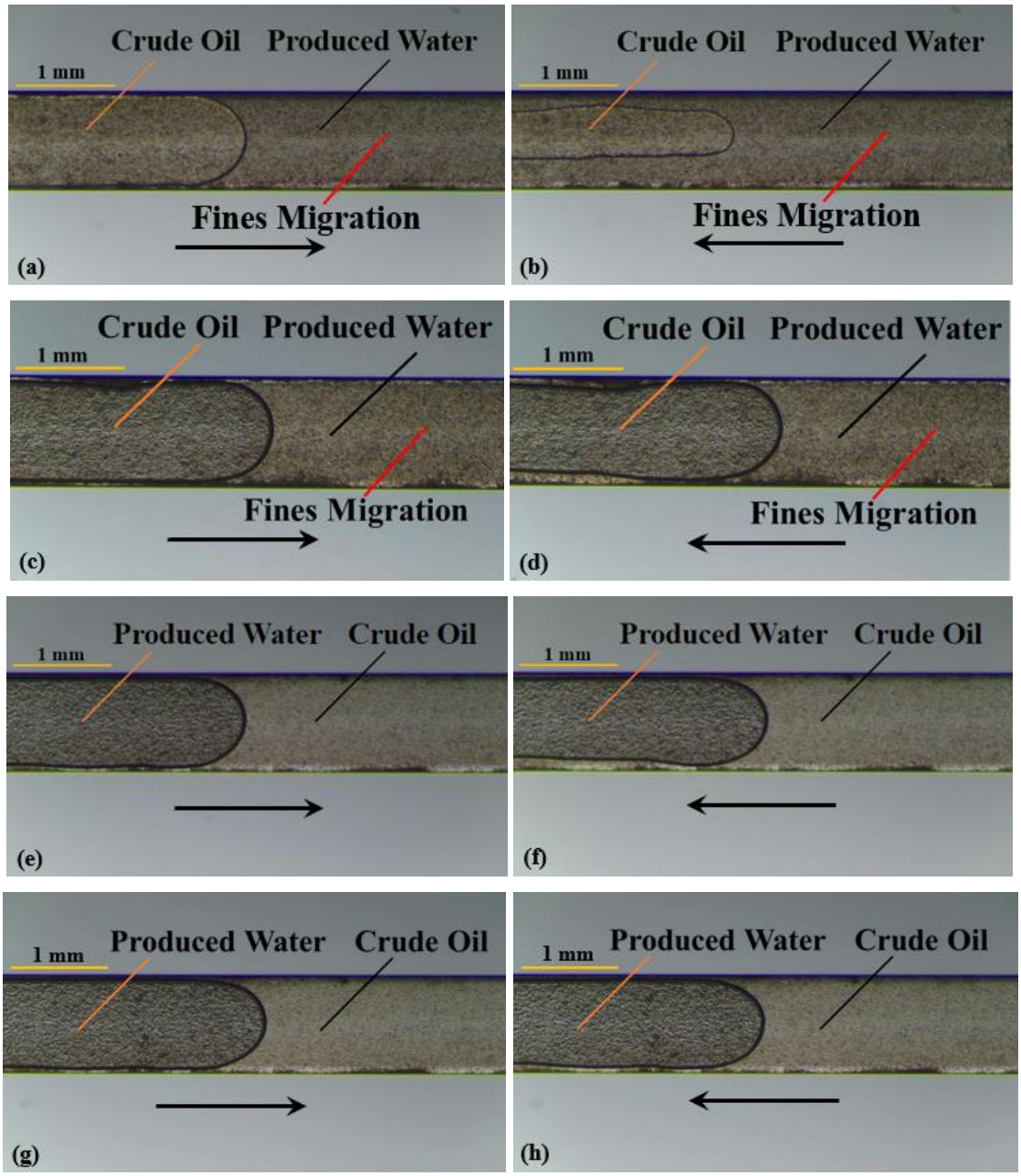


Figure 49: Illite clay-coated microfluidic channel contacted by produced water first: (a) produced water receding contact angle and (b) produced water advancing contact angle in produced water-crude oil system before aging; (c) produced water receding contact angle and (d) produced water advancing contact angle in produced water-crude oil system after aging. Illite clay-coated microfluidic channel contacted by crude oil first: (e) produced water advancing contact angle and (f) produced water receding contact angle in produced water-crude oil system before aging; (g) produced water advancing contact angle and (h) produced water receding contact angle in produced water-crude oil system after aging; Arrow indicates the direction of interface movement.

In the case of produced water contacted the channel first, both produced water advancing and receding angles after aging were ~0° indicating the surface is still strongly water-wet. In the case of crude oil contacted the channel first, both produced water advancing and receding angles after aging were ~180° indicating the surface is still strongly oil-wet. Fines migration was observed in the case of produced water-air system (Figures 48 (a) and (b)), and in the case of produced water - n-decane system when produced water first contacted the microfluidic channel (Figures 49 (a), (b), (c), and (d)).

#### 4.4.5.3 Illite-Smectite clay-coated microfluidic channel

Figure 50 represents the advancing and receding contact angles of produced water-air and crude oil-air system. Figure 51 represents the advancing and receding contact angles of produced water-crude oil before and after aging (produced water contacted the channel surface first), crude oil-produced water before and after aging (crude oil contacted the channel first) systems.

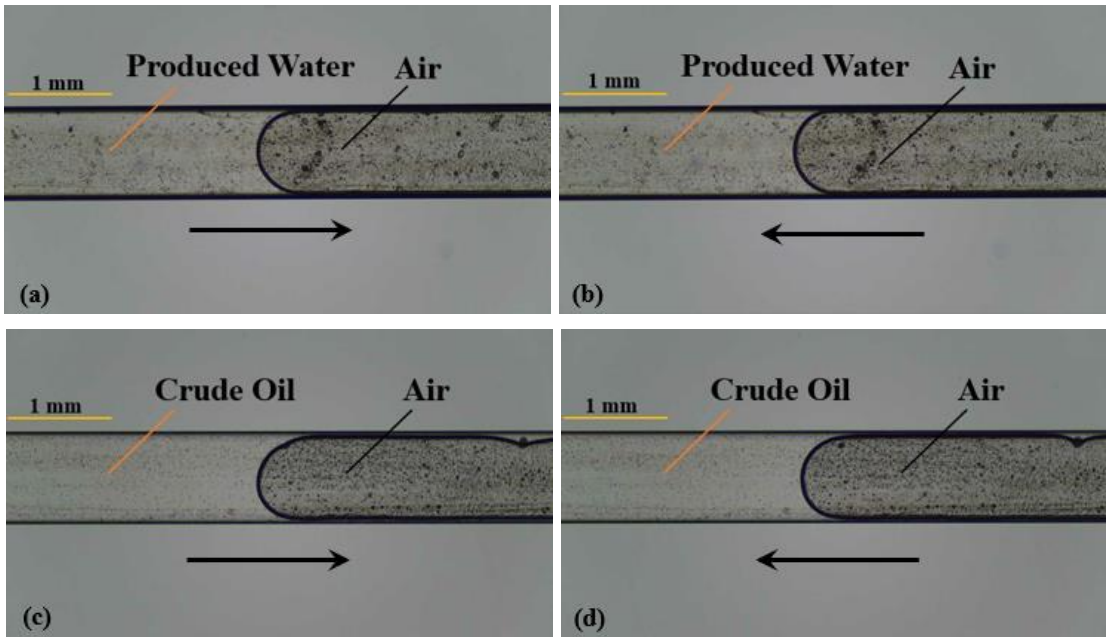


Figure 50: Illite-Smectite clay-coated microfluidic channel contacted by produced water first: (a) produced water advancing contact angle and (b) produced water receding contact angle in produced water-air system before aging; Illite-Smectite clay-coated microfluidic channel contacted by crude oil first: (c) crude oil advancing contact angle and (d) crude oil receding contact angle in crude oil-air system before aging.

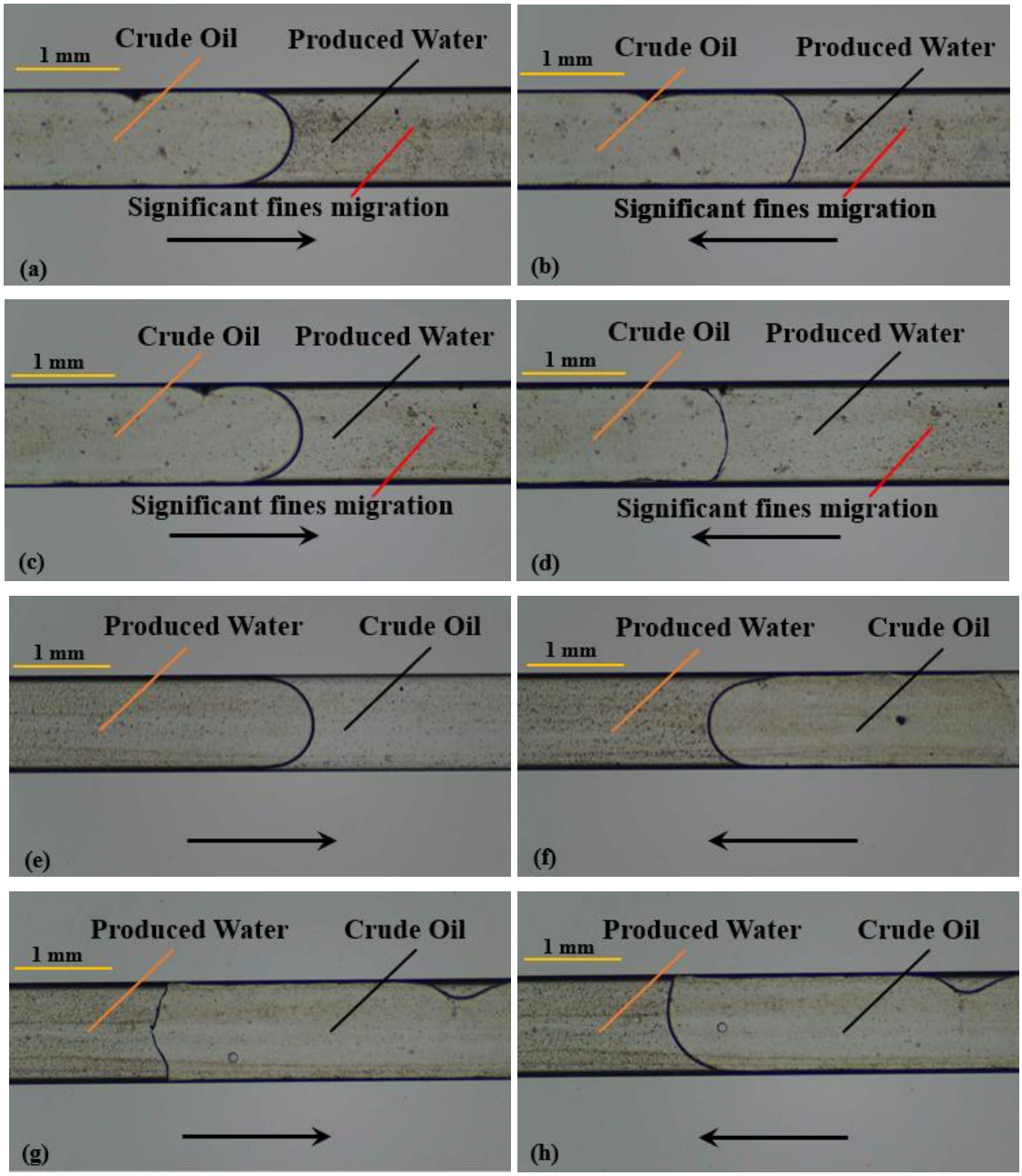


Figure 51: Illite-Smectite clay-coated microfluidic channel contacted by produced water first: (a) produced water receding contact angle and (b) produced water advancing contact angle in produced water-crude oil system before aging; (c) produced water receding contact angle and (d) produced water advancing contact angle in produced water-crude oil system after aging. Illite-Smectite clay-coated microfluidic channel contacted by crude oil first: (e) produced water advancing contact angle and (f) produced water receding contact angle in produced water-crude oil system before aging; (g) produced water advancing contact angle and (h) produced water receding contact angle in produced water-crude oil system after aging; Arrow indicates the direction of interface movement.

The before aging advancing and receding contact angles of produced water-air, and crude oil-air systems in Illite-Smectite clay-coated microfluidic channels were ~0°. In the case of produced water contacted the channel first, the produced water receding contact angle before aging in produced water-crude oil system is ~30°–40° and the produced water advancing contact angle before aging is ~60°–70° indicating that the surface is water-wet to intermediate-wet. In the case of crude oil first contacted the channel first, the produced water advancing and receding contact angle before aging is ~150°–160° and ~20°–30°, respectively, indicating that during produced water advancing the surface is behaving as oil-wet whereas when the produced water is receding the surface is behaving as water-wet. Snap off phenomenon was observed in the case of surface contacted by crude oil first. This is mainly due to surface heterogeneity. The aging effect was studied by retaining the crude oil and produced water in the corresponding microfluidic channels for approximately 24 h in the case of channels first contacted by produced water and crude oil, respectively. In the case of produced water first contacted the channel first, the produced water advancing and receding contact angle after aging is ~55°–60° and ~20°–30°, respectively, indicating the surface is preferentially water-wet. In the case of crude oil first contacted the channel first, the produced water advancing and receding contact angles were ~80°–85° and ~20°–30° indicating that during produced water advancing and receding the surface is intermediate wet and water-wet, respectively. Significant fines migration was observed in the case of produced water-air system (Figures 50 (a) and (b)), and in the case of produced water -n-decane system when produced water first contacted the microfluidic channel (Figures 51 (a), (b), (c), and (d)). Also, snap off phenomenon was observed after aging as well in the case of channel contacted by crude oil first. Figure 52 represents the snap off phenomenon in the case of surface contacted by crude oil first.

Table 9, 10, and 11 represents the wettability results for untreated, Illite clay-coated, and Illite-Smectite clay-coated microfluidic channels.

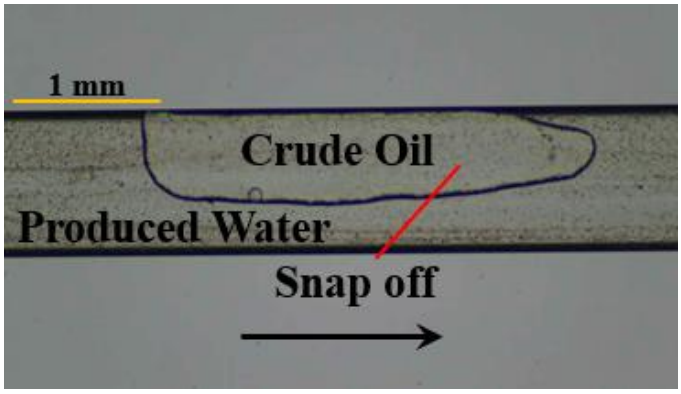


Figure 52: Snap off phenomenon in Illite-Smectite clay-coated surface contacted by crude oil first.

Table 9: Wettability states of untreated microfluidic channel-brine-oil systems.

| Experiment | Fluid contacting the microfluidic chip first | Wettability | | | |
|---|---|---|---|---|---|
| | | Advancing Contact Angle (°) | | Receding Contact Angle (°) | |
| | | Before Aging | After Aging | Before Aging | After Aging |
| **DI water/ n-decane** | n-decane | ~180° | ~85°–95° | ~180° | ~50°–65° |
| | DI water | ~0° | ~80°–90° | ~0° | ~60°–70° |
| **5k ppm brine/ n-decane** | n-decane | ~180° | ~0° | ~180° | ~0° |
| | 5k ppm brine | ~0° | ~0° | ~0° | ~0° |
| **10k ppm brine/ n-decane** | n-decane | ~180° | ~180° | ~180° | ~180° |
| | 10k ppm brine | ~0° | ~0° | ~0° | ~0° |
| **30k ppm brine/ n-decane** | n-decane | ~180° | ~180° | ~180° | ~180° |
| | 30k ppm brine | ~150° | ~150° | ~145° | ~150° |
| **Produced water/ Crude oil** | Crude oil | ~180° | ~180° | ~180° | ~180° |
| | Produced water | ~90° | ~130°–140° | ~25°–30° | ~30° |

Table 10: Wettability states of Illite clay-coated microfluidic channel-brine-oil systems.

| Experiment | Fluid contacting the microfluidic chip first | Wettability | | | |
|---|---|---|---|---|---|
| | | Advancing Contact Angle (°) | | Receding Contact Angle (°) | |
| | | Before Aging | After Aging | Before Aging | After Aging |
| **DI water/ n-decane** | n-decane | ~180° | ~180° | ~180° | ~180° |
| | DI water | ~0° | ~180° | ~0° | ~180° |
| **5k ppm brine/ n-decane** | n-decane | ~180° | ~0° | ~180° | ~0° |
| | 5k ppm brine | ~0° | ~0° | ~0° | ~0° |
| **10k ppm brine/ n-decane** | n-decane | ~180° | ~180° | ~180° | ~180° |
| | 10k ppm brine | ~0° | ~0° | ~0° | ~0° |
| **30k ppm brine/ n-decane** | n-decane | ~180° | ~180° | ~180° | ~180° |
| | 30k ppm brine | ~180° | ~180° | ~180° | ~180° |
| **Produced water/ Crude oil** | Crude oil | ~180° | ~180° | ~180° | ~180° |
| | Produced water | ~0° | ~0° | ~0° | ~0° |

Table 11: Wettability states of Illite-Smectite clay-coated microfluidic channel-brine-oil systems.

| Experiment | Fluid contacting the microfluidic chip first | Wettability | | | |
|---|---|---|---|---|---|
| | | Advancing Contact Angle (°) | | Receding Contact Angle (°) | |
| | | Before Aging | After Aging | Before Aging | After Aging |
| **DI water/ n-decane** | n-decane | ~180° | ~180° | ~180° | ~180° |
| | DI water | ~0° | ~180° | ~0° | ~180° |
| **5k ppm brine/ n-decane** | n-decane | ~180° | ~0° | ~180° | ~0° |
| | 5k ppm brine | ~0° | ~0° | ~0° | ~0° |
| **10k ppm brine/ n-decane** | n-decane | ~180° | ~180° | ~180° | ~180° |
| | 10k ppm brine | ~0° | ~0° | ~0° | ~0° |
| **30k ppm brine/ n-decane** | n-decane | ~180° | ~180° | ~180° | ~180° |
| | 30k ppm brine | ~0° | ~0° | ~0° | ~0° |
| **Produced water/ Crude oil** | Crude oil | ~150°–160° | ~80°–85° | ~20°–30° | ~20°–30° |
| | Produced water | ~60°–70° | ~55°–60° | ~30°–40° | ~20°–30° |

### 4.5 Wettability results using Caney shale core sample of reservoir zone

Figure 53 represents the before and after aging advancing and receding contact angles of produced water-crude oil-Caney shale rock from reservoir zone. Produced water advancing and receding contact angle in crude oil-produced water system before aging were ~43° and ~20°, respectively, indicating that the Caney shale from reservoir zone is water wet. Aging effect was observed by

having the crude oil-produced water system in equilibrium for approximately 24 h. After aging, the produced water advancing and receding contact angles were ~68° and ~31°, respectively, indicating that the surface is preferentially water-wet.

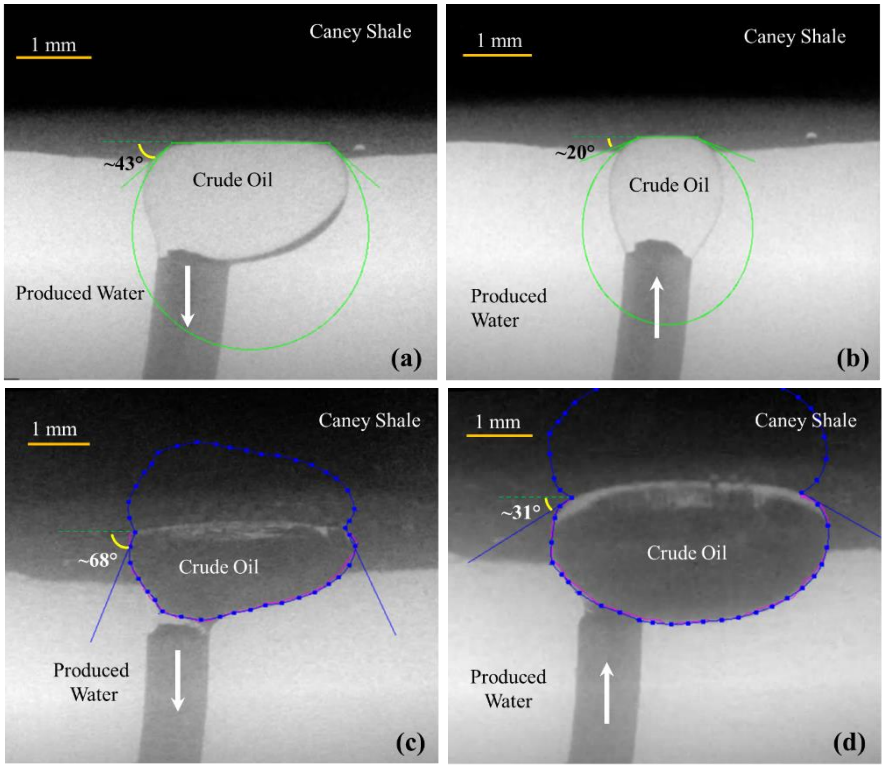


Figure 53: (a) Produced water advancing contact angle and (b) produced water receding contact angle in produced water-crude oil-Caney shale rock (reservoir zone) system before aging; (c) produced water advancing contact angle and (d) produced water receding contact angle in produced water-crude oil-Caney shale rock (reservoir zone) system after aging. Arrow indicates the direction of movement of crude oil droplet.

### 4.6 Wettability results using Caney shale core sample of non-reservoir zone

Figure 54 represents the before and after aging advancing and receding contact angles of produced water-crude oil-Caney shale rock from non-reservoir zone. Produced water advancing and receding contact angle in crude oil-produced water system before aging were ~32° and ~15°, respectively, indicating that the Caney shale from non-reservoir zone is water wet. Aging effect was observed by having the crude oil-produced water system in equilibrium for approximately 24 h. After aging, the produced water advancing and receding contact angles were ~36° and ~30°, respectively, indicating that the surface is preferentially water-wet.

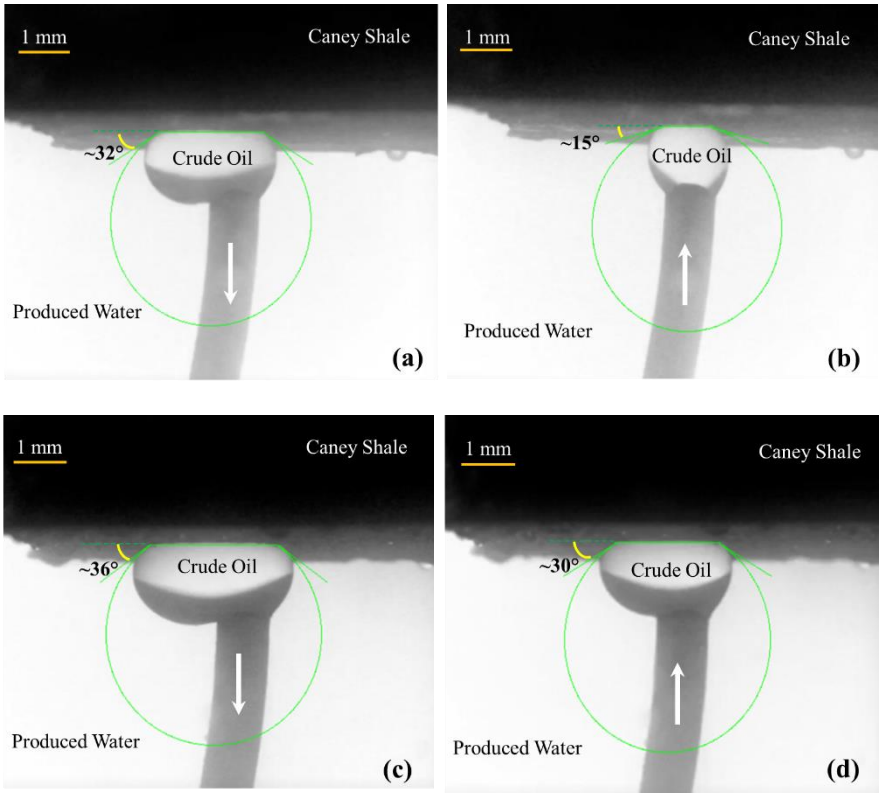


Figure 54: (a) Produced water advancing contact angle and (b) produced water receding contact angle in produced water-crude oil-Caney shale rock (non-reservoir zone) system before aging; (c) produced water advancing contact angle and (d) produced water receding contact angle in produced water-crude oil-Caney shale rock (non-reservoir zone) system after aging. Arrow indicates the direction of movement of crude oil droplet.

# CHAPTER V

## CONCLUSION

This study aimed to investigate the rock-brine interactions using geomaterial microfluidics. In this study, Illite and Illite-Smectite clay-coated surfaces were successfully generated in thin bottom flow cells microfluidic chips made of borosilicate glass. As this study is continuation of the work performed by Rupom et al. [62], Illite-Smectite coated surfaces were generated in glass capillary tubes to characterize the coating efficiency. For this purpose, NaCl brines of 4 different salinities (0ppm, 5000 ppm, 10,000 ppm, and 30,000 ppm) were used to test the effect of salinity on clay coating. It was observed that with increasing salinity, a more dense and uniform clay coating could be obtained on the glass surface.

This study provides insight about the behavior of clay formations (e.g., swelling potential, fines migration, wettability alteration, etc.) upon exposure to model (NaCl brine solutions and n-decane) and field fluids (produced water and crude oil).

In this study, the influence of brine salinity, first contact liquid, and aging in second contact liquid on the wettability of untreated, Illite and Illite-Smectite coated glass surfaces was evaluated. The study reported that low salinity brine injection results in wettability alteration in all cases i.e., untreated, Illite and Illite-Smectite coated surfaces. In high salinity environment, wettability of brine-first-contacted Illite and Illite-Smectite coated surfaces were different. In contrast, the wettability of brine-first-contacted untreated and Illite coated surface were similar. This study also

reports significant fines migration in the case of Illite-Smectite coated surface when brine contacted the channel at first. The wettability analysis of Caney shale core sample from reservoir and non-reservoir zones was also conducted in this study. The produced water advancing and receding contact angles before and after aging indicates that Caney shale from reservoir zone is predominantly water-wet.

There are further opportunities for conducting research on microfluidic chips coated with clay. The micromodel of geomaterial created in this study is a simple, straight channel with a single aspect ratio. Future studies could involve the development of a consistent coating on a more intricate flow network with narrower channels and various aspect ratios, resembling unconventional rocks. This would result in a more accurate representation of clay-rich rock formations using the geomaterial micromodel. Also, the wettability experiments conducted in this study are at atmospheric pressure and room temperature, therefore future studies may be conducted at high pressure and high temperature environment to resemble the reservoir conditions.

## REFERENCES


[1] "Field evaluation of the caney shale as an emerging unconventional play, southern oklahoma | netl.doe.gov." https://netl.doe.gov/node/9335.

[2] Z. Zhou, W. D. Gunter, B. Kadatz, and S. Cameron, "Effect of clay swelling on reservoir quality," *J. Can. Pet. Technol.*, vol. 35, no. 7, pp. 18–23, Jul. 1996, doi: 10.2118/96-07-02/182077/effect-of-clay-swelling-on-reservoir-quality.

[3] M. K. Rahman, Y. A. Suarez, Z. Chen, and S. S. Rahman, "Unsuccessful hydraulic fracturing cases in Australia: Investigation into causes of failures and their remedies," *J. Pet. Sci. Eng.*, vol. 57, no. 1–2, pp. 70–81, May 2007, doi: 10.1016/J.PETROL.2005.07.009.

[4] S. Farrokhpay, B. Ndlovu, and D. Bradshaw, "Behaviour of swelling clays versus non-swelling clays in flotation," *Miner. Eng.*, vol. 96–97, pp. 59–66, Oct. 2016, doi: 10.1016/j.mineng.2016.04.011.

[5] "USGS OFR01-041: Illite Group Minerals." https://pubs.usgs.gov/of/2001/of01-041/htmldocs/clays/illite.html.

[6] D. A. Laird, "Influence of layer charge on swelling of smectites," *Appl. Clay Sci.*, vol. 34, no. 1–4, pp. 74–87, Oct. 2006, doi: 10.1016/j.clay.2006.01.009.

[7] W. Song and A. R. Kovscek, "Direct visualization of pore-scale fines migration and formation damage during low-salinity waterflooding," *J. Nat. Gas Sci. Eng.*, vol. 34, pp. 1276–1283, Aug. 2016, doi: 10.1016/j.jngse.2016.07.055.

[8] "(PDF) A comprehensive review on formation damage due to fines migration." https://www.researchgate.net/publication/329058761.

[9] M. Buchgraber, M. Al-Dossary, C. M. Ross, and A. R. Kovscek, "Creation of a dual-porosity micromodel for pore-level visualization of multiphase flow," *J. Pet. Sci. Eng.*, vol. 86–87, pp. 27–38, May 2012, doi: 10.1016/j.petrol.2012.03.012.

[10] I. K. Shaik, C. P. Aichele, and P. K. Bikkina, "Microfluidics-based low salinity wettability alteration study of naphthenic-acid-adsorbed calcite surfaces," 2022, doi:

10.1021/acs.energyfuels.1c03837.

[11] "Microfluidics and their macro applications for the oil and gas industry." https://jpt.spe.org/twa/microfluidics-and-their-macro-applications-oil-and-gas-industry.

[12] M. Fani, P. Pourafshary, P. Mostaghimi, and N. Mosavat, "Application of microfluidics in chemical enhanced oil recovery: a review," *fuel*, vol. 315, p. 123225, may 2022, doi: 10.1016/j.fuel.2022.123225.

[13] P. Nguyen, J. W. Carey, H. S. Viswanathan, and M. Porter, "Effectiveness of supercritical-$CO_2$ and $N_2$ huff-and-puff methods of enhanced oil recovery in shale fracture networks using microfluidic experiments," *appl. energy*, vol. 230, pp. 160–174, nov. 2018, doi: 10.1016/j.apenergy.2018.08.098.

[14] F. Guo and S. Aryana, "An experimental investigation of nanoparticle-stabilized $CO_2$ foam used in enhanced oil recovery," *Fuel*, vol. 186, pp. 430–442, Dec. 2016, doi: 10.1016/j.fuel.2016.08.058.

[15] W. G. Anderson, "Wettability literature survey- part 1: rock/oil/brine interactions and the effects of core handling on wettability," *j. pet. technol.*, vol. 38, no. 10, pp. 1125–1144, oct. 1986, doi: 10.2118/13932-pa.

[16] B. Zhao, C. W. MacMinn, and R. Juanes, "Wettability control on multiphase flow in patterned microfluidics," *proc. natl. acad. sci. u. s. a.*, vol. 113, no. 37, pp. 10251–10256, sep. 2016, doi: 10.1073/pnas.1603387113/suppl_file/pnas.1603387113.sm04.mov.

[17] B. J. Adeyemi, P. Jadhawar, and L. Akanji, "Evolution and interfacial dynamics of thin electrolyte films in oil-brine-carbonate rock systems due to chemical equilibrium disruptions," *energy and fuels*, vol. 37, no. 1, pp. 175–190, jan. 2023, doi: 10.1021/acs.energyfuels.2c02513/asset/images/large/ef2c02513_0013.jpeg.

[18] G. Q. Tang and N. R. Morrow, "Salinity, temperature, oil composition, and oil recovery by waterflooding," *spe reserv. eng.*, vol. 12, no. 04, pp. 269–276, nov. 1997, doi: 10.2118/36680-pa.

[19] P. P. Jadhunandan and N. R. Morrow, "Effect of wettability on waterflood recovery for crude-oil/brine/rock systems," *spe reserv. eng. (society pet. eng. (united states)*, vol. 10:1, no. 1, pp. 40–46, feb. 1995, doi: 10.2118/22597-pa.

[20] R. A. Salathiel, "Oil recovery by surface film drainage in mixed-wettability rocks," *j. pet. technol.*, vol. 25, no. 10, pp. 1216–1224, oct. 1973, doi: 10.2118/4104-pa.

[21] J. E. Bobek, J. Member, A. C. C. Mattax, and M. O. Denekas, "Reservoir rock wettability - its significance and evaluation," *trans. aime*, vol. 213, no. 01, pp. 155–160, dec. 1958, doi: 10.2118/895-g.

[22] W. G. Anderson, "Wettability literature survey-part 6: the effects of wettability on waterflooding," *j. pet. technol.*, vol. 39, no. 12, pp. 1605–1622, dec. 1987, doi: 10.2118/16471-pa.

[23] P. Bikkina, J. Wan, Y. Kim, T. J. Kneafsey, and T. K. Tokunaga, "Influence of wettability and permeability heterogeneity on miscible $co_2$ flooding efficiency," *fuel*, vol. 166, pp. 219–226, oct. 2016, doi: 10.1016/j.fuel.2015.10.090.

[24] E. C. Donaldson Member Aime, R. D. Thomas, and P. B. Lorenz, "Wettability determination and its effect on recovery efficiency," *soc. pet. eng. j.*, vol. 9, no. 01, pp. 13–20, mar. 1969, doi: 10.2118/2338-pa.

[25] D. Arab, S. L. Bryant, O. Torsaeter, and A. Kantzas, "Water flooding of sandstone oil reservoirs: underlying mechanisms in imbibition vs. drainage displacement," *j. pet. sci. eng.*, vol. 213, p. 110379, jun. 2022, doi: 10.1016/j.petrol.2022.110379.

[26] H. Sharifigaliuk, S. M. Mahmood, M. Ahmad, V. Khosravi, and D. Matýsek, "Comparative analysis of conventional methods for the evaluation of wettability in shales," *j. pet. sci. eng.*, vol. 208, p. 109729, jan. 2022, doi: 10.1016/j.petrol.2021.109729.

[27] S. Guggenheim *et al.*, "Definition of clay and clay mineral: joint report of the aipea nomenclature and cms nomenclature committees," *clays clay miner.*, vol. 43, no. 2, pp. 255–256, 1995, doi: 10.1346/ccmn.1995.0430213.

[28] D. G. Schulze, "Clay Minerals," *Encycl. soils environ.*, vol. 4, pp. 246–254, jan. 2004, doi: 10.1016/b0-12-348530-4/00189-2.

[29] "Über kapillare leitung des wassers im boden: (aufstieg, versickerung u ... - josef kozeny - google books." https://books.google.com/books/about/.

[30] D. F. Boneau and R. L. Clampitt, "A surfactant system for the oil-wet sandstone of the north burbank unit," *j. pet. technol.*, vol. 29, no. 05, pp. 501–506, may 1977, doi: 10.2118/5820-pa.

[31] K. C. Khilar and H. S. Fogler, "The existence of a critical salt concentration for particle release," *j. colloid interface sci.*, vol. 101, no. 1, pp. 214–224, 1984, doi: 10.1016/0021-9797(84)90021-3.

[32] "Migration of fines | geothermperform." https://www.geothermperform.eu/fines-migration/#figure1.

[33] A. Marmur, "Thermodynamic aspects of contact angle hysteresis," *adv. colloid interface sci.*, vol. 50, no. c, pp. 121–141, may 1994, doi: 10.1016/0001-8686(94)80028-6.

[34] G. J. Hirasaki, "Wettability: fundamentals and surface forces," *spe form. eval.*, vol. 6, no. 02, pp. 217–226, jun. 1991, doi: 10.2118/17367-pa.

[35] F. Liu and M. Wang, "Review of low salinity waterflooding mechanisms: wettability alteration and its impact on oil recovery," *fuel*, vol. 267, p. 117112, may 2020, doi: 10.1016/j.fuel.2020.117112.

[36] M. Sadeqi-Moqadam, S. Riahi, and A. Bahramian, "An investigation into the electrical behavior of oil/water/reservoir rock interfaces: the implication for improvement in wettability prediction," *colloids surfaces a physicochem. eng. asp.*, vol. 490, pp. 268–282, feb. 2016, doi: 10.1016/j.colsurfa.2015.11.040.

[37] A. A. Yousef, S. Al-Saleh, A. Al-Kaabi, and M. Al-Jawfi, "Laboratory investigation of novel oil recovery method for carbonate reservoirs," *soc. pet. eng. - can. unconv. resour. int. pet. conf. 2010*, vol. 3, pp. 1825–1859, oct. 2010, doi: 10.2118/137634-ms.

[38] "Low salinity oil recovery - an experimental investigation1 | petrophysics | onepetro." https://onepetro.org/petrophysics/article-abstract/171146/low-salinity-oil-recovery-an-experimental.

[39] D. J. Ligthelm, J. Gronsveld, J. P. Hofman, N. J. Brussee, F. Marcelis, and H. A. van der Linde, "Novel waterflooding strategy by manipulation of injection brine composition.," *eurosurveillance*, jun. 2009, doi: 10.2118/119835-ms.

[40] Q. Xie, Y. Liu, J. Wu, and Q. Liu, "Ions tuning water flooding experiments and

interpretation by thermodynamics of wettability," *j. pet. sci. eng.*, vol. 124, pp. 350–358, dec. 2014, doi: 10.1016/j.petrol.2014.07.015.

[41] A. Katende and F. Sagala, "A critical review of low salinity water flooding: mechanism, laboratory and field application," *j. mol. liq.*, vol. 278, pp. 627–649, mar. 2019, doi: 10.1016/j.molliq.2019.01.037.

[42] H. Tian and M. Wang, "electrokinetic mechanism of wettability alternation at oil-water-rock interface," *surf. sci. rep.*, vol. 72, no. 6, pp. 369–391, dec. 2017, doi: 10.1016/j.surfrep.2018.01.001.

[43] A. Rezaeidoust, T. Puntervold, S. Strand, and T. Austad, "Smart water as wettability modifier in carbonate and sandstone: a discussion of similarities/differences in the chemical mechanisms," *energy and fuels*, vol. 23, no. 9, pp. 4479–4485, sep. 2009, doi: 10.1021/ef900185q.

[44] A. Kakati and J. S. Sangwai, "Effect of monovalent and divalent salts on the interfacial tension of pure hydrocarbon-brine systems relevant for low salinity water flooding," *j. pet. sci. eng.*, vol. 157, pp. 1106–1114, aug. 2017, doi: 10.1016/j.petrol.2017.08.017.

[45] T. Austad, S. F. Shariatpanahi, S. Strand, C. J. J. Black, and K. J. Webb, "Conditions for a low-salinity enhanced oil recovery (eor) effect in carbonate oil reservoirs," *energy and fuels*, vol. 26, no. 1, pp. 569–575, jan. 2012, doi: 10.1021/ef201435g/asset/images/large/ef-2011-01435g_0005.jpeg.

[46] H. Pu, X. Xie, P. Yin, and N. R. Morrow, "Low salinity waterflooding and mineral dissolution," *proc. - spe annu. tech. conf. exhib.*, vol. 2, pp. 1574–1590, sep. 2010, doi: 10.2118/134042-ms.

[47] W. B. Bartels, H. Mahani, S. Berg, and S. M. Hassanizadeh, "Literature review of low salinity waterflooding from a length and time scale perspective," *fuel*, vol. 236, pp. 338–353, jan. 2019, doi: 10.1016/j.fuel.2018.09.018.

[48] R. A. Nasralla *et al.*, "Potential of low-salinity waterflood to improve oil recovery in carbonates: demonstrating the effect by qualitative coreflood," *spe j.*, vol. 21, no. 05, pp. 1643–1654, oct. 2016, doi: 10.2118/172010-pa.

[49] S. Xu, J. Wu, W. Lv, J. Wang, and Q. Liu, "Experimental study on the wettability alteration

mechanism of ion tuning waterflooding," *spec. top. & rev. porous media an int. j.*, vol. 7, no. 4, pp. 373–376, 2016, doi: 10.1615/specialtopicsrevporousmedia.2016017437.

[50] H. Mahani *et al.*, "Insights into the impact of temperature on the wettability alteration by low salinity in carbonate rocks," *energy and fuels*, vol. 31, no. 8, pp. 7839–7853, aug. 2017, doi: 10.1021/acs.energyfuels.7b00776/suppl_file/ef7b00776_si_001.pdf.

[51] "Hydrocarbon potential of the caney shale in southeasteastern oklahoma - scott t. schad - google books.".

[52] P. J. Kamann, "Surface-to-subsurface correlation and lithostratigraphic framework of the caney shale (including the 'mayes' formation) in atoka, coal, hughes, johnston, pittsburg, and pontotoc counties, oklahoma," may 2006, accessed: mar. 14, 2023. [online]. available: https://shareok.org/handle/11244/14234

[53] M. Radonjic *et al.*, "Integrated microstructural characterisation of caney shale, ok," aug. 2020, doi: 10.15530/urtec-2020-2947.

[54] N.-T. Nguyen, S. T. Wereley, and S. A. M. Shaegh, "Fundamentals and applications of microfluidics".

[55] G. M. Whitesides, "The origins and the future of microfluidics.," *nature*, vol. 442, no. 7101, pp. 368–373, jul. 2006, doi: 10.1038/nature05058.

[56] A. Anbari, H.-T. Chien, S. S. Datta, W. Deng, D. A. Weitz, and J. Fan, "Microfluidic model porous media: fabrication and applications.," *small*, vol. 14, no. 18, p. e1703575, may 2018, doi: 10.1002/smll.201703575.

[57] N. S. K. Gunda, B. Bera, N. K. Karadimitriou, S. K. Mitra, and S. M. Hassanizadeh, "Reservoir-on-a-chip (roc): a new paradigm in reservoir engineering.," *lab chip*, vol. 11, no. 22, pp. 3785–3792, nov. 2011, doi: 10.1039/c1lc20556k.

[58] T. Amirian, *Pore-scale visualisation and geochemical modelling of low salinity water flooding as an enhanced oil recovery method*, no. july. 2019.

[59] A. Gerami, R. T. Armstrong, B. Johnston, M. E. Warkiani, N. Mosavat, and P. Mostaghimi, "Coal-on-a-chip: visualizing flow in coal fractures," *energy and fuels*, vol. 31, no. 10, pp. 10393–10403, oct. 2017, doi: 10.1021/acs.energyfuels.7b01046.

[60] I. K. Shaik, L. Zhang, S. Pradhan, A. K. Kalkan, C. P. Aichele, and P. K. Bikkina, "A parametric study of layer-by-layer deposition of $caco_3$ on glass surfaces towards fabricating carbonate reservoirs on microfluidic chips," *j. pet. sci. eng.*, vol. 198, p. 108231, mar. 2021, doi: 10.1016/j.petrol.2020.108231.

[61] W. Song and A. R. Kovscek, "Functionalization of micromodels with kaolinite for investigation of low salinity oil-recovery processes," *lab chip*, vol. 15, no. 16, pp. 3314–3325, jul. 2015, doi: 10.1039/c5lc00544b.

[62] R. Bhattacherjee and P. K. Bikkina, "Preparation of illite coated geomaterial microfluidic surfaces: effect of salinity and heat treatment," *j. pet. sci. eng.*, vol. 216, p. 110805, sep. 2022, doi: 10.1016/j.petrol.2022.110805.

[63] Y. Q. Zhang, A. Sanati-Nezhad, and S. H. Hejazi, "Geo-material surface modification of microchips using layer-by-layer (lbl) assembly for subsurface energy and environmental applications," *lab chip*, vol. 18, no. 2, pp. 285–295, 2018, doi: 10.1039/c7lc00675f.

[64] "Microscopes & microscope parts store | amscope." https://amscope.com/.

[65] "OSU microscopy laboratory | oklahoma state university." https://research.okstate.edu/microscopy/index.html.

VITA

AYUSH JOSHI

Candidate for the Degree of

Master of Science

Thesis: INVESTIGATION OF ROCK-FLUID INTERACTIONS USING GEOMATERIAL MICROFLUIDICS

Major Field: Petroleum Engineering
Biographical:

Education:

Completed the requirements for the Master of Science in Petroleum Engineering at Oklahoma State University, Stillwater, Oklahoma in May, 2023.

Completed the requirements for the Bachelor of Technology in Petroleum Engineering at Rajiv Gandhi Institute of Petroleum Engineering, Amethi, India in 2021.